

000 001 002 003 004 005 006 007 008 009 010 011 012 013 014 015 016 017 018 019 020 021 022 023 024 025 026 027 028 029 030 031 032 033 034 035 036 037 038 039 040 041 042 043 044 045 046 047 048 049 050 051 052 053 MEDIATOR: MEMORY-EFFICIENT LLM MERGING WITH LESS PARAMETER CONFLICTS AND UNCERTAINTY BASED ROUTING

Anonymous authors

Paper under double-blind review

ABSTRACT

Model merging aggregates Large Language Models (LLMs) finetuned on different tasks into a stronger one. However, parameter conflicts between models leads to performance degradation in averaging. While model routing addresses this issue by selecting individual models during inference, it imposes excessive storage and compute costs, and fails to leverage the common knowledge from different models. In this work, we observe that different layers exhibit varying levels of parameter conflicts. Building on this insight, we average layers with minimal parameter conflicts and use a novel task-level expert routing for layers with significant conflicts. To further reduce storage costs, inspired by task arithmetic sparsity, we decouple multiple fine-tuned experts into a dense expert and several sparse experts. Then, we select and merge appropriate experts based on the task uncertainty of the input data. We conduct extensive experiments on both LLaMA and Qwen with varying parameter scales, and evaluate on real-world reasoning tasks. Results demonstrate that our method consistently achieves significant performance improvements while requiring less system cost.

1 INTRODUCTION

Finetuning Large Language Models (LLMs) enables them to adapt to downstream applications including sentiment analysis (Sun et al., 2023), text summarization (Fang et al., 2024), mathematical reasoning (Ruis et al., 2024), code writing (Jiang et al., 2024a), roleplay chatting (Chen et al., 2025) so on. Open-source platforms such as Huggingface (Wolf et al., 2019) facilitate access to a diverse array of highly trained expert models with varying capabilities. Because the computational resources are scarce and implementing green computing (Stojkovic et al., 2024), the community is increasingly interested in how to merge these models to create a superior LLM that retains the strengths of finetuned ones without retraining (Yang et al., 2024a).

Current merging strategies generally fall into two categories, each with distinct limitations. The first is model averaging (Yang et al., 2024a; Thennal et al., 2024), which computes weighted averages of parameters to synthesize collective knowledge. However, this approach suffers from parameter conflicts arising from diverse finetuning tasks, leading to performance degradation as shown in Figure 1. The second direction is model routing (Lu et al., 2024a; He et al., 2024a; Wei et al., 2024a), which maintains multiple models and selects the best one during inference. While this avoids parameter conflicts, it incurs significant computing and storage costs due to the necessity of maintaining all finetuned models in memory, and loses aggregating shared knowledge into one model. This dichotomy motivates us to rethink the following question:

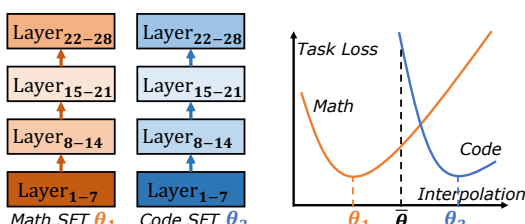


Figure 1: Knowledge conflict across finetuned LLMs and math and code dataset. Deeper color means larger parameter conflicts. And it is difficult for the linear averaged model to achieve low loss of both tasks.

054 *How to merge common and unique knowledge from various finetuned models while simultaneously
 055 avoiding parameter conflicts and minimizing system costs?*
 056

057 To address this, we first investigate the nature of parameter conflicts. By employing sign consistency
 058 between different task arithmetics to measure conflict levels, we discover that conflicts are not
 059 uniform: front and last layers tend to exhibit the highest levels of conflict (noise), while central layers
 060 demonstrate comparatively lower levels (Section 3). This insight drives our proposed framework,
 061 Mediator, which employs an adaptive merging strategy. We average layers with lower conflict levels
 062 to capture common knowledge (He et al., 2024b), while layers with significant conflicts are treated
 063 as distinct experts to be routed during inference (Section 4.1). This hybrid approach effectively
 064 preserves unique task-specific knowledge without dilution.

065 However, the "adaptive merging" strategy introduces a new challenge: maintaining multiple expert
 066 layers for the high-conflict regions remains memory-intensive. To resolve this storage bottleneck,
 067 we introduce expert decomposition. Leveraging the high sparsity of task arithmetics (Yadav et al.,
 068 2023a), we decouple finetuned models into a shared dense base and lightweight, sparse task-specific
 069 components (Δ_τ) (Ilharco et al., 2023; Tang et al., 2024a) (Section 4.2). By storing only one dense
 070 model and N sparse experts, we reduce storage requirements from 50% to 7%, making the system
 071 highly efficient.

072 With these sparse experts available, the challenge shifts to efficient selection. Existing token-level
 073 routing (Sukhbaatar et al., 2024a; Jiang et al., 2024b) often fragments the context, which is suboptimal
 074 given that LLMs are finetuned on complete sentences. Therefore, we propose a task-level expert
 075 router (Section 4.3). This mechanism selects the appropriate sparse experts based on the input prompt,
 076 better preserving the integrity of task-specific knowledge.

077 Furthermore, a static task-level router may struggle with complex or out-of-distribution (OOD) sam-
 078 ples. To address this, we incorporate uncertainty-based routing. Mediator estimates task uncertainty
 079 for input data. For ambiguous or OOD inputs, it intelligently merges multiple sparse experts to create
 080 a composite expert on the fly (Section 4.3). This allows the unified model to adapt dynamically to the
 081 characteristics of the input data.

082 Finally, to validate that our system preserves high-level capabilities, we evaluate Mediator using
 083 Chain-of-Thought (CoT) enhanced datasets (Wei et al., 2022; Guo et al., 2025) (Section 5). Our
 084 evaluations show that Mediator achieves minimal performance degradation (0.06% ~ 0.3%) while
 085 enabling a model comparable to a 7B \times 4 LLM ensemble to run effectively on a single consumer-
 086 grade RTX 4090 GPU (Appendix I.4).

087 Our main contributions can be summarized as follows:

- 089 • We quantify layer-wise parameter conflicts (Section 3) and propose Mediator, an adaptive merging
 090 framework that averages low-conflict layers to share common knowledge while routing high-conflict
 091 layers to avoid interference (Section 4.1).
- 092 • To solve the storage overhead of routing, we introduce expert decomposition (Section 4.2), separating
 093 models into one dense base and multiple sparse experts. This achieves a high compression ratio
 094 while maintaining accuracy.
- 095 • We develop an uncertainty-based routing mechanism (Section 4.3) that performs task-level selection
 096 for standard inputs and dynamic expert merging for OOD data. Experiments on LLaMA and Qwen
 097 with CoT datasets demonstrate that Mediator outperforms existing methods in both accuracy and
 098 system efficiency (Section 5).

101 2 PRELIMINARY AND RELATED WORKS

102 2.1 LANGUAGE MODELING AND LLM FINETUNING

103 **Task Data Distribution.** Given a set of different downstream tasks \mathcal{T} , based on the sampling
 104 task $\tau \in \mathcal{T}$, the pretraining data sample is a sequence $x_{1:T}$ of tokens with the maximum length
 105 T generated from a distribution $p_\tau = p(x_{1:T}|\tau) = p(o_1, \dots, o_T|\tau)$ (Xie et al., 2022; Wies et al.,
 106 2023; Hahn and Goyal, 2023; Li et al., 2024a). We define the pretraining data is sampled from

108 $p(x|\mathcal{T}^*) = \int_{\mathcal{T}^* \in \mathcal{T}^*} p(o_1, \dots, o_T|\tau)p(\tau^*)d\tau^*$. Each token o is sampled from a vocabulary \mathbb{O} . And
 109 both $(\mathcal{T}$ and \mathcal{T}^* belong to a large task family Ω , i.e. $\mathcal{T}, \mathcal{T}^* \subset \Omega$.

110 **Language Modeling.** Current LLMs (Brown et al., 2020; Touvron et al., 2023; Xie et al., 2022)
 111 usually utilize the next word prediction as the language modelling, which predicts the next token
 112 x_t given the previous tokens $x_{1:t-1}$ for all $t = 1, \dots, T$. Formally, a LLM parameterized by θ is
 113 a distribution $f_\theta(x_t|x_{1:t-1})$. And it is pretrained on a huge corpus sampled from the pretraining
 114 distribution $p(x|\mathcal{T}^*)$ (Xie et al., 2022).

115 **Finetuning LLM.** Normally, for each downstream task $\tau \in \mathcal{T}$, finetuning LLM is to minimize
 116 the cross-entropy loss function as $L_{CE}(\theta, \tau) = -\sum_{t=1}^T \mathbb{E}[p_\tau(x_t|x_{1:t-1}) \cdot \log f_\theta(x_t|x_{1:t-1})]$. After
 117 finetuning, the model parameters θ are updated to θ_τ .

118 2.2 MODEL MERGING

121 Given finetuned task-specific LLMs $\{\theta_1, \theta_2, \dots, \theta_{n_\tau}\}$ finetuned on task set \mathcal{T} , where $n_\tau = |\mathcal{T}|$,
 122 model merge aims to find a unified model parameterized by ϕ that can achieve the low loss on all
 123 tasks \mathcal{T} as following

$$126 \min_{\phi} L_{CE}(\phi, \mathcal{T}) = \frac{1}{n_\tau} \sum_{\tau \in \mathcal{T}} L_{CE}(\phi, \tau). \quad (1)$$

128 Different from training ϕ that can be optimized towards any direction, model merging aims to
 129 exploit combining $\{\theta, \theta_1, \theta_2, \dots, \theta_{n_\tau}\}$ to obtain the ϕ . The current model merging methods include
 130 following two categories.

132 **Model Averaging.** Averaging parameters to fuse the knowledge from different finetuned models is
 133 straightforward. Mathematically, averaged model is $\phi = \sum_{\tau \in \mathcal{T}} w_\tau \theta_\tau$, in which w_τ is the averaging
 134 weight and $\sum_{\tau \in \mathcal{T}} w_\tau = 1$. Because different model parameters have different importance on
 135 downstream tasks, some works (Kirkpatrick et al., 2017; Sun et al., 2024; Dong et al.) assign
 136 larger weights to more important parameters. Current methods usually utilize Taylor expansion (Lee
 137 et al., 2019; Matena and Raffel, 2022) to measure the importance of the parameters. However, the
 138 knowledge conflicts still exist for parameters that have high importance simultaneously.

139 **Model Routing.** To completely avoid conflicts, another way is to select the most relevant model
 140 for each task. This approach typically employs a selection mechanism to activate the most relevant
 141 model based on the input task τ (Yang et al., 2024b) or sequence $x_{1:t}$ at t -th token like the Mixture
 142 of Experts (MoE) (Tang et al., 2024b). Current methods propose different routing and re-training
 143 mechanisms to improve the performance (He et al., 2024a; Wei et al., 2024a; Sukhbaatar et al.,
 144 2024b). However, these methods fail to consider merging parameters to find the common knowledge
 145 that can be shared across different tasks, and cause large memory and computational costs. We leave
 146 detailed discussions about related works in Appendix C).

147 **Out-of-distribution Data.** In real-world deployment, the test data x may come from other distributions
 148 instead of the $p(x|\tau)_{\tau \in \mathcal{T}}$. To this end, we need to consider how to handle OOD data x within
 149 merging LLMs. In this work, we mainly consider two OOD cases and tackle them in Section 4.

150 3 UNDERSTANDING CONFLICT BETWEEN LLMs

151 **Preliminary Experiments.** Before introducing
 152 our framework, we first investigate the nature
 153 of parameter conflicts in model merging.
 154 We conduct preliminary experiments to quantify
 155 how conflicts arise and distribute across layers.
 156 We finetune Llama-3.2-3B on three datasets and
 157 evaluate them on corresponding tasks (experimental
 158 details in Section 5). Let $P(\theta, \tau)$ denote

159 the performance of model θ on task τ . We define three baselines: the original pretrained model
 160 (P_{ORI}), the simply averaged model (P_{AVG}), and an oracle selection model (P_{SEL}) that selects the
 161 optimal finetuned expert θ_τ for each task. As shown in Table 1, we observe the performance hierarchy
 $P_{ORI} < P_{AVG} < P_{SEL}$. This inequality implies two key insights. First, merging knowledge via

150 Table 1: Accuracy of finetuning Llama 3.2-3B.

Model	GSM8K Math	TriviaQA	H.Eval Code	All tasks
θ (Pretrained)	27.52	57.71	22.56	35.93
θ_1 (Math SFT)	46.47	54.59	25.00	42.02
θ_2 (QA SFT)	32.75	61.45	28.05	40.75
θ_3 (Coding SFT)	33.13	57.71	40.85	43.90
ϕ_{AVG}	42.61	60.99	31.30	44.97
ϕ_{SEL}	46.47	61.45	40.85	49.59

averaging (P_{AVG}) improves upon the base model (P_{ORI}). Second, simple averaging fails to fully recover the specialized capabilities of individual experts (P_{SEL}). This gap suggests that indiscriminate averaging dilutes task-specific knowledge due to parameter conflicts.

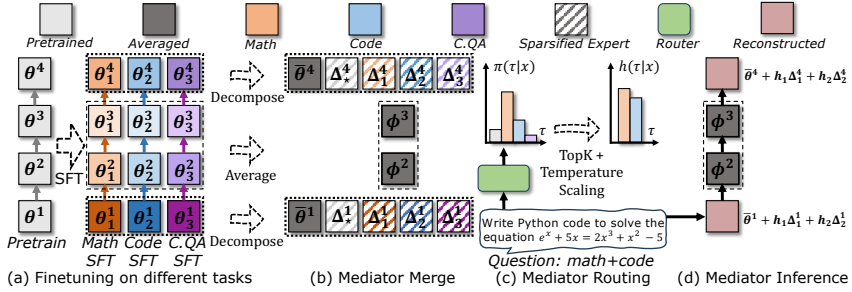


Figure 2: The framework of Mediator.

To close the gap between P_{AVG} and P_{SEL} , we must identify where conflicts occur. We utilize Task Arithmetic to isolate task-specific updates.

Definition 3.1 (Task Arithmetic). A task arithmetic on task τ is the parameter difference between the finetuned LLM θ_τ and the pre-trained LLM θ , i.e., $\Delta_\tau = \theta_\tau - \theta$.

Parameter Denoising. A critical challenge in measuring conflicts is the presence of stochastic noise. Finetuning is an optimization process where non-essential parameters often undergo random fluctuations (Yadav et al., 2023a; He et al., 2024b). For instance, a parameter might shift by $+10^{-5}$ in Task A and -10^{-5} in Task B purely by chance. Although these shifts are negligible for performance, a raw sign-based metric would incorrectly flag them as a "conflict" (+ vs -).

To prevent such false positives, we denoise the task arithmetic before measurement. We model the update elements of Δ_τ as a Gaussian distribution $\mathcal{N}_{\text{UPD}}(\mu_{\text{UPD}}, \sigma_{\text{UPD}}^2)$. We identify parameters within the range $(\mu_{\text{UPD}} - \sigma_{\text{UPD}}, \mu_{\text{UPD}} + \sigma_{\text{UPD}})$ as noise and prune them to zero. We then obtain the denoised arithmetic $\hat{\Delta}_\tau$ and the corresponding denoised model $\hat{\theta}_\tau = \theta + \hat{\Delta}_\tau$ (further details in Appendix F.1).

Measuring Parameter Conflict. Using the denoised parameters, we measure conflicts using sign consistency (Yadav et al., 2023a). For a layer l , given parameters $w_i^l \in \hat{\theta}_{\tau_i}^l$ and $w_j^l \in \hat{\theta}_{\tau_j}^l$, a conflict exists if $\text{sgn}(w_i^l w_j^l) = -1$. The conflict ratio d_l is the proportion of conflicting parameters:

$$d_l = \frac{\sum_{i,j} \mathbb{I}(\text{sgn}(w_i^l w_j^l) = -1)}{|\theta^l|} \quad (2)$$

Observation. Figure 3 illustrates the distribution of d_l across layers. We observe that conflict levels are non-uniform. Specifically, front layers consistently exhibit high conflict ratios, likely due to the divergence in shallow feature extraction for different tasks. In contrast, central layers demonstrate significantly lower conflict, suggesting a region of shared, common knowledge.

It is worth noting that while the final layers often show high conflict (as seen in Llama-3), this is not universal; for example, Qwen-4B exhibits relatively lower conflict in its final layers. This variability in conflict distribution—where the "safe-to-merge" zones differ by model architecture—underscores the necessity for an adaptive merging strategy rather than fixed layer selection.

4 THE DESIGN OF MEDIATOR

This section introduces Mediator, a unified framework designed to efficiently merge multiple finetuned LLMs. Our approach begins with **Adaptive Merging** (Section 4.1), which leverages our finding that parameter conflicts are concentrated in the front and last layers. By averaging low-conflict central layers and routing the high-conflict ones, we preserve task-specific capabilities without noise. To address the storage overhead of maintaining these multiple experts, we introduce **Expert Decomposition** (Section 4.2), which utilizes sparsity to decouple experts into lightweight task arithmetics. Finally, we implement **uncertainty-aware Expert Routing** (Section 4.3), a mechanism that dynamically selects or mixes these sparse experts to handle ambiguous or out-of-distribution inputs effectively.

4.1 ADAPTIVE LAYER-WISE MODEL AVERAGING AND ROUTING

The core challenge in model merging is that parameter conflicts are not uniformly distributed across the model. As analyzed in Section 3, averaging on high-conflict layers destroys task-specific information, while routing every layer is computationally prohibitive. Mediator solves this via an adaptive merging strategy: we average layers with shared knowledge (low conflict) and route layers with distinct task requirements (high conflict) as shown in Figure 2.

Dynamic Thresholding. Instead of manually designating "front" or "back" layers, Mediator dynamically identifies conflict zones. We first calculate the conflict score d_l for each layer l (as defined in Eq. 2). We model the distribution of these layer-wise conflicts as a Gaussian distribution $d_l \sim \mathcal{N}(\mu, \sigma)$. We apply the *Route operation* to layers falling above the adaptive threshold ($\mu + \sigma$) and *Average* those falling below it. Empirically, we observe that layers satisfying $d_l \geq \mu + \sigma$ (high conflict) are primarily located in the front and last layers of the model, corresponding to shallow feature processing and final output formatting as shown in Figure 3. Conversely, central layers typically satisfy $d_l < \mu + \sigma$, indicating they store common knowledge suitable for averaging. Additionally, following findings that attention mechanisms largely store non-specific domain knowledge (Sukhbaatar et al., 2024a), we default to averaging all attention layers.

Merging Operations. For layers designated for averaging (ϕ_{AVG}^l), we employ TIES-Merging (Yadav et al., 2023a) to compute a unified parameter set. For layers designated for routing (ϕ_{UP}^l), we maintain the distinct parameters for each task, which we address in the following subsection.

4.2 EXPERT DECOMPOSITION

The adaptive merging strategy creates a new challenge: maintaining N distinct experts for the routed layers (ϕ_{UP}^l) requires memory $N \times M_l$, where M_l is the layer size. This linear scaling with the number of tasks (N) is inefficient.

To resolve this, we introduce Expert Decomposition. We leverage the observation that while the base weights are dense, the task-specific updates (task arithmetics) are highly sparse and distinguishable

Algorithm 1 Adaptive Merging and Routing with Sparsified Expert Decomposition in Mediator

Input: Different finetuned models $\theta_1, \theta_2, \dots, \theta_{n_\tau}$.

Output: The merged layers Φ .

```

1: Calculate the conflict distribution  $\{d_l\}_{l=1, \dots, |\mathcal{L}|}$ ;
2: Estimate  $\mu, \sigma$  based on  $\{d_l\}_{l=1, \dots, |\mathcal{L}|}$ ;
3: for layer  $l = 1, \dots, |\mathcal{L}|$  do
4:   if  $d_l < \mu + \sigma$  then
5:      $\phi_{\text{AVG}}^l = \mathcal{M}(\theta_1^l, \theta_2^l, \dots, \theta_{n_\tau}^l)$ ;
6:   else
7:      $\bar{\theta}^l = 1/n_\tau \sum_{\tau \in \mathcal{T}} \theta_\tau^l$ ;
8:      $\Delta_\tau^l = \theta_\tau^l - \bar{\theta}^l$ ,  $\Delta_*^l = \theta^l - \bar{\theta}^l$ ;
9:      $\hat{\Delta}_\tau^l = \text{Denoise}(\Delta_\tau^l)$ ;
10:     $\phi_{\text{UP}}^l = \{\bar{\theta}^l, \hat{\Delta}_1^l, \hat{\Delta}_2^l, \dots, \hat{\Delta}_{n_\tau}^l, \Delta_*^l\}$ ;
11:   end if
12:   Insert  $\phi_{\text{AVG}}^l$  or  $\phi_{\text{UP}}^l$  into  $\Phi_{\text{AVG}}$  and  $\Phi_{\text{UP}}$ ;
13: end for
14: Return  $\Phi = \{\Phi_{\text{AVG}}, \Phi_{\text{UP}}\}$ . =0

```

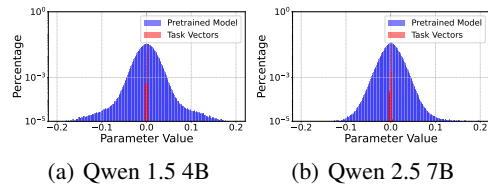


Figure 4: Comparing magnitudes of task arithmetic and pretrained model parameters.

270 from noise. As shown in Figure 4, the magnitude of task updates is significantly smaller than the
 271 pretrained parameters.
 272

273 We decompose each routed expert θ_τ into a shared base θ and a sparse task arithmetic Δ_τ :

$$\theta_\tau = \theta + \Delta_\tau \quad (3)$$

275 We then sparsify Δ_τ into $\hat{\Delta}_\tau$ by pruning parameters below a noise threshold (derived from Section 3).
 276 This reduces the storage cost from $N \times M_l$ to roughly $N \times M_l \times c$, where c is the sparsity ratio
 277 (typically $< 10\%$).
 278

279 **Preserving Pretraining Knowledge (OOD-I).** (OOD to \mathcal{T} but in-distribution to pretraining data
 280 $p(x|\mathcal{T}^*)$) Finetuning often induces catastrophic forgetting of the pretraining distribution. To ensure
 281 Mediator retains general capabilities for inputs that are Out-Of-Distribution (OOD) to the specific
 282 tasks but In-Distribution to the pretraining data ($x \sim p(x|\mathcal{T}^*)$), we explicitly store the "pretraining
 283 arithmetic" $\Delta_\star = \theta - \bar{\theta}$, where $\bar{\theta}$ is the average of the finetuned models. This allows us to revert to
 284 the generalist capability when necessary.
 285

4.3 EXPERT ROUTING

287 With the experts decomposed into sparse components $\hat{\Delta}_\tau$, the next challenge is selecting the correct
 288 expert during inference like the token-level expert routing in MoE (Sukhbaatar et al., 2024a).

289 **Task-level vs. Token-level Routing.** Standard
 290 MoE models use token-level routing. However, finetuned LLMs are trained on complete
 291 sequences $x_{1:T} \sim p_\tau$. Therefore, a subsequence $x_{1:t} \subset x_{1:T}$ might be OOD to the an-
 292 other model θ_τ . Switching experts mid-sentence
 293 (token-level) fragments the semantic context and
 294 degrades performance (theoretical analysis pro-
 295 vided in Appendix D). Therefore, Mediator em-
 296 ploys *Task-level Routing*, selecting experts once
 297 per input sequence. Besides, task-level routing
 298 is more system friendly than token-level rout-
 299 ing because there is no expert reloading during
 300 decoding process.
 301

302 **Handling Compositional Tasks (OOD-II).**
 303 (OOD but close to \mathcal{T} and Ω) A rigid selector
 304 fails on inputs x that do not belong strictly to
 305 a single training task τ (e.g., a query requiring
 306 both coding and reasoning). To handle such OOD samples, we propose **Uncertainty-based Expert**
 307 **Selection.** We treat the selection as a probabilistic merging problem.
 308

309 Specifically, we train a lightweight classifier κ to predict the task likelihood. During inference, we
 310 apply temperature scaling to the logits to estimate the posterior distribution (uncertainty) $h(\tau|x)$:

$$h(\tau|x) = \frac{e^{\pi_\kappa(\tau|x)/\beta}}{\sum_{\tau \in \mathcal{T} \cup \star} e^{\pi_\kappa(\tau|x)/\beta}} \quad (4)$$

311 For clear task inputs, this distribution is sharp (selecting a single $\hat{\Delta}_\tau$). For ambiguous or OOD inputs,
 312 the distribution flattens, effectively computing a weighted average of relevant experts. The final
 313 parameters for the routed layer are constructed dynamically as $\theta_{\text{routed}} = \theta_{\text{base}} + \sum_\tau h(\tau|x) \hat{\Delta}_\tau$. This
 314 process is summarized in Algorithm 2.
 315

4.4 SYSTEM-LEVEL OPTIMIZATION

316 The dynamic construction of θ_{routed} introduces latency due to memory loading. We implement two
 317 system-level optimizations to mitigate this overhead:
 318

319 **Asynchronous Prefetching.** The bottleneck lies in loading sparse experts from CPU/disk to GPU.
 320 We implement asynchronous prefetching: while the GPU computes layer l , the CPU prepares and
 321

324 transfers the sparse experts for layer $l + 1$ (i.e., Algorithm 2). This effectively masks the loading
 325 latency behind the computation time.
 326

327 **Fused Sparse Integration.** To accelerate the summation $\theta + \sum h\hat{\Delta}$, we utilize a custom CUDA
 328 kernel based on atomicAdd. This allows us to parallelize the addition of sparse matrices directly into
 329 the dense backbone without materializing intermediate dense tensors.

330 For non-sparse components stored on disk, we utilize ZipNN (Hershcovitch et al., 2024) for rapid
 331 decompression. As detailed in Appendix G, these optimizations result in an inference latency only
 332 0.2s \sim 0.4s higher than a standard single model, despite the dynamic routing capabilities.
 333

334 5 EXPERIMENTS

335 **Models and Evaluation Tasks.** We conduct comprehensive experiments on cutting-edge LLMs
 336 including Qwen-1.5-4B, Qwen-2.5-7B (Yang et al., 2024c), LLaMA-3.1-3B, and LLaMA-3.2-
 337 8B (Dubey et al., 2024). We select different evaluation tasks to effectively demonstrate model
 338 capability in resolving parameter conflicts during model merging, including GSM8K of mathematical
 339 question-answering (Cobbe et al., 2021), TriviaQA (Joshi et al., 2017) of a large-scale Wikipedia-
 340 based question answering dataset, HumanEval (Chen et al., 2021) of Python programming tasks,
 341 WinoGrande (Sakaguchi et al., 2019) of logical reasoning, MMLU (Hendrycks et al., 2021) of vertical
 342 domain knowledge (as OOD to the finetuned models).
 343

344 **Finetuning Settings.** The finetuning datasets are constructed by augmenting some publicly datasets
 345 (task related but without overlap) with GPT-4o (Gilardi et al., 2023) and Chain-of-Thoughts (Wei
 346 et al., 2022). For each finetuning process, we use at least 180K training samples to ensure sufficient
 347 performance improvement on the corresponding task, which helps validate the effectiveness of our
 348 experiments (Details of constructing finetuning datasets in Appendix H and hyperparameters in
 349 Appendix E). *To the best of our knowledge, this is the first LLM merging study with CoT enhanced
 350 finetuning and evaluated with generative tasks.*

351 **Table 2: Comparing performance of model merging methods on Llama 3.1 3B and Llama-3.2 8B.**

Model	Llama 3.1 3B						Llama-3.2 8B					
	Alg./Tasks	GSM.	TrA.	Wino.	H.Eval	MMLU	AVG.	GSM.	TrA.	Wino.	H.Eval	MMLU
Base	27.52	57.71	69.69	22.56	54.08	46.31	56.33	72.39	73.64	27.44	67.99	59.56
Math	46.47	54.59	69.06	25.00	52.73	49.57	77.18	73.99	74.98	20.12	62.10	61.67
QA	32.75	61.45	69.69	28.05	54.17	49.22	69.60	74.14	75.45	31.71	62.21	62.43
Code	33.13	57.71	68.59	40.85	53.09	50.67	61.41	73.94	74.59	62.80	62.73	67.09
All data	44.12	47.74	69.21	34.76	53.75	49.92	70.89	69.77	75.06	48.17	62.94	65.37
TIES	42.61	60.99	71.11	31.30	54.32	51.27	76.04	76.78	74.19	53.05	62.36	68.48
PCB	46.02	60.39	71.27	29.88	54.21	52.35	76.04	76.89	74.35	53.66	62.42	68.67
Twin	39.04	52.45	69.27	29.94	53.91	48.11	76.80	72.71	74.49	59.14	64.43	69.51
BTX	45.19	62.05	71.87	28.05	54.44	52.33	76.72	73.99	75.22	60.98	65.68	70.52
Mediator	46.47	61.02	72.03	40.42	54.91	54.97	76.95	76.70	75.69	62.80	67.87	71.80

362 **Table 3: Comparing performance of model merging methods on Qwen 1.5 4B and Qwen 2.5 7B.**

Models	Qwen 1.5 4B						Qwen 2.5 7B					
	Alg./Tasks	GSM.	TrA.	Wino.	H.Eval	MMLU	AVG.	GSM.	TrA.	Wino.	H.Eval	MMLU
base	47.16	44.54	56.75	41.46	54.45	48.87	83.41	51.67	67.68	67.68	67.70	67.63
Math	51.00	46.95	54.62	26.83	53.54	46.79	85.14	51.67	65.75	61.59	67.27	66.27
Code	43.29	46.39	54.14	43.29	54.82	48.39	52.31	49.47	64.64	71.95	72.30	62.13
QA	45.56	48.02	57.93	39.02	52.32	48.57	84.62	55.58	62.83	43.29	71.51	63.57
all-sft	48.52	47.73	55.88	39.14	53.93	49.04	64.90	52.98	69.30	65.85	69.66	64.59
TIES	47.76	46.59	54.14	44.51	54.58	49.5	84.76	54.46	66.46	65.85	71.55	68.62
PCB-merging	47.83	47.60	56.75	43.90	54.58	49.93	73.46	53.90	69.53	60.98	71.41	65.86
Twin-merging	47.99	44.63	57.54	40.85	52.98	48.80	83.46	54.64	66.37	69.51	70.56	68.91
BTX	48.44	46.94	57.77	42.68	53.88	49.94	84.46	55.89	67.72	67.68	72.30	69.61
Mediator	50.94	48.20	57.85	45.12	54.87	51.40	85.14	56.06	69.30	71.95	72.56	71.00

374 **Baselines.** We compare pretrained, finetuned models, and the state-of-the-art static and dynamic
 375 merging methods with Mediator. The *static merging methods* include TIES (Yadav et al., 2023b)
 376 and PCB-merging (Du et al., 2024) achieve the best performance in weighted average method
 377 and do not require calibration data, and also partly consider OOD evaluation tasks. The dynamic
 378 merging methods include BTX (Sukhbaatar et al., 2024b) with token-level routing and the twin-merge

378 with task-level routing and SVD decomposition (Lu et al., 2024b) (Details of hyperparameters and
 379 optimization of these baselines in Appendix E).
 380

381 5.1 MAIN RESULTS 382

383 **Fine-grained Comparison on All Tasks.** Table 2 and 3 show the fine-grained performance on each
 384 tasks and their overall averaged one of different methods and algorithms. In most of time, the finetuned
 385 LLM can achieve the best performance across all single and merged models on its specialized domain,
 386 like Math finetuned models on GSM8K and Code finetuned models on HumanEval. While merged
 387 LLMs can generally outperform single models on the averaged performance, their specialized domain
 388 performance is weaker. However, Mediator can catch up the domain performance of specialized
 389 models, and almost always outperform other merged models. Also, the overall performance on all
 390 tasks of Mediator is consistently better than other methods. Expert routing methods includes BTX
 391 and Mediator generally improve performance. This aligns with findings in TIES (Yadav et al., 2023b)
 392 and Twin-merging (Lu et al., 2024a). As model scale increases, the improvement of all merging
 393 algorithms decrease, which may be attributed to enhanced comprehensive capabilities of individual
 394 finetuned models.

395 **Overall Comparison.** As shown in Table 4,
 396 the advantages of PCB over TIES become less
 397 pronounced at larger model scales, and even
 398 shows performance degradation on Qwen-7B,
 399 which demonstrates PCB’s instability. Dynamic
 400 routing approaches include BTX and Mediator
 401 show stable performance improvements. Our
 402 method demonstrates consistent improvements
 403 across different models.

404 **Post-Training Time After Merging.** As many model
 405 merging methods like Twin, PCB and BTX require post-
 406 training, it is critical to compare the extra training time.
 407 Table 5 shows the post-training time of different methods.
 408 PCB merging require weight exploration thus leads to
 409 higher time. The BTX with token-level routing needs to
 410 completely train the layer-wise routers for each token, thus,
 411 the post-training time of them is significantly high. In contrast, for task-level routing approaches like
 412 Twin-merging and Mediator, taking the lowest time.

413 **Inference Time.** Table 6 shows the inference time of different methods. As the token-level routing
 414 methods need to load and compute the layer-wise routers for each token, the inference time of them
 415 is significantly higher (more than 2x) than our method. We have detailed our inference acceleration
 416 process in Section 4.4 and Appendix G.

Table 4: Overall Performance on all tasks.

Model/Algo.	Qwen-4B	Llama-3B	Qwen-7B	Llama-8B
base model	48.87	46.31	67.63	59.56
all data sft	49.04	49.92	64.59	65.37
TIES	49.50	51.27	68.62	68.48
Twin	48.80	48.11	68.91	69.51
PCB	49.93	52.35	65.86	68.67
BTX	49.94	52.33	69.61	70.52
Mediator	51.40 (↑2.9%)	54.97 (↑5.0%)	71.00 (↑2.0%)	71.80 (↑1.8%)

Table 5: Post Training Time (Hours).

Model/Algo	LlaMA-3B	LlaMA-8B	Qwen-4B	Qwen-7B
Twin	1.33	1.87	1.60	1.80
PCB	3.42	5.75	5.73	5.80
BTX	7.55	12.52	8.83	12.18
Mediator	1.35	2.03	1.57	1.78

Table 6: Inference time per sample (seconds).

Model/Algo	LlaMA-3B 32 layers	LlaMA-8B 32 layers	Qwen-4B 40 layers	Qwen-7B 28 layers
Base model	1.452	3.600	3.112	3.057
Twin	1.725	4.151	3.792	3.648
BTX	3.237	8.68	7.082	7.153
Mediator	1.609	4.053	3.674	3.489

Table 7: Comparing memory costs.

Model/Algo	LLaMA-3B	LLaMA-8B	Qwen-4B	Qwen-7B
Base model	9G	33G	11G	31G
Twin-merging	10G	35G	13G	32G
BTX (MOE)	37G	80G	40G	78G
Mediator	10G	35G	13G	33G

422 **Memory Cost.** Table 7 shows the memory costs of different methods. Our method significantly
 423 reduces the memory costs compared to saving all finetuned models because there is only one router
 424 for all experts, and the sparsified experts saving, and the layer-wise merging strategy (Details of
 425 formally comparing memory costs of merging methods in Appendix C).

426 5.2 ABLATION STUDIES 427

428 **Scalability of Finetuned Models.** To verify the scalability of Mediator, we finetune another 4
 429 LLMs according to the following 4 extra evaluation tasks including: (1) *Instruction Following*
 430 with IFEval. (Zhou et al., 2023) which assess models ability to accurately interpret and execute
 431 natural language instructions; (2-4) *Medicine, College Economics and Law* from CEval which assess

knowledge and capabilities across various academic and professional domains (Huang et al., 2023a). We utilize four accordingly domain datasets for finetuning including Magpie (Xu et al., 2024), IndustryInstruction (Ind), DISC-Med (Bao et al., 2023), DISC-Law (Yue et al., 2023a) without overlap with IFEval and CEval (Details in Appendix H).

Table 8 demonstrates several key findings: 1) Static merging methods like PCB and TIES show diminished performance improvements after task expansion, performing even worse than instruction-following finetuned models in overall scores. The similar performance between PCB merging and TIES aligns with findings from the TIES paper, which noted degraded model capabilities when merging more than three tasks; 2) Dynamic merging approaches like BTX, Twin and Mediator maintain relatively stable performance after task expansion; 3) Mediator consistently outperforms BTX by a margin of 2.09% and achieves the best scores across all individual tasks, showing its good scalability.

Layer-wise Merging. Layers with low conflicts are averaged thus reducing $n_\tau \times$ memory occupation. Table 9 averaging or not on Qwen-1.5 with 4 and 8 experts show almost no performance loss of the parameter averaging. Given the significant compression ratios achieved (3.5x for 4 experts, 7x for 8 experts), this minor performance trade-off is acceptable.

Comparison between Task-level routing and Token-level routing. Fig. 7 in Appendix demonstrates the expert selection probabilities of the BTX model across different tasks (MMLU, math, coding, and QA). The results indicate that 1) bottom and upper layers show obvious task preference; 2) middle layers suggesting some shared logical processing across tasks in these layers, which explains why averaging middle layers that have less conflicts in Mediator results in small performance loss.

Different Temperatures. In the routing process, the hyperparameter temperature β is a key factor. Table 10 shows performance change of Mediator with different temperatures. Results show that only around 2.2% score variation, the $\beta = 1.5$ achieves the highest performance, $\beta = 0.1$ almost equals to the Top-1 routing, results in the lowest performance.

Table 8: Performance of scaling up finetuned models.

Alg./Tasks	GSM.	TrA.	Wino.	H.Eval	MMLU	I.Eval	C.Eco	C.Med	C.law	Avg.
Base	47.16	44.54	56.75	41.46	54.45	30.70	49.09	55.10	41.67	46.77
Math	50.95	46.95	54.62	26.83	53.54	34.05	45.45	55.10	45.83	45.92
QA	45.56	48.02	57.93	39.02	52.32	31.65	43.64	59.18	45.83	47.02
code	43.29	46.39	54.14	43.29	54.82	31.65	43.64	59.18	45.83	46.91
Instruct.	47.54	40.96	55.09	37.80	54.88	38.37	52.73	59.18	50.00	48.51
Economy	45.56	46.24	57.93	28.86	54.21	32.13	56.36	55.10	45.83	46.78
medicine	39.12	44.50	56.67	1.83	54.63	28.30	50.09	61.22	41.66	42.00
Law	40.64	46.64	56.59	0.61	54.61	27.94	41.82	57.14	58.33	47.15
All Data	43.75	46.25	56.43	40.85	54.60	35.37	49.09	55.10	41.67	46.90
TIES	47.38	47.19	55.80	36.59	55.38	34.17	40.00	57.14	50.00	47.07
PCB	47.38	47.19	55.80	36.59	55.45	34.29	41.82	57.14	50.80	47.38
Twin	47.91	44.78	57.54	40.85	53.01	37.53	53.32	59.56	50.00	49.38
BTX	48.44	46.94	57.85	42.68	54.93	36.93	54.40	60.36	58.33	51.18
Mediator	50.64	48.04	57.93	44.51	55.12	38.50	56.01	61.17	58.33	52.25

Table 9: Model Performance w/o layer-wise merging.

Model scale	with averaging	w/o averaging	perf. gap
Qwen-1.5	51.40	51.43	-0.06%
Qwen-2.5	71.00	71.29	-0.27%

Table 10: Performance under Different Temperature β .

Temperature	0.1	0.5	1.0	1.25	1.50	1.75	2.0
Mediator	50.31	50.35	50.64	51.02	51.40	50.84	50.92

6 CONCLUSION

We propose Mediator, a framework for merging LLMs that addresses parameter conflicts through adaptive layer-wise strategies, which average low-conflict layers and routing high-conflict ones via task-specific experts. This preserves individual model strengths while integrating shared knowledge, improving performance and reducing system costs.

By decomposing experts into a dense core and sparse components, Mediator minimizes storage without sacrificing efficacy. Dynamic expert selection via task uncertainty enhances adaptability across diverse inputs. Experiments on LLaMA and Qwen demonstrate significant performance gains over existing methods, with CoT enhanced datasets further enhancing reasoning capabilities.

Mediator advances efficient LLM merging methods, balancing resource constraints with practical versatility. Future work should explore theoretical foundations of parameter conflicts, large-scale deployment optimizations, and faster expert loading mechanisms.

486 ETHICS STATEMENT
487488 We declare no conflicts of interest that could inappropriately influence our work. All experiments
489 were conducted using publicly available resources. Our study does not involve human subjects, data
490 collection from individuals, or experiments on protected groups. The models and basic datasets used
491 in this work are publicly available and widely used in the research community. We have made efforts
492 to ensure our experimental design and reporting of results are fair, unbiased, and do not misrepresent
493 the capabilities or limitations of the methods presented.
494495 REPRODUCIBILITY STATEMENT
496497 For openness of LLM research, we declare our code and the CoT enhanced crafted finetuning
498 datasets will be made available to ensure reproducibility. We will provide detailed documents of code
499 implemnetation. And we have provided the details of all hyper-parameters of implementing Mediator
500 and optimizing baselines.
501502 REFERENCES
503504 Xiaofei Sun, Xiaoya Li, Shengyu Zhang, Shuhe Wang, Fei Wu, Jiwei Li, Tianwei Zhang, and Guoyin
505 Wang. Sentiment analysis through llm negotiations, 2023. URL <https://arxiv.org/abs/2311.01876>.
506507 Jiangnan Fang, Cheng-Tse Liu, Jieun Kim, Yash Bhedaru, Ethan Liu, Nikhil Singh, Nedim Lipka,
508 Puneet Mathur, Nesreen K. Ahmed, Franck Dernoncourt, Ryan A. Rossi, and Hanieh Deilamsalehy.
509 Multi-llm text summarization, 2024. URL <https://arxiv.org/abs/2412.15487>.
510511 Laura Ruis, Maximilian Mozes, Juhan Bae, Siddhartha Rao Kamalakara, Dwarak Talupuru, Acyr
512 Locatelli, Robert Kirk, Tim Rocktäschel, Edward Grefenstette, and Max Bartolo. Procedural
513 knowledge in pretraining drives reasoning in large language models, 2024. URL <https://arxiv.org/abs/2411.12580>.
514515 Juyong Jiang, Fan Wang, Jiasi Shen, Sungju Kim, and Sunghun Kim. A survey on large language
516 models for code generation, 2024a. URL <https://arxiv.org/abs/2406.00515>.
517518 Nuo Chen, Yan Wang, Yang Deng, and Jia Li. The oscars of ai theater: A survey on role-playing
519 with language models, 2025. URL <https://arxiv.org/abs/2407.11484>.
520521 Thomas Wolf, Lysandre Debut, Victor Sanh, Julien Chaumond, Clement Delangue, Anthony Moi,
522 Pierrick Cistac, Tim Rault, Rémi Louf, Morgan Funtowicz, et al. Huggingface’s transformers:
523 State-of-the-art natural language processing. *arXiv preprint arXiv:1910.03771*, 2019.524 Jovan Stojkovic, Esha Choukse, Chaojie Zhang, Inigo Goiri, and Josep Torrellas. Towards greener
525 llms: Bringing energy-efficiency to the forefront of llm inference, 2024. URL <https://arxiv.org/abs/2403.20306>.
526527 Enneng Yang, Li Shen, Guibing Guo, Xingwei Wang, Xiaochun Cao, Jie Zhang, and Dacheng Tao.
528 Model merging in llms, mllms, and beyond: Methods, theories, applications and opportunities.
529 *arXiv preprint arXiv:2408.07666*, 2024a.
530531 DK Thennal, Ganesh Nathan, and MS Suchithra. Fisher mask nodes for language model merging. In
532 *LREC-COLING*, pages 7349–7355, 2024.
533534 Zhenyi Lu, Chenghao Fan, Wei Wei, Xiaoye Qu, Dangyang Chen, and Yu Cheng. Twin-merging:
535 Dynamic integration of modular expertise in model merging. *arXiv preprint arXiv:2406.15479*,
536 2024a.
537538 Ethan He, Abhinav Khattar, Ryan Prenger, Vijay Korthikanti, Zijie Yan, Tong Liu, Shiqing Fan,
539 Ashwath Aithal, Mohammad Shoeybi, and Bryan Catanzaro. Upcycling large language models
into mixture of experts. 10 2024a. URL <https://arxiv.org/pdf/2410.07524.pdf>.
540

540 Tianwen Wei, Bo Zhu, Liang Zhao, Cheng Cheng, Biye Li, Weiwei Lü, Peng Cheng, Jianhao Zhang,
 541 Xiaoyu Zhang, Liang Zeng, Xiaokun Wang, Yutuan Ma, Rui Hu, Shuicheng Yan, Han Fang, and
 542 Yahui Zhou. Skywork-moe: A deep dive into training techniques for mixture-of-experts language
 543 models. 06 2024a. URL <https://arxiv.org/pdf/2406.06563.pdf>.

544 Yifei He, Yuzheng Hu, Yong Lin, Tong Zhang, and Han Zhao. Localize-and-stitch: Efficient model
 545 merging via sparse task arithmetic. *arXiv preprint arXiv:2408.13656*, 2024b.

546 Prateek Yadav, Derek Tam, Leshem Choshen, Colin Raffel, and Mohit Bansal. Ties-merging:
 547 Resolving interference when merging models. 06 2023a. URL <https://arxiv.org/pdf/2306.01708.pdf>.

548 Gabriel Ilharco, Marco Tulio Ribeiro, Mitchell Wortsman, Ludwig Schmidt, Hannaneh Hajishirzi,
 549 and Ali Farhadi. Editing models with task arithmetic. In *ICLR*, 2023.

550 Anke Tang, Li Shen, Yong Luo, Nan Yin, Lefei Zhang, and Dacheng Tao. Merging multi-task models
 551 via weight-ensembling mixture of experts. *ICML*, 02 2024a. URL <https://arxiv.org/pdf/2402.00433.pdf>.

552 Sainbayar Sukhbaatar, Olga Golovneva, Vasu Sharma, Hu Xu, Xi Victoria Lin, Baptiste Rozière,
 553 Jacob Kahn, Daniel Li, Wen tau Yih, Jason Weston, and Xian Li. Branch-train-mix: Mixing
 554 expert llms into a mixture-of-experts llm. 03 2024a. URL <https://arxiv.org/pdf/2403.07816.pdf>.

555 Albert Q. Jiang, Alexandre Sablayrolles, Antoine Roux, Arthur Mensch, Blanche Savary, Chris
 556 Bamford, Devendra Singh Chaplot, Diego de las Casas, Emma Bou Hanna, Florian Bressand,
 557 Gianna Lengyel, Guillaume Bour, Guillaume Lample, Lélio Renard Lavaud, Lucile Saulnier, Marie-
 558 Anne Lachaux, Pierre Stock, Sandeep Subramanian, Sophia Yang, Szymon Antoniak, Teven Le
 559 Scao, Théophile Gervet, Thibaut Lavril, Thomas Wang, Timothée Lacroix, and William El Sayed.
 560 Mixtral of experts. 01 2024b. URL <https://arxiv.org/pdf/2401.04088.pdf>.

561 Jason Wei, Xuezhi Wang, Dale Schuurmans, Maarten Bosma, Fei Xia, Ed Chi, Quoc V Le, Denny
 562 Zhou, et al. Chain-of-thought prompting elicits reasoning in large language models. *Advances in
 563 neural information processing systems*, 35:24824–24837, 2022.

564 Daya Guo, Dejian Yang, Haowei Zhang, Junxiao Song, Ruoyu Zhang, Runxin Xu, Qihao Zhu,
 565 Shirong Ma, Peiyi Wang, Xiao Bi, et al. Deepseek-r1: Incentivizing reasoning capability in llms
 566 via reinforcement learning. *arXiv preprint arXiv:2501.12948*, 2025.

567 Sang Michael Xie, Aditi Raghunathan, Percy Liang, and Tengyu Ma. An explanation of in-context
 568 learning as implicit Bayesian inference. In *International Conference on Learning Representations*,
 569 2022.

570 Noam Wies, Yoav Levine, and Amnon Shashua. The learnability of in-context learning. In *Thirty-
 571 seventh Conference on Neural Information Processing Systems*, 2023.

572 Michael Hahn and Navin Goyal. A theory of emergent in-context learning as implicit structure
 573 induction. *arxiv*, arXiv:2303.07971, 2023. URL <https://arxiv.org/abs/2303.07971>.

574 Jiaoda Li, Yifan Hou, Mrinmaya Sachan, and Ryan Cotterell. What do language models learn in
 575 context? the structured task hypothesis. *arXiv preprint arXiv:2406.04216*, 2024a.

576 Tom Brown, Benjamin Mann, Nick Ryder, Melanie Subbiah, Jared D Kaplan, Prafulla Dhariwal,
 577 Arvind Neelakantan, Pranav Shyam, Girish Sastry, Amanda Askell, et al. Language models are
 578 few-shot learners. *NeurIPS*, 33:1877–1901, 2020.

579 Hugo Touvron, Louis Martin, Kevin Stone, Peter Albert, Amjad Almahairi, Yasmine Babaei, Nikolay
 580 Bashlykov, Soumya Batra, Prajjwal Bhargava, Shruti Bhosale, et al. Llama 2: Open foundation
 581 and fine-tuned chat models. *arXiv preprint arXiv:2307.09288*, 2023.

582 James Kirkpatrick, Razvan Pascanu, Neil Rabinowitz, Joel Veness, Guillaume Desjardins, Andrei A
 583 Rusu, Kieran Milan, John Quan, Tiago Ramalho, Agnieszka Grabska-Barwinska, et al. Overcoming
 584 catastrophic forgetting in neural networks. *Proceedings of the national academy of sciences*, 114
 585 (13):3521–3526, 2017.

594 Mingjie Sun, Zhuang Liu, Anna Bair, and J Zico Kolter. A simple and effective pruning approach
 595 for large language models. In *The Twelfth International Conference on Learning Representations*,
 596 2024. URL <https://openreview.net/forum?id=PxoFut3dWW>.

597

598 Peijie Dong, Lujun Li, Zhenheng Tang, Xiang Liu, Xinglin Pan, Qiang Wang, and Xiaowen Chu.
 599 Pruner-zero: Evolving symbolic pruning metric from scratch for large language models. In
 600 *Forty-first International Conference on Machine Learning*.

601

602 Namhoon Lee, Thalaiyasingam Ajanthan, and Philip Torr. SNIP: SINGLE-SHOT NETWORK
 603 PRUNING BASED ON CONNECTION SENSITIVITY. In *International Conference on Learning
 604 Representations*, 2019. URL <https://openreview.net/forum?id=B1VZqjAcYX>.

605 Michael S Matena and Colin A Raffel. Merging models with fisher-weighted averaging. *NeurIPS*,
 606 35:17703–17716, 2022.

607

608 Enneng Yang, Zhenyi Wang, Li Shen, Shiwei Liu, Guibing Guo, Xingwei Wang, and Dacheng
 609 Tao. Adamerging: Adaptive model merging for multi-task learning. *ICLR*, 10 2024b. URL
 610 <https://arxiv.org/pdf/2310.02575.pdf>.

611 Anke Tang, Li Shen, Yong Luo, Nan Yin, Lefei Zhang, and Dacheng Tao. Merging multi-task models
 612 via weight-ensembling mixture of experts. *ICML*, 2024b.

613

614 Sainbayar Sukhbaatar, Olga Golovneva, Vasu Sharma, Hu Xu, Xi Victoria Lin, Baptiste Roziere,
 615 Jacob Kahn, Shang-Wen Li, Wen tau Yih, Jason E Weston, and Xian Li. Branch-train-mix: Mixing
 616 expert LLMs into a mixture-of-experts LLM. In *First Conference on Language Modeling*, 2024b.
 617 URL <https://openreview.net/forum?id=nqLAuMOF6n>.

618 Moshik Herscovitch, Andrew Wood, Leshem Choshen, Guy Girmionsky, Roy Leibovitz, Ilias
 619 Ennmouri, Michal Malka, Peter Chin, Swaminathan Sundararaman, and Danny Harnik. Zipnn:
 620 Lossless compression for ai models. *arXiv preprint arXiv:2411.05239*, 2024.

621

622 An Yang, Baosong Yang, Beichen Zhang, Binyuan Hui, Bo Zheng, Bowen Yu, Chengyuan Li,
 623 Dayiheng Liu, Fei Huang, Haoran Wei, et al. Qwen2. 5 technical report. *arXiv preprint
 624 arXiv:2412.15115*, 2024c.

625

626 Abhimanyu Dubey, Abhinav Jauhri, Abhinav Pandey, Abhishek Kadian, Ahmad Al-Dahle, Aiesha
 627 Letman, Akhil Mathur, Alan Schelten, Amy Yang, Angela Fan, et al. The llama 3 herd of models.
 628 *arXiv preprint arXiv:2407.21783*, 2024.

629

630 Karl Cobbe, Vineet Kosaraju, Mohammad Bavarian, Mark Chen, Heewoo Jun, Lukasz Kaiser,
 631 Matthias Plappert, Jerry Tworek, Jacob Hilton, Reiichiro Nakano, Christopher Hesse, and John
 632 Schulman. Training verifiers to solve math word problems, 2021. URL <https://arxiv.org/abs/2110.14168>.

633

634 Mandar Joshi, Eunsol Choi, Daniel S. Weld, and Luke Zettlemoyer. Triviaqa: A large scale distantly
 635 supervised challenge dataset for reading comprehension, 2017. URL <https://arxiv.org/abs/1705.03551>.

636

637 Mark Chen, Jerry Tworek, Heewoo Jun, Qiming Yuan, and etc. Evaluating large language models
 638 trained on code, 2021. URL <https://arxiv.org/abs/2107.03374>.

639

640 Keisuke Sakaguchi, Ronan Le Bras, Chandra Bhagavatula, and Yejin Choi. Winogrande: An
 641 adversarial winograd schema challenge at scale, 2019. URL <https://arxiv.org/abs/1907.10641>.

642

643 Dan Hendrycks, Collin Burns, Steven Basart, Andy Zou, Mantas Mazeika, Dawn Song, and Jacob
 644 Steinhardt. Measuring massive multitask language understanding, 2021. URL <https://arxiv.org/abs/2009.03300>.

645

646 Fabrizio Gilardi, Meysam Alizadeh, and Maël Kubli. Chatgpt outperforms crowd workers for
 647 text-annotation tasks. *Proceedings of the National Academy of Sciences*, 120(30):e2305016120,
 2023.

648 Prateek Yadav, Derek Tam, Leshem Choshen, Colin Raffel, and Mohit Bansal. Resolving interference
 649 when merging models. *NeurIPS*, 2023b.

650

651 Guodong Du, Junlin Lee, Jing Li, Runhua Jiang, Yifei Guo, Shuyang Yu, Hanting Liu, Sim Kuan
 652 Goh, Ho-Kin Tang, Daojing He, and Min Zhang. Parameter competition balancing for model
 653 merging. *NIIPS*, 10 2024. URL <https://arxiv.org/pdf/2410.02396.pdf>.

654

655 Zhenyi Lu, Chenghao Fan, Wei Wei, Xiaoye Qu, Dangyang Chen, and Yu Cheng. Twin-merging:
 656 Dynamic integration of modular expertise in model merging. *NIPS*, 06 2024b. URL <https://arxiv.org/pdf/2406.15479v2.pdf>.

657

658 Jeffrey Zhou, Tianjian Lu, Swaroop Mishra, Siddhartha Brahma, Sujoy Basu, Yi Luan, Denny
 659 Zhou, and Le Hou. Instruction-following evaluation for large language models, 2023. URL
 660 <https://arxiv.org/abs/2311.07911>.

661

662 Yuzhen Huang, Yuzhuo Bai, Zhihao Zhu, Junlei Zhang, Jinghan Zhang, Tangjun Su, Junteng
 663 Liu, Chuancheng Lv, Yikai Zhang, Jiayi Lei, Yao Fu, Maosong Sun, and Junxian He. C-eval:
 664 A multi-level multi-discipline chinese evaluation suite for foundation models, 2023a. URL
 665 <https://arxiv.org/abs/2305.08322>.

666

667 Zhangchen Xu, Fengqing Jiang, Luyao Niu, Yuntian Deng, Radha Poovendran, Yejin Choi, and
 668 Bill Yuchen Lin. Magpie: Alignment data synthesis from scratch by prompting aligned llms with
 669 nothing. *arXiv preprint arXiv:2406.08464*, 2024.

670

671 BaaI/industryinstruction - finance - economics. URL https://huggingface.co/datasets/BAAI/IndustryInstruction_Finance-Economics.

672

673 Zhijie Bao, Wei Chen, Shengze Xiao, Kuang Ren, Jiaao Wu, Cheng Zhong, Jiajie Peng, Xuanjing
 674 Huang, and Zhongyu Wei. Disc-MedLLM: Bridging General Large Language Models and Real-
 675 World Medical Consultation. *arXiv*, abs/2308.14346, 2023.

676

677 Shengbin Yue, Wei Chen, Siyuan Wang, Bingxuan Li, Chenchen Shen, Shujun Liu, Yuxuan Zhou,
 678 Yao Xiao, Song Yun, Xuanjing Huang, and Zhongyu Wei. Disc-LawLLM: Fine-tuning Large
 679 Language Models for Intelligent Legal Services. *arXiv*, abs/2309.11325, 2023a.

680

681 Yuanchun Li, Hao Wen, Weijun Wang, Xiangyu Li, Yizhen Yuan, Guohong Liu, Jiacheng Liu,
 682 Wenxing Xu, Xiang Wang, Yi Sun, Rui Kong, Yile Wang, Hanfei Geng, Jian Luan, Xuefeng Jin,
 683 Zilong Ye, Guanjing Xiong, Fan Zhang, Xiang Li, Mengwei Xu, Zhijun Li, Peng Li, Yang Liu,
 684 Ya-Qin Zhang, and Yunxin Liu. Personal llm agents: Insights and survey about the capability,
 685 efficiency and security, 2024b. URL <https://arxiv.org/abs/2401.05459>.

686

687 Xin Chan, Xiaoyang Wang, Dian Yu, Haitao Mi, and Dong Yu. Scaling synthetic data creation with
 688 1,000,000,000 personas. *arXiv preprint arXiv:2406.20094*, 2024.

689

690 Le Yu, Bowen Yu, Haiyang Yu, Fei Huang, and Yongbin Li. Extend model merging from fine-tuned to
 691 pre-trained large language models via weight disentanglement. *arXiv preprint arXiv:2408.03092*,
 692 2024a.

693

694 Carlos Gómez-Rodríguez and Paul Williams. A confederacy of models: a comprehensive evaluation
 695 of llms on creative writing, 2023. URL <https://arxiv.org/abs/2310.08433>.

696

697 Joachim Utans. Weight averaging for neural networks and local resampling schemes. In *AAAI*
 698 *Workshop*, pages 133–138. Citeseer, 1996.

699

700 Ken Shoemake. Animating rotation with quaternion curves. In *Proceedings of the 12th annual*
 701 *conference on Computer graphics and interactive techniques*, pages 245–254, 1985.

702

703 Brendan McMahan, Eider Moore, Daniel Ramage, Seth Hampson, and Blaise Aguera y Arcas.
 704 Communication-efficient learning of deep networks from decentralized data. In *AISTATS*, pages
 705 1273–1282. PMLR, 2017.

706

707 Zhenheng Tang, Shaohuai Shi, Xiaowen Chu, Wei Wang, and Bo Li. Communication-efficient
 708 distributed deep learning: A comprehensive survey. *arXiv preprint arXiv:2003.06307*, 2020.

702 Jianyu Wang, Qinghua Liu, Hao Liang, Gauri Joshi, and H Vincent Poor. Tackling the objective
 703 inconsistency problem in heterogeneous federated optimization. *NeurIPS*, 33:7611–7623, 2020a.
 704

705 Divyansh Jhunjhunwala, Shiqiang Wang, and Gauri Joshi. Fedfisher: Leveraging fisher information
 706 for one-shot federated learning. In *AISTATS*, pages 1612–1620. PMLR, 2024a.

707 Mikhail Yurochkin, Mayank Agarwal, Soumya Ghosh, Kristjan Greenewald, Nghia Hoang, and
 708 Yasaman Khazaeni. Bayesian nonparametric federated learning of neural networks. In *ICML*,
 709 pages 7252–7261. PMLR, 2019a.

710

711 Sidak Pal Singh and Martin Jaggi. Model fusion via optimal transport. *NeurIPS*, 33:22045–22055,
 712 2020.

713 Hongyi Wang, Mikhail Yurochkin, Yuekai Sun, Dimitris Papailiopoulos, and Yasaman Khazaeni.
 714 Federated learning with matched averaging. In *ICLR*, 2020b.

715

716 Zhenheng Tang, Yonggang Zhang, Shaohuai Shi, Xinmei Tian, Tongliang Liu, Bo Han, and Xiaowen
 717 Chu. Fedimpro: Measuring and improving client update in federated learning. In *The Twelfth
 718 International Conference on Learning Representations*, 2024c. URL <https://openreview.net/forum?id=giU9fYGTND>.

719

720 Zhenheng Tang, Yonggang Zhang, Shaohuai Shi, Xin He, Bo Han, and Xiaowen Chu. Virtual
 721 homogeneity learning: Defending against data heterogeneity in federated learning. In *Proceedings
 722 of the 39th International Conference on Machine Learning*, volume 162 of *Proceedings of Machine
 723 Learning Research*, pages 21111–21132. PMLR, 17–23 Jul 2022.

724

725 Neel Guha, Ameet Talwalkar, and Virginia Smith. One-shot federated learning. *arXiv preprint
 726 arXiv:1902.11175*, 2019.

727

728 Zhenheng Tang, Yonggang Zhang, Peijie Dong, Yiu ming Cheung, Amelie Chi Zhou, Bo Han, and
 729 Xiaowen Chu. Fusefl: One-shot federated learning through the lens of causality with progressive
 730 model fusion. In *The Thirty-eighth Annual Conference on Neural Information Processing Systems*,
 731 2024d. URL <https://openreview.net/forum?id=E7fZ0oIEk1>.

732

733 Peijie Dong, Lujun Li, Yuedong Zhong, Dayou Du, Ruibo Fan, Yuhang Chen, Zhenheng Tang, Qiang
 734 Wang, Wei Xue, Yike Guo, and Xiaowen Chu. Stbllm: Breaking the 1-bit barrier with structured
 735 binary llms, 2024. URL <https://arxiv.org/abs/2408.01803>.

736

737 Anthony Robins. Catastrophic forgetting, rehearsal and pseudorehearsal. *Connection Science*, 1995.

738

739 Didi Zhu, Zhongyi Sun, Zexi Li, Tao Shen, Ke Yan, Shouhong Ding, Kun Kuang, and Chao Wu.
 740 Model tailor: Mitigating catastrophic forgetting in multi-modal large language models. *ICML*,
 741 2024.

742

743 Daniel Marczak, Bartłomiej Twardowski, Tomasz Trzciński, and Sebastian Cygert. Magmax: Lever-
 744 aging model merging for seamless continual learning. In *ECCV*, 2024.

745

746 Divyansh Jhunjhunwala, Shiqiang Wang, and Gauri Joshi. Towards a theoretical and practical
 747 understanding of one-shot federated learning with fisher information. In *Federated Learning and
 748 Analytics in Practice: Algorithms, Systems, Applications, and Opportunities*, 2023.

749

750 Zhe Qu, Xingyu Li, Rui Duan, Yao Liu, Bo Tang, and Zhuo Lu. Generalized federated learning
 751 via sharpness aware minimization. In *International Conference on Machine Learning*, pages
 752 18250–18280. PMLR, 2022.

753

754 Yuyan Zhou, Liang Song, Bingning Wang, and Weipeng Chen. Metagpt: Merging large language
 755 models using model exclusive task arithmetic. *arXiv preprint arXiv:2406.11385*, 2024.

756

757 Divyansh Jhunjhunwala, Neharika Jali, Gauri Joshi, and Shiqiang Wang. Erasure coded neural
 758 network inference via fisher averaging. In *ISIT*, pages 13–18. IEEE, 2024b.

759

760 Nico Daheim, Thomas Möllenhoff, Edoardo Ponti, Iryna Gurevych, and Mohammad Emtiyaz Khan.
 761 Model merging by uncertainty-based gradient matching. In *ICLR*, 2024.

756 Yang He and Lingao Xiao. Structured pruning for deep convolutional neural networks: A survey.
 757 *TPAMI*, 2023.

758 Tejalal Choudhary, Vipul Mishra, Anurag Goswami, and Jagannathan Sarangapani. A comprehensive
 759 survey on model compression and acceleration. *Artificial Intelligence Review*, 53:5113–5155,
 760 2020.

761 Pala Tej Deep, Rishabh Bhardwaj, and Soujanya Poria. Della-merging: Reducing interference in
 762 model merging through magnitude-based sampling. *arXiv preprint arXiv:2406.11617*, 2024.

763 Le Yu, Bowen Yu, Haiyang Yu, Fei Huang, and Yongbin Li. Language models are super mario:
 764 Absorbing abilities from homologous models as a free lunch. *ICML*, 11 2024b. URL <https://arxiv.org/pdf/2311.03099.pdf>.

765 Le Yu, Bowen Yu, Haiyang Yu, Fei Huang, and Yongbin Li. Language models are super mario:
 766 Absorbing abilities from homologous models as a free lunch. *ICML*, 2024c.

767 MohammadReza Davari and Eugene Belilovsky. Model breadcrumbs: Scaling multi-task model
 768 merging with sparse masks. *arXiv preprint arXiv:2312.06795*, 2023.

769 Ke Wang, Nikolaos Dimitriadis, Guillermo Ortiz-Jimenez, François Fleuret, and Pascal Frossard.
 770 Localizing task information for improved model merging and compression. *ICML*, 2024.

771 Fanshuang Kong, Richong Zhang, and Ziqiao Wang. Activated parameter locating via causal
 772 intervention for model merging. *arXiv preprint arXiv:2408.09485*, 2024.

773 Chenyu Huang, Peng Ye, Tao Chen, Tong He, Xiangyu Yue, and Wanli Ouyang. Emr-merging:
 774 Tuning-free high-performance model merging. *arXiv preprint arXiv:2405.17461*, 2024.

775 Anke Tang, Li Shen, Yong Luo, Liang Ding, Han Hu, Bo Du, and Dacheng Tao. Concrete
 776 subspace learning based interference elimination for multi-task model fusion. *arXiv preprint*
 777 *arXiv:2312.06173*, 2023.

778 Gabriel Ilharco, Marco Tulio Ribeiro, Mitchell Wortsman, Suchin Gururangan, Ludwig Schmidt,
 779 Hannaneh Hajishirzi, and Ali Farhadi. Editing models with task arithmetic. 12 2022. URL
 780 <https://arxiv.org/pdf/2212.04089.pdf>.

781 Donato Crisostomi, Marco Fumero, Daniele Baieri, Florian Bernard, and Emanuele Rodolà. Cycle-
 782 consistent multi-model merging. 05 2024. URL <https://arxiv.org/pdf/2405.17897.pdf>.

783 Pingzhi Li, Zhenyu Zhang, Prateek Yadav, Yi-Lin Sung, Yu Cheng, Mohit Bansal, and Tianlong Chen.
 784 Merge, then compress: Demystify efficient smoe with hints from its routing policy. *ICLR*, 2024c.

785 Mohammed Muqeeth, Haokun Liu, and Colin Raffel. Soft merging of experts with adaptive routing.
 786 *TMLR*, 2024.

787 Junmo Kang, Leonid Karlinsky, Hongyin Luo, Zhen Wang, Jacob Hansen, James Glass, David Cox,
 788 Rameswar Panda, Rogerio Feris, and Alan Ritter. Self-moe: Towards compositional large language
 789 models with self-specialized experts. *arXiv preprint arXiv:2406.12034*, 2024.

790 Lei Shen, Zhenheng Tang, Lijun Wu, Yonggang Zhang, Xiaowen Chu, Tao Qin, and Bo Han. Hot
 791 pluggable federated learning. In *International Workshop on Federated Foundation Models in*
 792 *Conjunction with NeurIPS 2024*, 2024. URL <https://openreview.net/forum?id=FazIrAXoM6>.

793 Anke Tang, Li Shen, Yong Luo, Shiwei Liu, Han Hu, and Bo Du. Towards efficient pareto set
 794 approximation via mixture of experts based model fusion. *arXiv preprint arXiv:2406.09770*,
 2024e.

795 R. A. Jacobs, M. I. Jordan, S. J. Nowlan, and G. E. Hinton. Adaptive mixtures of local experts.
 796 *Neural computation*, 3(1):79–87, 1991.

797 M. I. Jordan and R. A. Jacobs. Hierarchical mixtures of experts and the em algorithm. *Neural*
 798 *computation*, 6(2):181–214, 1994.

810 Noam Shazeer, Azalia Mirhoseini, Krzysztof Maziarz, Andy Davis, Quoc Le, Geoffrey Hinton, and
 811 Jeff Dean. Outrageously large neural networks: The sparsely-gated mixture-of-experts layer. 01
 812 2017. URL <https://arxiv.org/pdf/1701.06538.pdf>.

813

814 Dmitry Lepikhin, HyoukJoong Lee, Yuanzhong Xu, Dehao Chen, Orhan Firat, Yanping Huang,
 815 Maxim Krikun, Noam Shazeer, and Zhifeng Chen. Gshard: Scaling giant models with conditional
 816 computation and automatic sharding. 06 2020. URL <https://arxiv.org/pdf/2006.16668.pdf>.

817

818 Yanqi Zhou, Tao Lei, Hanxiao Liu, Nan Du, Yanping Huang, Vincent Zhao, Andrew Dai, Zhifeng
 819 Chen, Quoc Le, and James Laudon. Mixture-of-experts with expert choice routing. 02 2022. URL
 820 <https://arxiv.org/pdf/2202.09368.pdf>.

821

822 Damai Dai, Chengqi Deng, Chenggang Zhao, R. X. Xu, Huazuo Gao, Deli Chen, Jiashi Li, Wangding
 823 Zeng, Xingkai Yu, Y. Wu, Zhenda Xie, Y. K. Li, Panpan Huang, Fuli Luo, Chong Ruan, Zhifang Sui,
 824 and Wenfeng Liang. Deepseekmoe: Towards ultimate expert specialization in mixture-of-experts
 825 language models. 01 2024. URL <https://arxiv.org/pdf/2401.06066.pdf>.

826

827 Zewen Chi, Li Dong, Shaohan Huang, Damai Dai, Shuming Ma, Barun Patra, Saksham Singhal, Payal
 828 Bajaj, Xia Song, Xian-Ling Mao, Heyan Huang, and Furu Wei. On the representation collapse of
 829 sparse mixture of experts. 04 2022. URL <https://arxiv.org/pdf/2204.09179.pdf>.

830

831 Jianan Chen, Qin Hu, Fangtian Zhong, Yan Zhuang, and Minghui Xu. Upcycling noise for federated
 832 unlearning. 12 2024. URL <https://arxiv.org/pdf/2412.05529.pdf>.

833

834 Anonymous. Drop-upcycling: Training sparse mixture of experts with partial re-initialization. In
 835 *Submitted to The Thirteenth International Conference on Learning Representations*, 2024. URL
 836 <https://openreview.net/forum?id=gx1wHnf5Vp>. under review.

837

838 Margaret Li, Suchin Gururangan, Tim Dettmers, Mike Lewis, Tim Althoff, Noah A Smith, and Luke
 839 Zettlemoyer. Branch-train-merge: Embarrassingly parallel training of expert language models.
 840 *arXiv preprint arXiv:2208.03306*, 2022.

841

842 Chengsong Huang, Qian Liu, Bill Yuchen Lin, Tianyu Pang, Chao Du, and Min Lin. Lorahub:
 843 Efficient cross-task generalization via dynamic lora composition. 07 2023b. URL <https://arxiv.org/pdf/2307.13269.pdf>.

844

845 Sara Babakniya, Ahmed Roushdy Elkordy, Yahya H. Ezzeldin, Qingfeng Liu, Kee-Bong Song,
 846 Mostafa El-Khamy, and Salman Avestimehr. Slora: Federated parameter efficient fine-tuning of
 847 language models. 08 2023. URL <https://arxiv.org/pdf/2308.06522.pdf>.

848

849 Geoffrey E Hinton, Simon Osindero, and Yee-Whye Teh. A fast learning algorithm for deep belief
 850 nets. *Neural computation*, 18(7):1527–1554, 2006.

851

852 Joshua Bengio, Pascal Lamblin, Dan Popovici, and Hugo Larochelle. Greedy layer-wise training of
 853 deep networks. *Advances in neural information processing systems*, 19, 2006.

854

855 Naftali Tishby, Fernando C Pereira, and William Bialek. The information bottleneck method. *arXiv
 856 preprint physics/0004057*, 2000.

857

858 Rabeeh Karimi Mahabadi, Yonatan Belinkov, and James Henderson. Variational information bottleneck
 859 for effective low-resource fine-tuning. *arXiv preprint arXiv:2106.05469*, 2021.

860

861 Naftali Tishby and Noga Zaslavsky. Deep learning and the information bottleneck principle. In *2015
 862 ieee information theory workshop (itw)*, pages 1–5. IEEE, 2015.

863

864 Yuwen Xiong, Mengye Ren, and Raquel Urtasun. Loco: Local contrastive representation learning.
 865 *Advances in neural information processing systems*, 33:11142–11153, 2020.

866

867 Aidan N Gomez, Oscar Key, Kuba Perlin, Stephen Gou, Nick Frosst, Jeff Dean, and Yarin Gal.
 868 Interlocking backpropagation: Improving depthwise model-parallelism. *The Journal of Machine
 869 Learning Research*, 23(1):7714–7741, 2022.

864 Hesham Mostafa, Vishwajith Ramesh, and Gert Cauwenberghs. Deep supervised learning using local
 865 errors. *Frontiers in neuroscience*, 12:608, 2018.

866

867 Eugene Belilovsky, Michael Eickenberg, and Edouard Oyallon. Greedy layerwise learning can scale
 868 to imagenet. In *International conference on machine learning*, pages 583–593. PMLR, 2019.

869

870 Eugene Belilovsky, Michael Eickenberg, and Edouard Oyallon. Decoupled greedy learning of cnns.
 871 In *International Conference on Machine Learning*, pages 736–745. PMLR, 2020.

872

873 Mandar Kulkarni and Shirish Karande. Layer-wise training of deep networks using kernel similarity.
 874 *arXiv preprint arXiv:1703.07115*, 2017.

875

876 Arild Nøkland and Lars Hiller Eidnes. Training neural networks with local error signals. In
 877 *International conference on machine learning*, pages 4839–4850. PMLR, 2019.

878

879 Shoaib Ahmed Siddiqui, David Krueger, Yann LeCun, and Stéphane Deny. Blockwise self-supervised
 880 learning at scale. *arXiv preprint arXiv:2302.01647*, 2023.

881

882 Yulin Wang, Zanlin Ni, Shiji Song, Le Yang, and Gao Huang. Revisiting locally supervised learning:
 883 an alternative to end-to-end training. In *International Conference on Learning Representations*,
 884 2020c.

885

886 Maithra Raghu, Justin Gilmer, Jason Yosinski, and Jascha Sohl-Dickstein. Svcca: Singular vector
 887 canonical correlation analysis for deep learning dynamics and interpretability, 2017. URL <https://arxiv.org/abs/1706.05806>.

888

889 Chaoyang He, Shen Li, Mahdi Soltanolkotabi, and Salman Avestimehr. Pipetransformer: Automated
 890 elastic pipelining for distributed training of large-scale models. In Marina Meila and Tong Zhang,
 891 editors, *Proceedings of the 38th International Conference on Machine Learning*, volume 139 of
 892 *Proceedings of Machine Learning Research*, pages 4150–4159. PMLR, 18–24 Jul 2021.

893

894 Rui Pan, Xiang Liu, Shizhe Diao, Renjie Pi, Jipeng Zhang, Chi Han, and Tong Zhang. Lisa:
 895 Layerwise importance sampling for memory-efficient large language model fine-tuning. 03 2024.
 896 URL <https://arxiv.org/pdf/2403.17919.pdf>.

897

898 Pengxiang Li, Lu Yin, and Shiwei Liu. Mix-In: Unleashing the power of deeper layers by combining
 899 pre-In and post-In. 12 2024d. URL <https://arxiv.org/pdf/2412.13795.pdf>.

900

901 Balaji Lakshminarayanan, A. Pritzel, and C. Blundell. Simple and scalable predictive uncertainty
 902 estimation using deep ensembles. In *Neural Information Processing Systems*, 2016.

903

904 C. Blundell, Julien Cornebise, K. Kavukcuoglu, and D. Wierstra. Weight uncertainty in neural
 905 networks. *arXiv.org*, 2015.

906

907 Dan Hendrycks and Kevin Gimpel. A baseline for detecting misclassified and out-of-distribution
 908 examples in neural networks. *International Conference on Learning Representations*, 2016.

909

910 Chuan Guo, Geoff Pleiss, Yu Sun, and Kilian Q. Weinberger. On calibration of modern neural
 911 networks. In *International Conference on Machine Learning*, 2017.

912

913 Ian J Goodfellow, Jonathon Shlens, and Christian Szegedy. Explaining and harnessing adversarial
 914 examples. *arXiv preprint arXiv:1412.6572*, 2014.

915

916 P Izmailov, AG Wilson, D Podoprikhin, D Vetrov, and T Garipov. Averaging weights leads to wider
 917 optima and better generalization. In *UAI*, pages 876–885, 2018.

918

919 Wesley J Maddox, Pavel Izmailov, Timur Garipov, Dmitry P Vetrov, and Andrew Gordon Wilson.
 920 A simple baseline for bayesian uncertainty in deep learning. In H. Wallach, H. Larochelle,
 921 A. Beygelzimer, F. d’Alché-Buc, E. Fox, and R. Garnett, editors, *Advances in Neural Information
 922 Processing Systems*, volume 32. Curran Associates, Inc., 2019.

923

924 A. Wilson and Pavel Izmailov. Bayesian deep learning and a probabilistic perspective of generalization.
 925 *Neural Information Processing Systems*, 2020.

918 Xiang Liu, Liangxi Liu, Feiyang Ye, Yunheng Shen, Xia Li, Linshan Jiang, and Jialin Li. Fedlpa:
 919 One-shot federated learning with layer-wise posterior aggregation. *Neural Information Processing*
 920 *Systems*, 2024a.

921 Liang Liu, Xi Jiang, Feng Zheng, Hong Chen, Guo-Jun Qi, Heng Huang, and Ling Shao. A bayesian
 922 federated learning framework with online laplace approximation. *IEEE Transactions on Pattern*
 923 *Analysis and Machine Intelligence*, 2021.

924 Maruan Al-Shedivat, Jennifer Gillenwater, E. Xing, and Afshin Rostamizadeh. Federated learning
 925 via posterior averaging: A new perspective and practical algorithms. *International Conference on*
 926 *Learning Representations*, 2020.

927 Mikhail Yurochkin, Mayank Agarwal, Soumya Ghosh, Kristjan Greenewald, Nghia Hoang, and
 928 Yasaman Khazaeni. Bayesian nonparametric federated learning of neural networks. In Kamalika
 929 Chaudhuri and Ruslan Salakhutdinov, editors, *Proceedings of the 36th International Conference*
 930 *on Machine Learning*, volume 97 of *Proceedings of Machine Learning Research*, pages
 931 7252–7261. PMLR, 09–15 Jun 2019b. URL <https://proceedings.mlr.press/v97/yurochkin19a.html>.

932 Hongyi Wang, Mikhail Yurochkin, Yuekai Sun, Dimitris Papailiopoulos, and Yasaman Khazaeni. Fed-
 933 erated learning with matched averaging. In *International Conference on Learning Representations*,
 934 2020d.

935 Deyuan Liu, Zecheng Wang, Bingning Wang, Weipeng Chen, Chunshan Li, Zhiying Tu, Dianhui
 936 Chu, Bo Li, and Dianbo Sui. Checkpoint merging via bayesian optimization in lilm pretraining.
 937 *arXiv preprint arXiv:2403.19390*, 2024b.

938 Weitang Liu, Xiaoyun Wang, John Douglas Owens, and Yixuan Li. Energy-based out-of-distribution
 939 detection. *Neural Information Processing Systems*, 2020.

940 Yaniv Ovadia, Emily Fertig, Jie Jessie Ren, Zachary Nado, D. Sculley, Sebastian Nowozin, Joshua V.
 941 Dillon, Balaji Lakshminarayanan, and Jasper Snoek. Can you trust your model’s uncertainty?
 942 evaluating predictive uncertainty under dataset shift. *Neural Information Processing Systems*,
 943 2019.

944 Alex Kendall and Yarin Gal. What uncertainties do we need in bayesian deep learning for computer
 945 vision? In I. Guyon, U. Von Luxburg, S. Bengio, H. Wallach, R. Fergus, S. Vishwanathan, and
 946 R. Garnett, editors, *Advances in Neural Information Processing Systems*, volume 30. Curran
 947 Associates, Inc., 2017.

948 John Duchi and Hongseok Namkoong. Learning models with uniform performance via distributionally
 949 robust optimization. *arXiv preprint arXiv:1810.08750*, 2018.

950 Martin Arjovsky, Léon Bottou, Ishaan Gulrajani, and David Lopez-Paz. Invariant risk minimization.
 951 *arXiv preprint arXiv:1907.02893*, 2019.

952 Elliot Creager, Jörn-Henrik Jacobsen, and Richard Zemel. Environment inference for invariant
 953 learning. In *ICML*, pages 2189–2200. PMLR, 2021.

954 Yoshua Bengio, Aaron Courville, and Pascal Vincent. Representation learning: A review and new
 955 perspectives. *IEEE TPAMI*, 35(8):1798–1828, 2013.

956 Francesco Locatello, Stefan Bauer, Mario Lucic, Gunnar Raetsch, Sylvain Gelly, Bernhard Schölkopf,
 957 and Olivier Bachem. Challenging common assumptions in the unsupervised learning of disentan-
 958 gled representations. In *ICML*, pages 4114–4124. PMLR, 2019.

959 Mengyue Yang, Furui Liu, Zhitang Chen, Xinwei Shen, Jianye Hao, and Jun Wang. Causalvae:
 960 disentangled representation learning via neural structural causal models. In *CVPR*, pages 9593–
 961 9602, 2021.

962 Peter Bühlmann. Invariance, causality and robustness. *arXiv preprint arXiv:1812.08233*, 2018.

963 Krikamol Muandet, David Balduzzi, and Bernhard Schölkopf. Domain generalization via invariant
 964 feature representation. In *ICML*, 2013.

972 Isabela Albuquerque, João Monteiro, Mohammad Darvishi, Tiago H Falk, and Ioannis Mitliagkas.
 973 Adversarial target-invariant representation learning for domain generalization. 2020.
 974

975 Haoliang Li, Sinno Jialin Pan, Shiqi Wang, and Alex C Kot. Domain generalization with adversarial
 976 feature learning. In *CVPR*, pages 5400–5409, 2018.

977 Rui Gong, Wen Li, Yuhua Chen, and Luc Van Gool. Dlow: Domain flow for adaptation and
 978 generalization. In *CVPR*, pages 2477–2486, 2019.

979

980 Anthony Sicilia, Xingchen Zhao, and Seong Jae Hwang. Domain adversarial neural networks for
 981 domain generalization: When it works and how to improve. *arXiv preprint arXiv:2102.03924*,
 982 2021.

983 Geli Fei and Bing Liu. Breaking the closed world assumption in text classification. In *NAACL*, 2016.

984

985 Stefan Larson, Anish Mahendran, Joseph J Peper, Christopher Clarke, Andrew Lee, Parker Hill,
 986 Jonathan K Kummerfeld, Kevin Leach, Michael A Laurenzano, Lingjia Tang, et al. An evaluation
 987 dataset for intent classification and out-of-scope prediction. In *EMNLP-IJCNLP*, 2019.

988

989 Amita Kamath, Robin Jia, and Percy Liang. Selective question answering under domain shift. In
 990 *ACL*, 2020.

991

992 Joo-Kyung Kim and Young-Bum Kim. Joint learning of domain classification and out-of-domain
 993 detection with dynamic class weighting for satisfying false acceptance rates. *arXiv preprint
 994 arXiv:1807.00072*, 2018.

995

996 Dan Hendrycks, Mantas Mazeika, and Thomas Dietterich. Deep anomaly detection with outlier
 997 exposure. In *ICLR*, 2019.

998

999 Kimin Lee, Honglak Lee, Kibok Lee, and Jinwoo Shin. Training confidence-calibrated classifiers for
 1000 detecting out-of-distribution samples. In *ICLR*, 2018.

1001

1002 Zhiyuan Zeng, Hong Xu, Keqing He, Yuanmeng Yan, Sihong Liu, Zijun Liu, and Weiran Xu.
 1003 Adversarial generative distance-based classifier for robust out-of-domain detection. In *ICASSP*,
 1004 2021a.

1005

1006 Zhiyuan Zeng, Keqing He, Yuanmeng Yan, Zijun Liu, Yanan Wu, Hong Xu, Huixing Jiang, and
 1007 Weiran Xu. Modeling discriminative representations for out-of-domain detection with supervised
 1008 contrastive learning. In *ACL*, 2021b.

1009

1010 Wenxuan Zhou, Fangyu Liu, and Muhamo Chen. Contrastive out-of-distribution detection for pretrained
 1011 transformers. In *EMNLP*, 2021.

1012

1013 Hyunsoo Cho, Choonghyun Park, Jaewook Kang, Kang Min Yoo, Taeuk Kim, and Sang-goo Lee.
 1014 Enhancing out-of-distribution detection in natural language understanding via implicit layer
 1015 ensemble. In *EMNLP*, 2022.

1016

1017 Yutao Mou, Pei Wang, Keqing He, Yanan Wu, Jingang Wang, Wei Wu, and Weiran Xu. Uninl:
 1018 Aligning representation learning with scoring function for ood detection via unified neighborhood
 1019 learning. In *EMNLP*, 2022.

1020

1021 Geoffrey E. Hinton, O. Vinyals, and J. Dean. Distilling the knowledge in a neural network. *arXiv.org*,
 1022 2015.

1023

1024 Shiyu Liang, Yixuan Li, and R. Srikant. Enhancing the reliability of out-of-distribution image
 1025 detection in neural networks. *International Conference on Learning Representations*, 2017.

1026

1027 Elias Frantar and Dan Alistarh. Sparsegpt: Massive language models can be accurately pruned
 1028 in one-shot. In Andreas Krause, Emma Brunskill, Kyunghyun Cho, Barbara Engelhardt, Sivan
 1029 Sabato, and Jonathan Scarlett, editors, *International Conference on Machine Learning, ICML
 1030 2023, 23-29 July 2023, Honolulu, Hawaii, USA*, volume 202 of *Proceedings of Machine Learning
 1031 Research*, pages 10323–10337. PMLR, 2023. URL <https://proceedings.mlr.press/v202/frantar23a.html>.

1026 Hang Shao, Bei Liu, and Yanmin Qian. One-shot sensitivity-aware mixed sparsity pruning for large
 1027 language models. In *ICASSP 2024 - 2024 IEEE International Conference on Acoustics, Speech
 1028 and Signal Processing (ICASSP)*, pages 11296–11300, 2024.

1029 Yuxin Zhang, Lirui Zhao, Mingbao Lin, Sun Yunyun, Yiwu Yao, Xingjia Han, Jared Tanner, Shiwei
 1030 Liu, and Rongrong Ji. Dynamic sparse no training: Training-free fine-tuning for sparse LLMs.
 1031 In *The Twelfth International Conference on Learning Representations*, 2024. URL <https://openreview.net/forum?id=1ndDmZdT4g>.

1032 Pavlo Molchanov, Arun Mallya, Stephen Tyree, Iuri Frosio, and Jan Kautz. Importance estimation for
 1033 neural network pruning. In *IEEE Conference on Computer Vision and Pattern Recognition, CVPR
 1034 2019, Long Beach, CA, USA, June 16-20, 2019*, pages 11264–11272. Computer Vision Foundation
 1035 / IEEE, 2019. doi: 10.1109/CVPR.2019.01152.

1036 Xinyin Ma, Gongfan Fang, and Xinchao Wang. LLM-pruner: On the structural pruning of large
 1037 language models. In *Thirty-seventh Conference on Neural Information Processing Systems*, 2023.
 1038 URL <https://openreview.net/forum?id=J8Ajf9WfXP>.

1039 Bo-Kyeong Kim, Geonmin Kim, Tae-Ho Kim, Thibault Castells, Shinkook Choi, Junho Shin, and
 1040 Hyoung-Kyu Song. Shortened llama: A simple depth pruning for large language models. *ICLR
 1041 Workshop on Mathematical and Empirical Understanding of Foundation Models (ME-FoMo)*,
 1042 2024.

1043 Song Han, Jeff Pool, John Tran, and William Dally. Learning both weights and connections for
 1044 efficient neural network. In C. Cortes, N. Lawrence, D. Lee, M. Sugiyama, and R. Garnett, editors,
 1045 *Advances in Neural Information Processing Systems*, volume 28. Curran Associates, Inc., 2015.

1046 Wei Wen, Chunpeng Wu, Yandan Wang, Yiran Chen, and Hai Li. Learning structured sparsity in
 1047 deep neural networks. In D. Lee, M. Sugiyama, U. Luxburg, I. Guyon, and R. Garnett, editors,
 1048 *Advances in Neural Information Processing Systems*, volume 29. Curran Associates, Inc., 2016.

1049 Yifei He, Yuzheng Hu, Yong Lin, Tong Zhang, and Han Zhao. Localize-and-stitch: Efficient model
 1050 merging via sparse task arithmetic. *Transactions on Machine Learning Research*, 2025. ISSN
 1051 2835-8856. URL <https://openreview.net/forum?id=9CWU80i86d>.

1052 Gunho Park, Baeseong park, Minsub Kim, Sungjae Lee, Jeonghoon Kim, Beomseok Kwon, Se Jung
 1053 Kwon, Byeongwook Kim, Youngjoo Lee, and Dongsoo Lee. LUT-GEMM: Quantized matrix
 1054 multiplication based on LUTs for efficient inference in large-scale generative language models.
 1055 In *The Twelfth International Conference on Learning Representations*, 2024. URL <https://openreview.net/forum?id=gLARhFLE0F>.

1056 Mohammad Rastegari, Vicente Ordonez, Joseph Redmon, and Ali Farhadi. Xnor-net: Imagenet
 1057 classification using binary convolutional neural networks. In Bastian Leibe, Jiri Matas, Nicu Sebe,
 1058 and Max Welling, editors, *Computer Vision - ECCV 2016 - 14th European Conference, Amsterdam,
 1059 The Netherlands, October 11-14, 2016, Proceedings, Part IV*, volume 9908 of *Lecture Notes in
 1060 Computer Science*, pages 525–542. Springer, 2016. doi: 10.1007/978-3-319-46493-0_32. URL
 1061 https://doi.org/10.1007/978-3-319-46493-0_32.

1062 Elias Frantar, Saleh Ashkboos, Torsten Hoefer, and Dan Alistarh. OPTQ: Accurate quantization
 1063 for generative pre-trained transformers. In *The Eleventh International Conference on Learning
 1064 Representations*, 2023. URL <https://openreview.net/forum?id=tcbBPnfwxs>.

1065 Elias Frantar and Dan Alistarh. Optimal brain compression: A framework for accurate post-training
 1066 quantization and pruning. In Alice H. Oh, Alekh Agarwal, Danielle Belgrave, and Kyunghyun
 1067 Cho, editors, *Advances in Neural Information Processing Systems*, 2022.

1068 Jerry Chee, Yaohui Cai, Volodymyr Kuleshov, and Christopher De Sa. QuIP: 2-bit quantization
 1069 of large language models with guarantees. In *Thirty-seventh Conference on Neural Information
 1070 Processing Systems*, 2023. URL <https://openreview.net/forum?id=xrk9g5vcXR>.

1071 Ji Lin, Jiaming Tang, Haotian Tang, Shang Yang, Xingyu Dang, and Song Han. AWQ: activation-
 1072 aware weight quantization for LLM compression and acceleration. *CoRR*, abs/2306.00978,
 1073 2023. doi: 10.48550/arXiv.2306.00978. URL [https://doi.org/10.48550/arXiv.
 1074 2306.00978](https://doi.org/10.48550/arXiv.2306.00978).

1080 Changhun Lee, Jungyu Jin, Taesu Kim, Hyungjun Kim, and Eunhyeok Park. OWQ: outlier-aware
 1081 weight quantization for efficient fine-tuning and inference of large language models. In Michael J.
 1082 Wooldridge, Jennifer G. Dy, and Sriraam Natarajan, editors, *Thirty-Eighth AAAI Conference on*
 1083 *Artificial Intelligence*, pages 13355–13364. AAAI Press, 2024. doi: 10.1609/AAAI.V38I12.29237.
 1084 URL <https://doi.org/10.1609/aaai.v38i12.29237>.

1085 Tim Dettmers, Ruslan A. Svirchevski, Vage Egiazarian, Denis Kuznedelev, Elias Frantar, Saleh
 1086 Ashkboos, Alexander Borzunov, Torsten Hoefer, and Dan Alistarh. SpQR: A sparse-quantized
 1087 representation for near-lossless LLM weight compression. In *The Twelfth International Conference*
 1088 *on Learning Representations*, 2024. URL <https://openreview.net/forum?id=Q1u25ahSuy>.

1089

1090 Sehoon Kim, Coleman Hooper, Amir Gholami, Zhen Dong, Xiuyu Li, Sheng Shen, Michael W.
 1091 Mahoney, and Kurt Keutzer. Squeezellm: Dense-and-sparse quantization. *CoRR*, abs/2306.07629,
 1092 2023. doi: 10.48550/ARXIV.2306.07629. URL <https://doi.org/10.48550/arXiv.2306.07629>.

1093

1094 Yiming Zhu, Peixian Zhang, Ehsan-Ul Haq, Pan Hui, and Gareth Tyson. Can chatgpt reproduce
 1095 human-generated labels? a study of social computing tasks. *arXiv preprint arXiv:2304.10145*,
 1096 2023.

1097

1098 Meysam Alizadeh, Maël Kubli, Zeynab Samei, Shirin Dehghani, Juan Diego Bermeo, Maria Ko-
 1099 robeynikova, and Fabrizio Gilardi. Open-source large language models outperform crowd workers
 1100 and approach chatgpt in text-annotation tasks. *arXiv preprint arXiv:2307.02179*, 101, 2023.

1101

1102 Petter Törnberg. Chatgpt-4 outperforms experts and crowd workers in annotating political twitter
 1103 messages with zero-shot learning. *arXiv preprint arXiv:2304.06588*, 2023.

1104

1105 Weihao Zeng, Can Xu, Yingxiu Zhao, Jian-Guang Lou, and Weizhu Chen. Automatic instruction
 1106 evolving for large language models. *arXiv preprint arXiv:2406.00770*, 2024.

1107

1108 Lifan Yuan, Ganqu Cui, Hanbin Wang, Ning Ding, Xingyao Wang, Jia Deng, Boji Shan, Huimin
 1109 Chen, Ruobing Xie, Yankai Lin, et al. Advancing llm reasoning generalists with preference trees.
 1110 *arXiv preprint arXiv:2404.02078*, 2024.

1111

1112 Tanay Dixit, Bhargavi Paranjape, Hannaneh Hajishirzi, and Luke Zettlemoyer. Core: A retrieve-then-
 1113 edit framework for counterfactual data generation. *arXiv preprint arXiv:2210.04873*, 2022.

1114

1115 Lisa Dunlap, Alyssa Umino, Han Zhang, Jiezhi Yang, Joseph E Gonzalez, and Trevor Darrell.
 1116 Diversify your vision datasets with automatic diffusion-based augmentation. *Advances in neural*
 1117 *information processing systems*, 36:79024–79034, 2023.

1118

1119 Zeming Chen, Qiyue Gao, Antoine Bosselut, Ashish Sabharwal, and Kyle Richardson. Disco:
 1120 Distilling counterfactuals with large language models. *arXiv preprint arXiv:2212.10534*, 2022.

1121

1122 Qingxiu Dong, Lei Li, Damai Dai, Ce Zheng, Zhiyong Wu, Baobao Chang, Xu Sun, Jingjing Xu, and
 1123 Zhifang Sui. A survey on in-context learning. *arXiv preprint arXiv:2301.00234*, 2022.

1124

1125 Yizhong Wang, Yeganeh Kordi, Swaroop Mishra, Alisa Liu, Noah A Smith, Daniel Khashabi, and
 1126 Hannaneh Hajishirzi. Self-instruct: Aligning language models with self-generated instructions. In
 1127 *The 61st Annual Meeting Of The Association For Computational Linguistics*, 2023.

1128

1129 Or Honovich, Thomas Scialom, Omer Levy, and Timo Schick. Unnatural instructions: Tuning
 1130 language models with (almost) no human labor. *arXiv preprint arXiv:2212.09689*, 2022.

1131

1132 Minghao Wu, Abdul Waheed, Chiyu Zhang, Muhammad Abdul-Mageed, and Alham Fikri Aji.
 1133 Lamini-lm: A diverse herd of distilled models from large-scale instructions. *arXiv preprint*
 1134 *arXiv:2304.14402*, 2023.

1135

1136 Xian Li, Ping Yu, Chunting Zhou, Timo Schick, Luke Zettlemoyer, Omer Levy, Jason Weston, and
 1137 Mike Lewis. Self-alignment with instruction backtranslation. *arXiv preprint arXiv:2308.06259*,
 1138 2023a.

1134 Ronen Eldan and Yuanzhi Li. Tinystories: How small can language models be and still speak coherent
 1135 english? *arXiv preprint arXiv:2305.07759*, 2023.

1136 Suriya Gunasekar, Yi Zhang, Jyoti Aneja, Caio César Teodoro Mendes, Allie Del Giorno, Sivakanth
 1137 Gopi, Mojan Javaheripi, Piero Kauffmann, Gustavo de Rosa, Olli Saarikivi, et al. Textbooks are all
 1138 you need. *arXiv preprint arXiv:2306.11644*, 2023.

1139

1140 Yuanzhi Li, Sébastien Bubeck, Ronen Eldan, Allie Del Giorno, Suriya Gunasekar, and Yin Tat Lee.
 1141 Textbooks are all you need ii: phi-1.5 technical report. *arXiv preprint arXiv:2309.05463*, 2023b.

1142 Rohan Taori, Ishaan Gulrajani, Tianyi Zhang, Yann Dubois, Xuechen Li, Carlos Guestrin, Percy
 1143 Liang, and Tatsunori B. Hashimoto. Stanford alpaca: An instruction-following llama model, March
 1144 2023a. URL https://github.com/tatsu-lab/stanford_alpaca.

1145

1146 Lichang Chen, Shiyang Li, Jun Yan, Hai Wang, Kalpa Gunaratna, Vikas Yadav, Zheng Tang, Vijay
 1147 Srinivasan, Tianyi Zhou, Heng Huang, et al. Alpagasus: Training a better alpaca with fewer data.
 1148 *arXiv preprint arXiv:2307.08701*, 2023.

1149 Yuxiang Wei, Zhe Wang, Jiawei Liu, Yifeng Ding, and LINGMING ZHANG. Magicoder: Empow-
 1150 ering Code Generation with OSS-Instruct. In *Forty-first International Conference on Machine*
 1151 *Learning*, 2024b.

1152

1153 Ziyang Luo, Can Xu, Pu Zhao, Qingfeng Sun, Xiubo Geng, Wenxiang Hu, Chongyang Tao, Jing Ma,
 1154 Qingwei Lin, and Daxin Jiang. Wizardcoder: Empowering Code Large Language Models with
 1155 Evol-Instruct. In *International Conference on Learning Representations (ICLR)*, 2024.

1156 Aitor Lewkowycz, Anders Andreassen, David Dohan, Ethan Dyer, Henryk Michalewski, Vinay Ra-
 1157 masesh, Ambrose Sloane, Cem Anil, Imanol Schlag, Theo Gutman-Solo, et al. Solving quantitative
 1158 reasoning problems with language models. *Advances in Neural Information Processing Systems*,
 1159 35:3843–3857, 2022.

1160

1161 Huajian Xin, Daya Guo, Zhihong Shao, Zhizhou Ren, Qihao Zhu, Bo Liu, Chong Ruan, Wenda Li,
 1162 and Xiaodan Liang. Deepseek-Prover: Advancing Theorem Proving in LLMs through Large-Scale
 1163 Synthetic Data. *arXiv*, abs/2405.14333, 2024.

1164

1165 Haoxiong Liu, Yifan Zhang, Yifan Luo, and Andrew C Yao. Augmenting Math Word Problems
 1166 via Iterative Question Composing. In *ICLR 2024 Workshop on Navigating and Addressing Data*
 1167 *Problems for Foundation Models*, 2024c.

1168

1169 Chen Li, Weiqi Wang, Jingcheng Hu, Yixuan Wei, Nanning Zheng, Han Hu, Zheng Zhang, and
 1170 Houwen Peng. Common 7b language models already possess strong math capabilities. *arXiv preprint*
 1171 *arXiv:2403.04706*, 2024e.

1172

1173 Xiang Yue, Xingwei Qu, Ge Zhang, Yao Fu, Wenhao Huang, Huan Sun, Yu Su, and Wenhui Chen.
 1174 Mammoth: Building math generalist models through hybrid instruction tuning. *arXiv preprint*
 1175 *arXiv:2309.05653*, 2023b.

1176

1177 Yichao Fu, Peter Bailis, Ion Stoica, and Hao Zhang. Break the sequential dependency of llm inference
 1178 using lookahead decoding. In *Forty-first International Conference on Machine Learning*.

1179

1180 Ingo Steinwart. How to compare different loss functions and their risks. *Constructive Approx-
 1181 imation*, 26:225–287, 2007. URL <https://api.semanticscholar.org/CorpusID:16660598>.

1182

1183 Bernardo Ávila Pires and Csaba Szepesvári. Multiclass classification calibration functions. *arXiv*
 1184 *preprint arXiv:1609.06385*, 2016.

1185

1186 Kleijn and Van der Vaart. The bernstein-von-mises theorem under misspecification. *Electronic Journal*
 1187 *of Statistics*, 6:354–381, 2012. URL <https://api.semanticscholar.org/CorpusID:85548207>.

1188

1189 Yuze Zhao, Jintao Huang, Jinghan Hu, Xingjun Wang, Yunlin Mao, Daoze Zhang, Zeyinzi Jiang,
 1190 Zhikai Wu, Baole Ai, Ang Wang, Wenmeng Zhou, and Yingda Chen. Swift:a scalable lightweight
 1191 infrastructure for fine-tuning, 2024. URL <https://arxiv.org/abs/2408.05517>.

1188 Xisen Jin, Xiang Ren, Daniel Preotiuc-Pietro, and Pengxiang Cheng. Dataless knowledge fusion
 1189 by merging weights of language models. *ICLR*, 12 2023. URL <https://arxiv.org/pdf/2212.09849.pdf>.
 1190

1191 Sainbayar Sukhbaatar, Olga Golovneva, Vasu Sharma, Hu Xu, Xi Victoria Lin, Baptiste Rozière,
 1192 Jacob Kahn, Daniel Li, Wen-tau Yih, Jason Weston, et al. Branch-train-mix: Mixing expert llms
 1193 into a mixture-of-experts llm. *arXiv preprint arXiv:2403.07816*, 2024c.
 1194

1195 Arindam Mitra, Hamed Khanpour, Corby Rossset, and Ahmed Awadallah. Orca-math: Unlocking
 1196 the potential of slms in grade school math, 2024. URL <https://arxiv.org/abs/2402.14830>.
 1197

1198 Rohan Taori, Ishaan Gulrajani, Tianyi Zhang, Yann Dubois, Xuechen Li, Carlos Guestrin, Percy
 1199 Liang, and Tatsunori B. Hashimoto. Stanford alpaca: An instruction-following llama model.
 1200 https://github.com/tatsu-lab/stanford_alpaca, 2023b.
 1201

1202 Antoine Bordes, Sumit Chopra, and Jason Weston. Question answering with subgraph embeddings,
 1203 2014. URL <https://arxiv.org/abs/1406.3676>.
 1204

1205 Pranav Rajpurkar, Jian Zhang, Konstantin Lopyrev, and Percy Liang. Squad: 100,000+ questions for
 1206 machine comprehension of text, 2016. URL <https://arxiv.org/abs/1606.05250>.
 1207

1208 Jacob Austin, Augustus Odena, Maxwell Nye, Maarten Bosma, Henryk Michalewski, David Dohan,
 1209 Ellen Jiang, Carrie Cai, Michael Terry, Quoc Le, and Charles Sutton. Program synthesis with large
 1210 language models, 2021. URL <https://arxiv.org/abs/2108.07732>.
 1211

1212 Tristan Coignion, Clément Quinton, and Romain Rouvoy. A performance study of llm-generated code
 1213 on leetcode. In *Proceedings of the 28th International Conference on Evaluation and Assessment in
 1214 Software Engineering*, EASE 2024, page 79–89. ACM, June 2024. doi: 10.1145/3661167.3661221.
 1215 URL <http://dx.doi.org/10.1145/3661167.3661221>.
 1216

1217 Pengcheng Yin, Bowen Deng, Edgar Chen, Bogdan Vasilescu, and Graham Neubig. Learning to
 1218 mine aligned code and natural language pairs from stack overflow. In *International Conference on
 1219 Mining Software Repositories*, MSR, pages 476–486. ACM, 2018. doi: <https://doi.org/10.1145/3196398.3196408>.
 1220

1221

1222

1223

1224

1225

1226

1227

1228

1229

1230

1231

1232

1233

1234

1235

1236

1237

1238

1239

1240

1241

1242 APPENDIX
12431244 A THE USE OF LARGE LANGUAGE MODELS
12451246 We used LLMs solely for grammar and wording improvements. It did not generate ideas, analyses, or
1247 results. No additional or undisclosed LLM use occurred.
12481249 B BROADER IMPACT
12501252 **Societal Impacts.** Our approach demonstrates significant effectiveness by enabling the deployment
1253 of merging 7B x 4 LLMs with only 24GB VRAM. Compared to ensemble learning with these models,
1254 our method not only maintains better accuracy but also requires significantly less computational
1255 resources and demonstrates superior performance. This breakthrough in resource efficiency makes
1256 advanced language models more accessible and cost-effective.
12571258 **Potential Applications.** The technology may have significant potential across specialized vertical
1259 domains. Considering that many vertical domains, personalized LLM agents (Li et al., 2024b), LLM
1260 applications like roleplay chatting (Chan et al., 2024; Yu et al., 2024a) and professional domain-
1261 specific writing (Gómez-Rodríguez and Williams, 2023), an LLM service provider may need to
1262 simultaneously deploy different finetuned LLMs. Our technology enables efficient and effective
1263 serving multiple popular LLM applications, and merging knowledge from different LLMs together.
12641265 C MORE RELATED WORKS
12661267 We introduce more related works about model merging and routing in this section. Current common
1268 methods include: (1) **Averaging based merging.** This direction combines multiple models into a
1269 single model while preserving their capabilities with minimal or no additional training; (2) **Routing**
1270 **based merging.** It considers to route inputs to specialized expert modules like mixture-of-experts
(MoE) approaches but completely different.
12711272 Table 11 provides an overview of comparing different model merging methods and our framework.
1273 Given n_τ different finetuned models, averaging based methods do not completely address the
1274 parameter conflicts, thus having higher parameter conflicts than routing based merging. The weighted
1275 averaging requires calibration data to compute the importance metrics. The token-level routing
1276 requires routing for each layer, thus having totally $n_\mathcal{L}$ routers. Our framework Mediator exploits
1277 layer-wise characteristics to both reduce parameter conflict and improve common knowledge fusion.
1278 And Mediator utilizes compression to further reduce the memory costs. To the best of our knowledge,
1279 the most of previous model merging works focus on experiments on traditional CV and NLP
1280 tasks (Matena and Raffel, 2022), while Mediator conducts experiments on modern LLMs and
1281 real-world experiments.
12821283 Table 12 provides the system performance comparison. Because token-level routing like MoE
1284 requires to route each token towards different (possibly) experts, its inference cost is significantly
1285 large as more than $T \times n_\mathcal{L}$ times than task-level routing, where T is the sequence length. Besides,
1286 the token-level routing requires more than $n_\mathcal{L}$ times routers in memory costs. With the layer-wise
1287 adaptive averaging and Routing, Mediator significantly reduce the memory costs of from $M_\theta \times n_\tau$ to
1288 $M_\theta \times (c_{\text{avg}} + c_{\text{route}} \times n_\tau \times c)$ ¹. The experimental memory reduction and the system performance
1289 comparisons are shown in the Section 5.1. We also provide system optimization to accelerate
1290 the inference during the deployment of Mediator in Section 4.4 and Appendix H. And the hyper-
1291 parameters c_{avg} and c_{route} are adaptively decided by the parameter conflict estimation.
12921293 Besideds, we also review some highly related works include following directions that are closely
1294 related to our framework. Insights from these directions have provided valuable guidance for our
1295 framework.
12961297 1. **Layer-wise training dynamics and optimization.** This direction discusses the layer-wise training
1298 dynamics to help shed some light on the paramter conflicts and the layer-wise adaptivity.
12991¹Normally, each transformer layer occupies the same memory.

1296 Table 11: Demystifying different merging methods. The n_τ represents the number of finetuning tasks,
 1297 n_L the number of layers in the model.

Method Type	Parameter Conflict Level	Merging Common Knowledge	Require Calibration Data	Routing Type	Considering Layer-wise Characteristics	Considering Compression	Considering OOD Samples	Experimental Scenario
Basic Averaging	High	✓	✗	NA	✗	✗	✗	Traditional CV, NLP
Weighted Averaging	Middle	✓	✓	NA	✗	✗	✗	Traditional CV, NLP
Subspace Averaging	Middle	✓	✗	NA	✗	✗	✗	Traditional CV, NLP
Token-Level Routing	Low	✗	✗	Token-level	✗	✗	✗	Traditional CV, NLP
Task-Level Routing	Low	✗	✗	Task-level	✗	✗	✗	Traditional CV, NLP
Mediator	Low	✓	✗	Task-level	✓	✓	✓	Generative LLMs

1303 Table 12: Demystifying different merging methods in system performance costs. Considering the
 1304 memory costs of the base model and one router are M_θ and M_h , each layer occupies the same
 1305 memory M_l , compression ratio c , the ratio of selected layers for averaging is c_{avg} , for routing is c_{route} ,
 1306 FP_θ and BP_θ are the forward time and backward time of the model. FP_h and BP_h are the forward
 1307 time and backward time of the router.

Method Type	Requiring # of routers	Costs of Trainig Routers	Memory Costs After Merging	Inference Cost
Basic Averaging	NA	NA	M_θ	FP_θ
Weighted Averaging	NA	NA	M_θ	FP_θ
Subspace Averaging	NA	NA	M_θ	FP_θ
Token-Level Routing	$n_L \times n_\tau$	High	$M_\theta \times n_\tau + M_h \times n_L$	$FP_\theta + FP_h \times T \times n_L \times n_\tau$
Task-Level Routing	n_τ	Middle	$M_\theta \times n_\tau + M_h$	$FP_\theta + FP_h \times n_\tau$
Mediator	n_τ	Low	$M_\theta \times (c_{avg} + c_{route} \times n_\tau \times c) + M_h$	$FP_\theta + FP_h \times n_\tau$

1315 2. **Bayesian deep learning.** This direction reviews some works of the Bayesian deep learning,
 1316 discussing the uncertainty and Bayesian model averaging.

1317 3. **OOD Detection & Generalization.** This direction reviews some works of the OOD Detection
 1318 and Generalization, shedding light on deployment of the model merging on the out-of-distribution
 1319 data.

1320 4. **Model compression.** This direction shortly review some works about the model compression, in
 1321 which many methods can be directly applied into our framework to further reduce the memory
 1322 costs. Note that in our paper we propose a general framework instead of a new model compression
 1323 method. Different model compression methods can be combined into our framework.

1324 5. **Data Synthesis.** This direction reviews some works about how to generate new synthetic data to
 1325 improve the model merging performance. In our framework, we exploit the CoT to generate new
 1326 synthetic data to improve the finetuning performance on downstream tasks, which is a real-world
 1327 downstream task instead of traditional model fine-tuning using the in-domain training and testing
 1328 data.

C.1 AVERAGING-BASED MODEL MERGING

1330 Model merging, also known as model fusion, combines the parameters of multiple separate models
 1331 with different capabilities to create a universal model. In this paper, we temporarily focus on models
 1332 that have the same architecture but different parameters that are finetuned on different downstream
 1333 tasks.

1334 **Basic Averaging.** The traditional approach to merge different trained or finetuned models is to evenly
 1335 average the parameters of different models (Utans, 1996; Shoemake, 1985). This process does not
 1336 require access to the original training data and allows for enhanced performance without the need
 1337 for expensive computation. However, the performance of these simply weight averaging is generally
 1338 unsatisfactory.

1339 Some related directions of model averaging also include Federated learning (FL) (McMahan et al.,
 1340 2017; Tang et al., 2020). In FL, the model averaging is performed on the server side to reduce
 1341 the communication costs after the local training. Many methods have been proposed to stable and
 1342 smooth the model averaging process (Wang et al., 2020a; Jhunjhunwala et al., 2024a; Yurochkin
 1343 et al., 2019a; Singh and Jaggi, 2020; Wang et al., 2020b; Tang et al., 2024c; 2022) to enhance the
 1344 averaging performance. Different from the multi-rounds FL, the model merging is performed in a
 1345 single round, which is more similar to the one-shot FL (Guha et al., 2019; Tang et al., 2024d).

1346 **Weighted Averaging.** Rethinking the cause of the poor performance of the basic averaging method,
 1347 many works propose to use the weighted averaging method to improve the merging performance.

1350
 1351 Intuitively, different model parameters have different importance on downstream tasks. Such a
 1352 heterogeneity of the parameter importance motivates other research directions including model
 1353 sparsification (Sun et al., 2024; Dong et al.; 2024; Tang et al., 2020), continual learning (Robins,
 1354 1995; Kirkpatrick et al., 2017; Zhu et al., 2024; Marczak et al., 2024) and FL (Jhunjhunwala et al.,
 1355 2024a; Yurochkin et al., 2019a; Singh and Jaggi, 2020). Thus, to avoid the important parameters being
 1356 overwhelmed by the unimportant parameters, during averaging, we can assign large weights to those
 1357 important parameters. To this end, the importance measurement is crucial. Many works propose to
 1358 use *first or second orders of Taylor expansion* to measure the importance of the parameters (Lee et al.,
 1359 2019; Jhunjhunwala et al., 2023; Qu et al., 2022). Some works employ *local linearization and task*
 1360 *vectors* to measure the importance of the parameters (Zhou et al., 2024). The *fisher information* also
 1361 a kind of importance measurement (Matena and Raffel, 2022; Jhunjhunwala et al., 2024b; Thennal
 1362 et al., 2024; Jhunjhunwala et al., 2024a; Thennal et al., 2024; Daheim et al., 2024).
 1363

1364 While these importance measurement methods can improve the merging performance than the basic
 1365 averaging method, they still face some typical challenges.
 1366

- 1367 1. *Require Calibration Dataset.* The importance measurement is based on the calibration dataset.
 1368 In the LLM era, the pretrained dataset is significantly large, it is difficult to collect the complete
 1369 pretrained dataset and measure the importance of the parameters on it.
 1370
2. *Computation Costs.* Because that the importance measurement is based on the calibration dataset,
 1371 the computation costs is almost similar to conduct the complete forward process of the different
 1372 models. In traditional small models, such a computaton cost is acceptable. However, in the LLM
 1373 era, the model size is significantly large, such a computation cost is unbearable.
 1374
3. *Unaddressed Parameter Conflicts.* While methods in these importance based weighted averaging
 1375 methods can improve the merging performance, they still face the parameter conflicts between
 1376 different models. Because of the highly non-convex structure of the LLMs, it is difficult to find a
 1377 optimal merging method based on averaging the parameters of different models.
 1378

1379 **Subspace Averaging.** Considering that the neural networks are over-parameterized, removing most
 1380 of the parameters from the model barely affects its accuracy (He and Xiao, 2023; Choudhary et al.,
 1381 2020). Besides, during the training or finetuning, some parameters might be optimized towards a
 1382 random direction which has small impact on the model performance (Yadav et al., 2023b). Thus,
 1383 works propose to firstly process different models in a subspace manner. Then, the parameter conflicts
 1384 can be mitigated by the subspace averaging methods (Deep et al., 2024; He et al., 2024b).
 1385

1386 DARE (Drop and Rescale) (Yu et al., 2024b;c) introduces a parameter pruning and rescaling strat-
 1387 egy that significantly reduces the number of parameters in SFT models while preserving their
 1388 performance, thereby serving as an effective preprocessing step for model merging. Similarly,
 1389 Model Breadcrumbs (Davari and Belilovsky, 2023) enhances sparsification by eliminating both
 1390 low-magnitude parameters and outlier parameters with exceptionally high weights, thereby reducing
 1391 noise and improving the generalization of hyperparameters during model merging.
 1392

1393 TALL-masks (Wang et al., 2024) creates task-specific mask matrices based on predefined thresholds
 1394 tailored to individual models, while Model Tailor (Zhu et al., 2024) further refines this approach
 1395 by masking parameters according to their sensitivity to loss changes and deviations from pre-
 1396 trained values. APL (Kong et al., 2024) advances parameter importance estimation through causal
 1397 interventions, providing a robust metric for selective parameter retention.
 1398

1399 EMR-Merging (Huang et al., 2024) departs from traditional model merging by maintaining a shared
 1400 model across multiple tasks alongside sparse task-specific models, where each shared parameter is
 1401 determined by the maximum value among corresponding parameters from all models. Concrete (Tang
 1402 et al., 2023) further innovates by framing mask construction and model merging as a learnable bi-level
 1403 optimization problem, with the outer level optimizing the mask matrix and the inner level performing
 1404 model merging and optimization utilizing unlabeled test samples.
 1405

1406 Task Arithmetic (Ilharco et al., 2022) exploits parameter-space arithmetic operations, treating model
 1407 parameters as vectors and employing addition and subtraction to synthesize new model capabilities.
 1408 However, many of these approaches, including DARE and Task Arithmetic, heavily rely on hyper-
 1409 parameters for parameter fusion, which can negatively impact the performance of model merging.
 1410 Additionally, as highlighted in studies such as TIES (Yadav et al., 2023a) and Crisostomi (Crisostomi
 1411

et al., 2024), model merging often encounters parameter conflicts that degrade performance when integrating multiple models.

Addressing these challenges, TIES (Trim, Elect, and Disjoint Merge) (Yadav et al., 2023a) implements a comprehensive approach by trimming parameters based on magnitude, selecting relevant weights, and disjointly merging weights using outcomes from task arithmetic operations. This methodology mitigates parameter conflicts and enhances the overall performance of the merged model, positioning TIES as a robust solution in the domain of model merging.

C.2 ROUTING-BASED MODEL MERGING.

Average-based methods primarily aim to enhance the averaging process of client models. However, the inherently non-linear architecture of deep neural networks complicates the derivation of a globally comparable model through simple averaging.

The basic, weighted-based, and subspace-based merging methods are *static* merging techniques. This implies that the merged model remains consistent across all samples or tasks. Given the variability among input samples and tasks, the model’s performance can fluctuate when processing diverse inputs. To this end, certain studies advocate for the *dynamic* merging of models (or subsets of layers) tailored to specific samples or tasks (Li et al., 2024c; Muqeeth et al., 2024; Tang et al., 2024b; Lu et al., 2024a; Kang et al., 2024; Tang et al., 2024d; Shen et al., 2024) during the inference phase.

For each input instance, SMEAR (Muqeeth et al., 2024) initially computes a weighted average of the parameters from each expert by leveraging the distribution of router inputs to the expert modules. This approach maintains a computational cost comparable to that of a single expert. Similarly, Twin-Merging (Lu et al., 2024a) adaptively integrates task-shared and task-specific knowledge based on routing mechanisms during inference. In the same vein, Weight-Ensembling MoE (Tang et al., 2024b) introduces a dynamic merging Transformer architecture. This method identifies that the parameters of the linear layer in the fine-tuned model undergo more significant changes compared to the nonlinear layers, which adversely affects merging performance. Consequently, Weight-Ensembling MoE employs a standard weighted average for all modules except the linear layer, which is dynamically weighted and merged based on the routing network (utilizing sample features as input and merging coefficients as output) during inference. PWE MoE (Tang et al., 2024e) extends Weight-Ensembling MoE to a multi-objective optimization framework, incorporating the preference vector as an input for routing.

AdaMerging (Yang et al., 2024b) adaptively learns merging coefficients in a task-aware or layer-wise manner, offering an automated and unsupervised approach to task arithmetic. While this method significantly enhances performance, it incurs high computational costs. *PCB Merge* (Du et al., 2024) introduces a parameter importance detection mechanism that accounts for parameter conflicts and employs heuristic algorithms to explore model fusion parameters, thereby achieving superior results. *TwinMerge* (Lu et al., 2024b) utilizes LoRA or SVD techniques in conjunction with supervised training for parameter fusion, resulting in improved performance.

Nevertheless, these methods encounter inherent limitations. Both AdaMerging and PCB Merge utilize static fusion approaches, which can lead to performance degradation when the actual sample distribution varies during runtime. Meanwhile, TwinMerge performs parameter fusion at the task level; however, the application of LoRA and SVD matrix decomposition markedly reduces model accuracy and introduces substantial online computational overhead. Besides, the code implementation of the TwinMerge actually exploits the LoRA finetuning to replace SVD decomposition. Using SVD decomposition in compressing model parameters leads to disturbed LLMs and significantly degraded model performance.

Mixture-of-Experts (MoE) (Jacobs et al., 1991; Jordan and Jacobs, 1994) is a foundational model concatenation and routing strategy comprising multiple expert networks and a router that dynamically selects relevant experts based on the input. This methodology has been extensively adopted in large language models, offering significant reductions in computational costs while preserving model performance. Recent studies, particularly sparse gated MoE (Shazeer et al., 2017) in transformer-based large language models (Lepikhin et al., 2020), have concentrated on maintaining load balancing among experts during training (Zhou et al., 2022; Jiang et al., 2024b), reducing training costs (Dai

et al., 2024), and mitigating performance degradation due to uncoordinated expert training (Chi et al., 2022).

Upcycling Methods have been developed to alleviate the high computational demands of training MoE models from scratch by initializing experts from existing dense models. These methods encompass copying existing dense models as experts (He et al., 2024a; Wei et al., 2024a), introducing noise to the MLP layers of dense models to create experts (Noise upcycling) (Chen et al., 2024), and drop upcycling (Anonymous, 2024), which combines parameter dropout with expert copying during training to enhance model robustness, reduce overfitting, and improve performance.

Branch-Train-Merge (BTM) (Li et al., 2022) and *Branch-Train-Mix (BTX)* (Sukhbaatar et al., 2024b) are methodologies aimed at further optimizing model training efficiency. These approaches employ different SFT-trained dense models derived from the same base LLM as MoE experts. The experts are interconnected via a router without necessitating additional training, while non-expert components are amalgamated through model merging techniques such as parameter averaging. Only the router undergoes training, thereby substantially reducing overall training costs. Although these methods achieve lower training expenses and marginally outperform traditional model merging approaches, our research indicates that token-level routing can partially degrade model performance. Additionally, maintaining all experts in GPU memory leads to significant parameter redundancy and escalates inference costs, which motivates our ongoing research endeavors.

However, the token-level routing methods are not suitable for model merging. We have provided detailed discussions in the main text Section 4.1 and Appendix D. The token-level routing methods after merging normally require re-training based on all training datasets to obtain a better token-level router, which significantly increases the computational costs, which is discussed in the main text Section 4.4 and Appendix G.

LoRA based Routing. Routing samples to different LoRA experts is a promising direction to dynamically route the input to different LoRA experts. This direction includes the *LoraHub* (Huang et al., 2023b) and *sLora* (Babakniya et al., 2023), which explore serving multiple LoRA adapters through techniques like unified paging and tensor parallelism. However, these methods do not consider the better dynamic expert merging method to further improve the model merging performance. In real-world applications, the input distribution is dynamic and the input samples are diverse, which motivates our ongoing research endeavors. Besides, their reliance on LoRA matrix decomposition significantly degrades model serving performance. Additionally, they do not consider model compression opportunities or the potential to average similar layers between models, which could further optimize storage and computation costs while maintaining model capabilities.

C.3 LAYER-WISE TRAINING DYNAMICS AND OPTIMIZATION

Layer-wise training was initially explored to achieve effective initialization (Hinton et al., 2006; Bengio et al., 2006). From the perspective of the information propagation (Tishby et al., 2000; Mahabadi et al., 2021; Tishby and Zaslavsky, 2015), the fundamental issue with layer-wise training is that each layer is unable to access information from the layers that precede it. Some works (Xiong et al., 2020) proposed a method that permits backpropagation within a local block, allowing information from subsequent layers to progressively influence earlier layers by training them sequentially. Furthermore, (Gomez et al., 2022) builds upon the concept of “overlapping local updates”, introducing a learning strategy that harmonizes the high parallelism characteristic of layer-wise training with the superior predictive accuracy associated with end-to-end (E2E) learning. Besides, classification-based loss functions are employed at each layer (Mostafa et al., 2018; Belilovsky et al., 2019; 2020), whereas similarity-based loss functions are utilized in other scenarios (Kulkarni and Karande, 2017; Nøkland and Eidnes, 2019; Siddiqui et al., 2023). Additionally, (Wang et al., 2020c) incorporates a reconstruction error term into the local objective function, drawing from an information-theoretic perspective.

Some works find that different layers have different convergence rates during the whole training process (Raghu et al., 2017). This property can be used to freeze front layers and only train the later layers, thus reducing the training costs. The PipeTransformer (He et al., 2021) utilizes this property to reduce the training costs of transformer models.

1512 LISA (Pan et al., 2024) discovered that the weight norm distributions across layers in LoRA and full
 1513 parameter fine-tuning are skewed, indicating varying layer importance in large-scale LLM training.
 1514 Based on this observation, LISA applies importance sampling to different layers in LLMs, randomly
 1515 freezing most intermediate layers during optimization. It periodically samples Transformer layers
 1516 from the model, randomly selecting r layers for fine-tuning while keeping others frozen. The initial
 1517 word/position embeddings (wte/wpe) and final language modeling head (lm_head) are consistently
 1518 fine-tuned. This aligns with our observations regarding layer merging.

1519 Layer-wise model training and merging approaches have also provided inspiration for our research
 1520 direction. (Li et al., 2024d) discovered that in the field of large language models, the effectiveness
 1521 of deeper layers gradually diminishes, with many studies showing that deeper layers can be pruned
 1522 without significantly affecting model performance - a phenomenon often viewed as an opportunity for
 1523 model compression. To address this, they proposed a novel normalization technique called Mix-LN,
 1524 which combines pre-LN and post-LN within the same model. Specifically, Mix-LN applies post-LN
 1525 to earlier layers and pre-LN to deeper layers, ensuring more uniform gradients across all layers.

1526 Different from these methods that focus on improving the layer-wise training and optimization, we
 1527 focus on improving merging LLMs inspired from the layer-wise training dynamics.

1529 C.4 BAYESIAN DEEP LEARNING

1530 **Bayesian Neural Networks.** Considering the uncertainty of the model parameters, sampling bias in
 1531 the training datasets, predictive uncertainty to domain shift (also referred to as out-of-distribution
 1532 examples) (Lakshminarayanan et al., 2016; Blundell et al., 2015; Hendrycks and Gimpel, 2016),
 1533 Bayesian Neural Networks (BNNs) view the model parameters as a random variable. Then, optimizing
 1534 the model parameters is equivalent to optimizing the posterior distribution of the model parameters
 1535 conditioned on the training datasets) (Blundell et al., 2015). However, the training costs of BNNs
 1536 are significantly higher than the non-Bayesian neural networks (Lakshminarayanan et al., 2016).
 1537 A proper scoring criterion for training non-Bayesian NN (Lakshminarayanan et al., 2016), model
 1538 ensemble (Guo et al., 2017) and adversarial training (Goodfellow et al., 2014) are found to be a good
 1539 way to improve the robustness of neural networks as an alternative to BNNs.

1540 **Bayesian Model Averaging (BMA).** Except for the static importance measurement mentioned in
 1541 previous section, Bayesian model averaging is another promising direction to improve the model
 1542 merging performance based on the Bayesian inference. The deep model ensemble and Stochastic
 1543 Weight Averaging (Izmailov et al., 2018; Maddox et al., 2019) are actually a compelling approach
 1544 to BMA (Wilson and Izmailov, 2020). The Bayesian marginalization can particularly improve the
 1545 accuracy and calibration of modern deep neural networks (Wilson and Izmailov, 2020).

1546 However, the previous works in BNN and BMA consider the model parameters trained with the same
 1547 datasets. How to merge models trained with different datasets is a new open problem which also
 1548 emerges in FL (Tang et al., 2024d; Liu et al., 2024a; 2021; Al-Shedivat et al., 2020; Yurochkin et al.,
 1549 2019b; Wang et al., 2020d) and merging LLM models in pretraining (Liu et al., 2024b).

1551 C.5 OOD DETECTION AND GENERALIZATION

1552 The input test samples in the real-world deployment are usually diverse and the distribution of the
 1553 input test samples is dynamic. Normally, these samples are not shown in the training datasets, and their
 1554 distribution might be different from the training distribution, which is called out-of-distribution (OOD)
 1555 data. It is important to detect the OOD data (**OOD Detection**) (Liu et al., 2020; Hendrycks and Gimpel,
 1556 2016) and improve the model generalization on the OOD data (**OOD Generalization**) (Ovadia et al.,
 1557 2019; Kendall and Gal, 2017; Lakshminarayanan et al., 2016). When confronted with distributional
 1558 shifts, models optimized purely based on average training errors lead to poor performance (Duchi
 1559 and Namkoong, 2018; Arjovsky et al., 2019; Creager et al., 2021).

1560 **OOD Generalization.** Some methods seek to find better invariant representations in neural net-
 1561 works (Bengio et al., 2013; Locatello et al., 2019), which means the representations are invariant to
 1562 the distribution shift. From the causal perspective, the invariant representations are the representations
 1563 that are invariant to the causal factors (Yang et al., 2021). Causal learning methods aim to learn the
 1564 underlying causal structure of the data and to predict the outcome variable based on the identified
 1565 causal variables. By correctly identifying the cause-effect relationships, these methods are expected

1566 to perform well even when the data distribution changes, as the underlying causal structure is often as-
 1567 sumed to remain invariant across different environments or domains (Bühlmann, 2018). The invariant
 1568 learning is to learn an invariant representation or model across environments leveraging contextual
 1569 information such as domain labels (Muandet et al., 2013; Arjovsky et al., 2019; Albuquerque et al.,
 1570 2020), where methods can be mainly divided into invariant risk minimization (Arjovsky et al., 2019)
 1571 and domain-irrelevant representation learning (Li et al., 2018; Gong et al., 2019; Sicilia et al., 2021).

1572 **OOD Detection.** Some methods assume access to extensive OOD data alongside in-distribution (ID)
 1573 data during training, formulating OOD detection as a discriminative classification task by allocating a
 1574 special label for OOD samples (Fei and Liu, 2016; Larson et al., 2019; Kamath et al., 2020; Kim
 1575 and Kim, 2018). Another approach optimizes outlier exposure regularization terms on OOD samples
 1576 to refine the representations and OOD scores, such as the generalized outlier exposure (OE) loss
 1577 introduced by (Hendrycks et al., 2019), which pushes the predicted distribution of OOD samples
 1578 toward uniformity (Hendrycks et al., 2019; Lee et al., 2018), and entropy regularization objectives
 1579 employed by (Zeng et al., 2021a) to enforce high entropy predictions for OOD samples. Additionally,
 1580 leveraging contrastive learning techniques (Zeng et al., 2021b; Zhou et al., 2021; Cho et al., 2022;
 1581 Mou et al., 2022) to increase inter-class discrepancies and enhance discriminative features for ID and
 1582 OOD samples has been demonstrated to improve OOD detection performance.

1583 Previous works have found that the softmax outputs from models can be used as a measurement of the
 1584 uncertainty of model predictions (Guo et al., 2017; Hinton et al., 2015). And the early work in model
 1585 distillation utilizes the softmax outputs as a kind of soft labels to guide the model training (Hinton
 1586 et al., 2015). Some works propose to scale the logits with the temperature scaling (Liang et al., 2017),
 1587 thus the ID and OOD samples are more distinguishable based on the scaled softmax scores.

1588 Our work proposes dynamically merging task arithmetics from the Bayesian perspective to improve
 1589 the OOD generalization. Inspired by the temperature scaling and the uncertainty measurement,
 1590 we propose to scale the logits with the temperature scaling and to use the softmax outputs as an
 1591 adjustment factor to estimating the likelihood of the task arithmetics conditioned on the input.

1593 C.6 MODEL COMPRESSION

1595 **Pruning.** *Unstructured pruning* (Frantar and Alistarh, 2023; Sun et al., 2024; Shao et al., 2024;
 1596 Zhang et al., 2024; Dong et al.; Tang et al., 2020) effectively maintains LLM performance without
 1597 requiring retraining, but leads to irregular structures that necessitate specialized optimizations for
 1598 inference. SparseGPT (Frantar and Alistarh, 2023) offers a novel one-shot pruning strategy by
 1599 framing it as a sparse regression problem, achieving over 50% sparsity with minimal perplexity
 1600 increase. Wanda (Sun et al., 2024) reduces weight update costs by pruning low-magnitude weights
 1601 scaled by input activations, while SAMSP (Shao et al., 2024) adjusts sparsity based on weight
 1602 sensitivity using the Hessian matrix. DSnoT (Zhang et al., 2024) iteratively prunes and grows weights
 1603 to minimize reconstruction error in sparse models.

1604 *Structured pruning* is hardware-agnostic, facilitating accelerated inference but may degrade per-
 1605 formance due to the removal of critical components, often necessitating fine-tuning. Loss-based
 1606 Pruning (Molchanov et al., 2019) measures the impact of unit removal on loss. LLM-Pruner (Ma et al.,
 1607 2023) uses gradient information to identify dependent structures for optimal pruning. In contrast,
 1608 Shortened LLaMA (Kim et al., 2024) focuses on depth pruning of Transformer blocks based on
 1609 loss derivatives, employing LoRA to quickly recover performance post-pruning. Magnitude-based
 1610 Pruning (Han et al., 2015) assesses pruning unit importance based on their magnitudes, pruning those
 1611 below a set threshold. Regularization-based Pruning (Wen et al., 2016) incorporates regularization
 1612 terms to induce sparsity.

1613 Different from these pruning methods which focus on the weight pruning, our method is inspired
 1614 from the sparse property of the task arithmetics to reduce the expert memory occupation (He et al.,
 1615 2025; Tang et al., 2020). We sparsify the task arithmetics based on denoising and the magnitudes
 1616 in our work. Note that our framework is a general framework, any other sparsity method can be
 1617 combined with our framework.

1618 **Quantization.** Weight-only quantization is the most conventional and widespread method. For
 1619 example, LUT-GEMM (Park et al., 2024) uses binary-coding quantization (BCQ) (Rastegari et al.,
 2016) format, which factorizes the parameters of LLMs into binary parameters and a set of scaling

1620 factors, to accelerate quantized matrix multiplications in weight-only quantization. GPTQ (Frantar
 1621 et al., 2023) proposes a layer-wise quantization method based on Optimal Brain Quantization
 1622 (OBQ) (Frantar and Alistarh, 2022), which updates weights with inverse Hessian information, and
 1623 quantizes LLMs into 3/4-bit. QuIP (Chee et al., 2023) optimally adjusts weights by utilizing the
 1624 LDL decomposition of the Hessian matrix derived from vectors drawn uniformly at random from
 1625 a calibration set, and multiplies weight and Hessian matrices with a Kronecker product of random
 1626 orthogonal matrices to ensure incoherence between weight and Hessian matrices. Combining these
 1627 two steps, QuIP successfully quantizes LLMs into 2-bits with minimal performance loss.

1628 To further minimize quantization errors in the weight-only quantization of LLMs, lots of works
 1629 identify sensitive weights, which have an important effect on LLMs' quantization performance, and
 1630 store these sensitive weights in high precision. For example, AWQ (Lin et al., 2023) stores the top
 1631 1% of weights that have the most significant impact on LLM performance in high-precision, and
 1632 integrates a per-channel scaling method to identify optimal scaling factors. Here, "channel" denotes
 1633 individual dimensions or feature maps within the model. Similar with AWQ, OWQ (Lee et al., 2024)
 1634 store weights sensitive to activation outliers in high-precision, and quantizes other non-sensitive
 1635 weights. Different from OWQ, SpQR (Dettmers et al., 2024) employs the L2 error between the
 1636 original and quantized predictions as a weight sensitivity metric. Furthermore, SqueezeLLM (Kim
 1637 et al., 2023) introduces a weights clusters algorithm based on sensitivity, using k-means centroids as
 1638 quantized weight values, to identify sensitive weights.

1640 C.7 DATA SYNTHESIS

1641 **Data Labeling.** The data labeling process utilizes the advanced language comprehension capabilities
 1642 of large language models (LLMs) to annotate extensive unlabeled datasets, proving particularly
 1643 beneficial in areas like cross-lingual processing and multimodal learning (Zhu et al., 2023; Gilardi
 1644 et al., 2023; Alizadeh et al., 2023). Automating this process enhances data preparation efficiency.
 1645 Recent studies have investigated the zero-shot potential of models like GPT-4 for annotating political
 1646 discourse on platforms like Twitter (Törnberg, 2023). Some works consider constructing a preference
 1647 tree (Zeng et al., 2024; Yuan et al., 2024) from LLM responses to refine incorrect responses based on
 1648 feedback from models like GPT-4, creating more diverse and robust preference data.

1649 **Data Reformation.** Data reformation aims to transform existing datasets into diverse variations
 1650 to improve data augmentation (Dixit et al., 2022; Dunlap et al., 2023). This enriches the training
 1651 set with varied examples, enhancing model robustness and generalization. Novel approaches
 1652 leveraging LLMs have emerged, such as Disco by Chen et al. (Chen et al., 2022), which generates
 1653 large-scale, high-quality counterfactual datasets. A prominent method in this area is in-context
 1654 learning (Dong et al., 2022), where examples embedded in prompts guide LLMs to generate re-
 1655 sponds that reflect the provided patterns. Early works, such as Self-Instruct (Wang et al., 2023) and
 1656 Unnatural Instructions (Honovich et al., 2022), utilized task pools with hand-crafted seed examples.
 1657 In contrast, LaMini-LM (Wu et al., 2023) built on this foundation by leveraging extensive data
 1658 from Wikipedia to generate a wider range of instructions. Auto Evol-Instruct (Zeng et al., 2024),
 1659 originally designed to evolve instructions, automates the optimization of evolution rules through an
 1660 Optimizer LLM that iteratively refines these rules based on evolving feedback data. Furthermore,
 1661 Instruction Backtranslation (Li et al., 2023a) enhances instruction-following capabilities by creating
 1662 instruction-response pairs from unannotated data, thus minimizing the need for manual annotation.
 1663 This ongoing refinement of data reformation is essential for enhancing performance across various
 1664 tasks.

1665 **Generation from LLMs.** Model generation utilizes powerful models—such as ChatGPT, StableVi-
 1666 cuna, and GPT-4—to create datasets that enhance the performance of weaker models. Techniques
 1667 include generating concise narratives through templates (Eldan and Li, 2023) and assessing dataset
 1668 quality with LLMs. Research by Phi-1 and its subsequent studies (Gunasekar et al., 2023; Li et al.,
 1669 2023b) indicates that even a small volume of high-quality data can effectively train models via
 1670 generated textbooks and exercises using GPT-3.5. Additionally, performance has been improved by
 1671 developing instructional datasets and fine-tuning models to enhance dataset quality (Honovich et al.,
 1672 2022; Taori et al., 2023a; Chen et al., 2023). Domain model generation concentrates on the use of
 1673 specialized models to produce domain-specific data. For example, domain generation can provide
 instructional materials for specific programming tasks in coding (Wei et al., 2024b; Luo et al., 2024).

1674 In mathematics, initiatives like Minerva (Lewkowycz et al., 2022) and DeepSeekMath (Xin et al.,
 1675 2024) focus on generating accurate solutions.

1676 **Synthetic Multi-step Reasoning.** To enhance reasoning in LLMs, additional reasoning steps are
 1677 incorporated into data synthesis. The MMIC framework (Liu et al., 2024c) iteratively creates
 1678 synthetic question-response pairs by expanding problems and integrating reasoning steps while
 1679 preserving logical structure. A complementary strategy involves generating chain-of-thought (CoT)
 1680 answers based on questions (Li et al., 2024e). Building on question-CoT pairs through Self-Instruct,
 1681 MathInstruct (Yue et al., 2023b) introduces the Program-of-Thought (PoT) rationale to streamline
 1682 mathematical problem-solving.

1683 In this work, we utilize the stronger LLM to generate CoT based domain training data to enhance the
 1684 reasoning performance of the downstream tasks. As far as we know, *this work is the first to explore*
 1685 *whether the model merging influences the CoT based reasoning performance.*

1687 D THEORETICAL UNDERSTANDING

1688 In this section, we provide the theoretical interpretation from the perspective from the In-context
 1689 learning (ICL) to further understand why routing *finetuned models* with task-level router instead of
 1690 token-level ones might be better. Note that here the *different finetuned models have been trained*
 1691 *on individual tasks and never see other tasks*. We re-write the preliminary in Section 2 here for
 1692 convenience of reading.

1693 **Task Data Distribution.** Given a set of different downstream tasks \mathcal{T} , based on the sampling task
 1694 $\tau \in \mathcal{T}$, the pretraining document (data sample) is a sequence $o_{1:T}$ of tokens with the maximum
 1695 length T generated from a distribution $p_\tau = p(x_{1:T}|\tau) = p(o_1, \dots, o_T|\tau)$ (Xie et al., 2022; Wies
 1696 et al., 2023; Hahn and Goyal, 2023; Li et al., 2024a).

1697 **Pretraining Data Distribution.** And we define the pretraining data is sampled from $p(o|\mathcal{T}^*) =$
 1698 $\int_{\tau^* \in \mathcal{T}^*} p(o_1, \dots, o_T|\tau)p(\tau^*)d\tau^*$. Each token o is sampled from a vocabulary \mathbb{O} . $p(\tau^*)$ is a prior
 1699 distribution about τ^* . And both $(\mathcal{T}$ and \mathcal{T}^* belong to a large task family Ω , i.e. $\mathcal{T}, \mathcal{T}^* \subset \Omega$.

1700 **Language Modeling.** Current LLMs (Brown et al., 2020; Touvron et al., 2023; Xie et al., 2022)
 1701 usually utilize the next word prediction as the language modelling, which predicts the next token
 1702 o_t given the previous tokens $o_{1:t-1}$ for all $t = 1, \dots, T$. Formally, a LLM parameterized by θ is
 1703 a distribution $f_\theta(o_t|o_{1:t-1})$. And it is pretrained on a huge corpus sampled from the pretraining
 1704 distribution $p(o_{1:T}|\mathcal{T}^*)$ (Xie et al., 2022).

1705 **Finetuning LLM.** Normally, for each downstream task $\tau \in \mathcal{T}$, finetuning LLM is to minimize the
 1706 cross-entropy loss function as below:

$$1707 L_{CE}(\theta, \tau) = - \sum_{t=1}^T \mathbb{E}[p_\tau(x_t|x_{1:t-1}) \cdot \log f_\theta(x_t|x_{1:t-1})].$$

1708 After finetuning, the model parameters θ are updated to θ_τ for each task τ .

1709 **Prompt distribution in Pretraining & Finetuing.** Following (Xie et al., 2022), a prompt is
 1710 composed of an input token sequence $o_{1:T}$ followed by an output token y . Then, the i -th training
 1711 example² that can appear in any place in the whole prompt $o_{1:T}$ is defined as O_i consisting of an
 1712 input $s_i = O_i[1:k-1]$ (the first $k-1$ tokens) followed by the output $y_i = O_i[k]$ at the end, where
 1713 the length k is fixed for simplicity.

1714 The i -th training example is independently generated as follows: 1) Generate a start hidden state h_i^{start}
 1715 from a *prompt start distribution* p_{prompt} ; 2) Given h_i^{start} , generate the example sequence $O_i = [s_i, y_i]$
 1716 from $p(O_i|h_i^{\text{start}}, \tau^\perp)$. The test input $x_{\text{test}} = s_{n+1}$ is sampled similarly. Between each example, a
 1717 special delimiter token o^{delim} “reset” the transition between examples (Xie et al., 2022). Then, the
 1718 prompt consists of a sequence of training examples (S_n) followed by the example x_{test} :

$$1725 [S_n, x_{\text{test}}] = [s_1, y_1, o^{\text{delim}}, s_2, y_2, o^{\text{delim}}, \dots, s_n, y_n, o^{\text{delim}}, x_{\text{test}}] \sim p_{\text{prompt}}. \quad (5)$$

1726 ²Here, training example in prompts means happens during the prompt learning, instead of the pretraining or
 1727 the finetuning.

Different from (Xie et al., 2022), here we distinguish the pretraining tasks (concepts) \mathcal{T}^* and the finetuning tasks (concepts) $\mathcal{T} = \{\tau_1, \tau_2, \dots, \tau_{n_\tau}\}$, from which the prompts might be sampled. We mainly consider $\tau^\perp \in \mathcal{T}$.

In-context learning setups and Assumptions. We follow other settings and assumptions in (Xie et al., 2022). With the greedy decoding (Fu et al.), sampling the next token from the language modeling $f_\theta(o_t|o_{1:t-1})$ becomes the predictor as $y = \arg \max_{o_t} f_\theta(o_t|o_{1:t-1})$. For simplicity, following (Xie et al., 2022), we consider that the finetuned LLMs have been aligned with its pretraining and finetuning data distribution, i.e. $p_{\mathcal{T}^* \cup \tau} = p(o_{1:T}|\mathcal{T}^* \cup \tau)$ for any task $\tau \in \mathcal{T}$. For convenience, we write $p_{A\tau} = p_{\mathcal{T}^* \cup \tau}$ which means that the \mathcal{T}^* is augmented with τ .

Thus, for $[S_n, x_{\text{test}}]$, the in-context learning predictor can be written as $f_{\theta_\tau}^n(x_{\text{test}}) := \arg \max_y p_{A\tau}(y|S_n, x_{\text{test}})$, which outputs the most likely prediction over the *pretraining distribution* conditioned on the *prompt distribution*. Its expected 0-1 error with n examples is $L_{0-1}(f_{\theta_\tau}^n) = \mathbb{E}_{x_{\text{test}}, y_{\text{test}} \sim p_{\text{prompt}}} [\mathbf{1}[f_{\theta_\tau}^n(x_{\text{test}}) \neq y_{\text{test}}]]$.

We define $p_\tau^i(o) := p(O[i] = o|O[1:i-1], \tau)$ of the i -th token with previous tokens and the analogous distribution $p_{\text{prompt}}^i := p_{\text{prompt}}(O[i] = o|O[1:i-1])$ under the prompt distribution. Following (Xie et al., 2022), there is a distinguishability condition formalizes when in-context learning occurs giving the downstream task τ .

The distinguishability condition is dependent on a KL divergence between the previous two distributions and the error terms ϵ_τ resulting from the distribution mismatch between the prompt and the pertaining distributions for each example. Letting $p_\tau^i(o)$ and p_{prompt}^i correspond to the task τ and and τ^\perp .

Condition D.1 (distinguishability (Xie et al., 2022)). The τ^\perp is distinguishable if for all $\tau \in \Omega$, $\tau \neq \tau^\perp$,

$$\sum_{i=1}^k \text{KL}_i(\tau^\perp || \tau) > \epsilon_\tau, \quad (6)$$

where the $\text{KL}_i(\tau^\perp || \tau) := \mathbb{E}_{O[1:i-1] \sim p_{\text{prompt}}} [\text{KL}(p_{\text{prompt}}^i || p_\tau^i)]$.

Lemma D.2. (Xie et al., 2022) let \mathcal{B} denotes the set of τ which does not satisfy Condition D.1. We assume that $\text{KL}(p_{\text{prompt}}(y_{\text{test}}|x_{\text{test}}))||p(y_{\text{test}}|x_{\text{test}}, \tau)$ is bounded for all τ and that τ^\perp minimizes the multi-class logistic risk as,

$$L_{CE}(\tau) = -\mathbb{E}_{x_{\text{test}} \sim p_{\text{prompt}}} [p_{\text{prompt}}(y_{\text{test}}|x_{\text{test}}) \cdot \log p(y_{\text{test}}|x_{\text{test}}, \tau)]. \quad (7)$$

If

$$\mathbb{E}_{x_{\text{test}} \sim p_{\text{prompt}}} [\text{KL}(p_{\text{prompt}}(y_{\text{test}}|x_{\text{test}}))||p(y_{\text{test}}|x_{\text{test}}, \tau)] \leq \epsilon_\tau, \quad \forall \tau \in \mathcal{B}, \quad (8)$$

then

$$\lim_{n \rightarrow \infty} L_{0-1}(f_{\theta_\tau}^n) \leq \inf_f L_{0-1}(f) + g^{-1} \left(\sup_{\tau \in \mathcal{B}} (\epsilon_\tau) \right), \quad (9)$$

where $g(\nu) = \frac{1}{2}((1-\nu)\log(1-\nu) + (1+\nu)\log(1+\nu))$ is the calibration function (Steinwart, 2007; Pires and Szepesvári, 2016) for the multiclass logistic loss for $\nu \in [0, 1]$.

Following (Kleijn and der Vaart, 2012; Xie et al., 2022), the task parameter τ is assumed to have the continuity, where the KL divergence is assumed to have the 2nd-order Taylor expansion. Then, we have the following theorem and proof.

Theorem D.3. (Xie et al., 2022) Let the set of τ which does not satisfy Equation 6 in Condition D.1 to be \mathcal{B} . Assume that KL divergences have a 2nd-order Taylor expansion around τ^\perp :

$$\forall j > 1, \quad \text{KL}_i(\tau^\perp || \tau) = \frac{1}{2}(\tau - \tau^\perp)^\top I_{j, \tau^\perp}(\tau - \tau^\perp) + O(\|\tau - \tau^\perp\|^3) \quad (10)$$

where I_{j, τ^\perp} is the Fisher information matrix of the j -th token distribution with respect to τ^\perp . Let $\gamma_{\tau^\perp} = \frac{\max_j \lambda_{\max}(I_{j, \tau^\perp})}{\min_j \lambda_{\min}(I_{j, \tau^\perp})}$ where $\lambda_{\max}, \lambda_{\min}$ return the largest and smallest eigenvalues. Then for $k \geq 2$ and as $n \rightarrow \infty$, the 0-1 risk of the in-context learning predictor $f_{\theta_\tau}^n$ is bounded as

$$\lim_{n \rightarrow \infty} L_{0-1}(f_{\theta_\tau}^n) \leq \inf_f L_{0-1}(f) + g^{-1} \left(O \left(\frac{\gamma_{\tau^\perp} \sup_{\tau \in \mathcal{B}} (\epsilon_{\text{start}}^\theta + \epsilon_{\text{delim}}^\theta)}{k-1} \right) \right) \quad (11)$$

1782 *Proof.* (Xie et al., 2022) By the continuity assumption, we have for any τ in \mathcal{B} that
 1783

$$1784 \quad \sum_{j=2}^k \text{KL}_i(\tau^\perp \parallel \tau) \geq \frac{1}{2} \sum_{j=2}^k (\tau - \tau^\perp)^\top I_{j,\tau^\perp} (\tau - \tau^\perp) + (k-1)O(\|\tau - \tau^\perp\|^3) \quad (12)$$

$$1787 \quad \geq \frac{1}{2}(k-1)\lambda_{\min}(I_{j,\tau^\perp})\|\tau - \tau^\perp\|^2 \quad (13)$$

$$1789 \quad \implies \|\tau - \tau^\perp\|^2 \leq \frac{\epsilon_{\text{start}}^\theta + \epsilon_{\text{delim}}^\theta}{\frac{1}{2}(k-1)(\min_j \lambda_{\min}(I_{j,\tau^\perp}))}. \quad (14)$$

1792 Using the above term to bound the last KL term (k -th token), we have:

$$1793 \quad \text{KL}_k(\tau^\perp \parallel \tau) = \frac{1}{2}(\tau - \tau^\perp)^\top I_{k,\tau^\perp} (\tau - \tau^\perp) + O(\|\tau - \tau^\perp\|^3) \quad (15)$$

$$1795 \quad \leq \frac{1}{2}(\max_j \lambda_{\max}(I_{j,\tau^\perp}))\|\tau - \tau^\perp\|^2 + O(\|\tau - \tau^\perp\|^2) \quad (16)$$

$$1797 \quad \leq \frac{(\epsilon_{\text{start}}^\theta + \epsilon_{\text{delim}}^\theta)(\max_j \lambda_{\max}(I_{j,\tau^\perp}) + O(1))}{(k-1) \min_j \lambda_{\min}(I_{j,\tau^\perp})}. \quad (17)$$

1800 Rearranging above equation, and with the defintion that $\text{KL}_k(\tau^\perp \parallel \tau) = \mathbb{E}_{x_{\text{test}} \sim p_{\text{prompt}}} [KL(p_{\text{prompt}}(y_{\text{test}}|x_{\text{test}}) \| p(y_{\text{test}}|x_{\text{test}}, \tau))]$, we have
 1801

$$1803 \quad \mathbb{E}_{x_{\text{test}} \sim p_{\text{prompt}}} [KL(p_{\text{prompt}}(y_{\text{test}}|x_{\text{test}}) \| p(y_{\text{test}}|x_{\text{test}}, \tau))] \leq \frac{(\epsilon_{\text{start}}^\theta + \epsilon_{\text{delim}}^\theta)(\max_j \lambda_{\max}(I_{j,\tau^\perp}) + O(1))}{(k-1) \min_j \lambda_{\min}(I_{j,\tau^\perp})} \quad (18)$$

1807 Combining Equation 18 with Equation 8 into Lemma D.2 completes the proof. \square
 1808

1809 **Task-level Routing.** Observing the Equation 7 in Lemma D.2, the $L_{\text{CE}}(\tau^\perp)$ is the optimal risk over
 1810 $\tau \in \Omega$. The $\tau \in \mathcal{B}$ which does not satisfy Condition D.1 means that the $\tau \in \mathcal{B}$ should be close to
 1811 τ^\perp enough. Thus, we can have $L_{0-1}(f_{\theta_\tau}^n)$ converges with $n \rightarrow \infty$ as in Lemma D.2. The task-level
 1812 routing means to route τ^\perp to the finetuned LLM that has been trained on $p(o_{1:T}|\tau^\perp)$. Thus, the
 1813 task-level routing can satisfy the requirement of $\tau \in \mathcal{B}$.

1814 **Token-level Routing.** The core motivation of using token-level routing is that different tokens
 1815 prefer different routers. Here, inspired by the distinguishability condition D.1, we can interpret the
 1816 token-level router which dynamically finds the expert model i^* for i -th token that satistifies:
 1817

$$1818 \quad \sum_i^k \arg \min_{i^*} \text{KL}_i(\tau^\perp \parallel \tau_{i^*}). \quad (19)$$

1821 However, there is distribution shift between the τ^\perp and different τ_{i^*} . Revisiting the prompt sequence
 1822 sampled as $[S_n, x_{\text{test}}] = [s_1, y_1, o_{\text{delim}}^{\text{delim}}, s_2, y_2, o_{\text{delim}}^{\text{delim}}, \dots, s_n, y_n, o_{\text{delim}}^{\text{delim}}, x_{\text{test}}] \sim p_{\text{prompt}}$, each pair
 1823 $O_i = [s_i, y_i]$ is sampled from $p(O_i|h_i^{\text{start}}, \tau^\perp)$. If the τ_{i^*} is choosed as different from τ^\perp , the
 1824 distribution shift implies that the KL_i cannot be minimized.

1825 **Out-of-distribution Cases.** While the above intuition illustrates that the task-level routing might
 1826 be more suitable for the in-distribution test data $x_{\text{test}} \sim p_{\text{prompt}}$, we illustrate that two cases of new
 1827 prompt sampling might need need combination of different LLM experts.
 1828

- 1829 • **OOD task.** Considering that the τ^\perp is different from all $\tau \in \mathcal{T}$, there might be needs to process
 1830 different tokens with different experts following equation 19.
- 1831 • **Compositional task.** Considering that $O_i = [s_i, y_i]$ might be sampled from $p(O_i|h_i^{\text{start}}, \tau_i)$, and
 1832 each τ_i is different from others, the Equation 19 may helps to find the suitable experts.
 1833

1834 However, the theoretical analysis of how Equation 19 benefits ICL is difficult and we left it as the
 1835 future work, which might also be beneficial to analyse the MoE models (Dai et al., 2024). Currently,
 we utilize the uncertainty-based model task-level routing and merging to address the OOD problem.

1836 **E DETAILED EXPERIMENT SETTIGNS**
18371838 **E.1 DETAILED EXPERIMENTAL SETUP**
18391840 **Hardware.** All experiments were conducted on an A800 GPU with 80GB VRAM, Intel Xeon 6348
1841 CPU, and 100GB RAM.1842 **Models and Datasets.** We conduct comprehensive experiments on two cutting-edge large language
1843 model families: Qwen and LLaMA. Table 13 shows the number of parameters, memory occupation
1844 and release data of these models. These models represent the latest advancements in language model
1845 development. *To the best of our knowledge, this is the first model merging study focusing primarily*
1846 *on generative tasks, finetuning with CoT based data and cutting-edge LLM tasks.*1847 **Table 13: Backbone Models Overview**
1848

Model	Number of Parameters	Release Date	Memory Occupation (GB)
Qwen-1.5-4B	4 Billion	February 2024	15.26
Qwen-2.5-7B	7 Billion	September 2024	26.00
LLaMA-3.1-3B	3 Billion	April 2024	11.31
LLaMA-3.2-8B	8 Billion	September 2024	30.52

1849 **Generative and Reasoning Tasks in Evaluation.** In designing our evaluation tasks, we strategically
1850 selected orthogonal benchmarks to effectively demonstrate our method’s capability in resolving
1851 parameter conflicts during model merging. Our task selection follows these principles:
18521853

- (1) *The mathematical reasoning and code generation tasks represent fundamentally different parameter spaces.* Specifically, mathematical computation requires numerical reasoning parameters, while code generation relies on syntax and programming logic parameters, allowing us to evaluate how well our merging approach handles potentially conflicting parameter updates.
- (2) *Knowledge-based QA (TriviaQA) and concept understanding tasks (MMLU) evaluate distinct knowledge representations.* TriviaQA focusing on factual retrieval parameters and MMLU covering broader conceptual understanding parameters across domains. This helps assess our method’s ability to preserve different types of knowledge without interference.
- (3) The logical reasoning task (WinoGrande) may prefer to yet another independent parameter space focused on *abstract reasoning*, providing insights into how well our merging technique maintains reasoning capabilities while optimizing for other tasks.

1854 Based on above principle, we utilize the following cutting-edge LLM evaluation tasks about math
1855 reasoning, code generation, common sense QA, common sense logical reasoning, multi-domain
1856 knowledge.
18571858

- **Mathematical Reasoning:** We evaluate mathematical question-answering capabilities using the
1859 GSM8K dataset (Cobbe et al., 2021), which contains 8,500 high-quality elementary school math
1860 word problems (about 7,500 training, about 1,000 test) designed to evaluate mathematical reasoning
1861 capabilities. The problems feature diverse language styles and formats while avoiding templated
1862 designs. They use basic arithmetic operations with natural language solutions.
- **Knowledge-based QA:** We utilize TriviaQA (Joshi et al., 2017), a large-scale Wikipedia-based
1863 question answering dataset, where models are required to generate direct answers without multiple-
1864 choice options. It contains complex questions requiring cross-sentence inference, with significant
1865 syntactic and lexical variations between questions and answer sentences. The dataset provides
1866 challenging evaluation scenarios that better approximate human-like question answering.
- **Code Generation:** The HumanEval (Chen et al., 2021) consists of human-written programming
1867 tasks where models must complete missing Python code snippets based on provided inputs. The
1868 problems simulate real-world programming challenges requiring context understanding, reasoning,
1869 and multi-step operations across varying difficulty levels and abstraction layers.
- **Logical Reasoning:** WinoGrande (Sakaguchi et al., 2019) is a large-scale commonsense reasoning
1870 dataset of approximately 2800 questions developed by University of Washington researchers.

1890 Questions are presented as fill-in-the-blank tasks with two options and correct answers, with dataset
 1891 bias reduced through the AfLite algorithm. The benchmark evaluates models' commonsense
 1892 reasoning abilities in understanding and generating relevant text.

1893 • **Multi-domain Knowledge:** We employ MMLU (Hendrycks et al., 2021) to assess knowledge
 1894 retention across diverse 57 subjects ranging from basic mathematics to US history, computer
 1895 science, law, and ethics. Using multiple-choice questions of varying difficulty levels. Notably,
 1896 we exploit the generation-based approach for multiple-choice evaluation, analyzing knowledge
 1897 preservation across base models, fine-tuned variants, and merged models. The generation-based
 1898 evaluation is better to measure the generative abilities of LLMs than choice-based evaluation.

1899 In the experiments of evaluating the scalability of Mediator, we also finetune another 4 LLMs
 1900 according to the following 4 extra evaluation tasks.

1902 **IFEval.** (Zhou et al., 2023) A comprehensive benchmark dataset designed to evaluate instruction-
 1903 following capabilities of language models. It contains carefully curated instruction-response pairs
 1904 across diverse task categories including text generation, analysis, and reasoning. The dataset aims
 1905 to assess models' ability to accurately interpret and execute natural language instructions while
 1906 maintaining coherence and relevance in responses. The evaluation spans multiple dimensions
 1907 including instruction comprehension, output quality, and adherence to specified constraints.

1909 **CEval.** (Huang et al., 2023a) A comprehensive Chinese evaluation suite designed to assess
 1910 language models' knowledge and capabilities across various academic and professional domains.
 1911 It consists of multiple-choice questions drawn from professional qualification exams and academic
 1912 tests in China. For our evaluation, we specifically focus on three key subjects: (1) *Medicine*: testing
 1913 clinical knowledge, diagnosis, and treatment principles from medical licensing exams; (2) *College
 1914 Economics*: evaluating understanding of micro/macroeconomics concepts, market principles, and
 1915 economic theories; (3) *Law*: assessing comprehension of Chinese legal principles, regulations, and
 1916 judicial procedures. These subjects were chosen to evaluate models' domain-specific expertise in
 1917 technically demanding professional fields.

1918 **Finetuning Settings.** We adopt the ms-swift (Zhao et al., 2024) to finetune the given pretrained
 1919 LLM. The finetuning datasets are constructed by augmenting some publicly datasets (task related
 1920 but without overlap) with GPT-4o (Gilardi et al., 2023) and Chain-of-Thoughts (Wei et al., 2022).
 1921 For each finetuning process, we use at least 180K training samples to ensure sufficient performance
 1922 improvement on the corresponding task, which helps validate the effectiveness of our experiments.
 1923 We provide the details of how we construct the finetuning datasets in Section H.

1924 **Baselines.** Following the summary of the related works in Section C, we compare methods in
 1925 following four categories:

- 1926 • **Pretrained model.** The pretrained models are directly downloaded from its open-source
 1927 repository. These models are pretrained on the large corpus and have included enormous
 1928 knowledge about the evaluation tasks.
- 1929 • **Finetuned Models:** We finetune the pretrained models on datasets that we construct for
 1930 each domain. Then, each finetuned model is evaluated on all tasks. The results help to show
 1931 whether finetuning on task A enhance or decrease model performance on task B.
- 1932 • **Static merging methods.** These methods use fixed weights to merge multiple finetuned
 1933 models. The advanced static merging methods like Fisher merging (Matena and Raffel,
 1934 2022) and RegMean (Jin et al., 2023) require extra dataset and forward process to estimate
 1935 some information like gradients, hessian, features to estimate parameter importance, which
 1936 causes significant computational costs. Furthermore, considering that LLMs need to be
 1937 deployed on various tasks, the utilized dataset actually cannot reflect the real-world data
 1938 distribution. Therefore, these methods are shown empirically to perform worse than some
 1939 calibration-less methods (Du et al., 2024). Recently, TIES (Yadav et al., 2023b) and PCB-
 1940 merging (Du et al., 2024) achieve the best performance in weighted average method and do
 1941 not require calibration data. Thus, we choose it for comparison.
- 1942 • **Dynamic Advanced Methods:** We compare with state-of-the-art dynamic merging tech-
 1943 niques that adapt model fusion parameters based on the input data. For example, Branch-
 train-mix dynamically routes different tokens to corresponding experts for generation

1944 through token-level routing. Similarly, the twin-merge (Lu et al., 2024b) computes merging
 1945 weights through task-level routing mechanisms and dynamically fuses SVD-decomposed
 1946 task vectors into the pretrained model in real-time.
 1947

1948 **E.2 HYPERPARAMETERS OF FINETUNING AND IMPLEMENTING BASELINES**
 1949

1950 **Hyperparameters for Single-task Finetuning.** For single-task finetuning, we utilize a set of
 1951 hyperparameters that remain consistent across all models and tasks. The learning rate is set at 1.2e-5,
 1952 applying a cosine decay schedule. The batch size varies, with one sequence per batch for both the
 1953 7B and 8B models, while the 3B and 4B models use two sequences per batch considering the GPU
 1954 memory limitation. The maximum sequence length is confined to 4096 tokens for both math and
 1955 QA tasks and extends to 7000 tokens for coding tasks. The training consists of two epochs, and we
 1956 employ the AdamW optimizer with parameters $\beta_1 = 0.9$, $\beta_2 = 0.999$, and $\epsilon = 1e - 8$. Additionally,
 1957 warmup steps constitute 5% of the total steps.
 1958

1959 For all model merging baselines, the finetuned LLMs are the same. And all finetuned LLMs have
 1960 shown that they can successfully improve the performance of the pretrained model on various tasks.
 1961 The following is the details of how we tune and implement baseline methods.
 1962

1963 **Hyperparameters for PCB-merging.** We follow the original paper of PCB merging and have
 1964 searched its hyperparameters. The weight clipping ratio is established at 0.1, which means weights
 1965 with magnitudes in the bottom 10% are clipped to zero, following recommendations from the original
 1966 paper concerning LLM generalization tasks. For model merging exploration, we perform 200 random
 1967 exploration steps. The initial weights for random exploration are set to (0.4, 0.4, 0.4, 0.4) for the
 1968 3B, 4B, 7B, and 8B models with four experts, while for all models with eight experts, they are set to
 1969 a repeated value of 0.2 across eight instances. The validation batch size is configured to handle 8
 1970 samples per task, and we implement early stopping with a patience of 10 steps without improvement.
 1971 The weight clipping ratio and exploration parameters are uniform across all model sizes and tasks to
 1972 facilitate fair comparison. It's worth noting that for the 7B and 8B models, the validation batch size is
 1973 reduced to 4 due to memory limitations.
 1974

1975 **Optimizing PCB-merging.** To enhance the computational speed of PCB-merging, several optimizations
 1976 were introduced based on the original framework, which do not influence its task performance.
 1977 Instead of merging entire models simultaneously, we adopt a layer-wise model merging strategy. This
 1978 layer-by-layer merging approach has multiple benefits: it decreases memory overhead during the
 1979 merging process, facilitates parallel processing of different layers, and allows for the assignment
 1980 of layer-specific merging weights. Moreover, we implemented asynchronous model input/output
 1981 operations which enable overlapping of I/O with computational processes. This adjustment is instru-
 1982 mental in reducing the total merging time by as much as 40%, enabling the seamless streaming of
 1983 large models. These optimizations have significantly boosted both the efficiency and effectiveness of
 1984 PCB-merging, particularly the layer-wise method, which has lowered peak memory usage by approx-
 1985 imately 60% while maintaining or enhancing final model performance. And other hyper-parameters
 1986 and settings are completely followed as the original paper.
 1987

1988 **Hyperparameters for Twin-merging finetuning.** For Twin-merging, we leverage LoRA finetuning
 1989 in lieu of SVD to attain greater precision following the original paper. The rank is set as 32, and
 1990 both the alpha and dropout parameters are also set at 32 and 0.1, respectively. The target modules
 1991 involved in this finetuning process include the query and value matrices within the attention layers.
 1992 And we also have conducted grid search for the hyper-parameters. Each task involves training over
 1993 two epochs, with a batch size set at 16; this batch size is reduced to 8 for the 7B and 8B models. The
 1994 learning rate is specified at 1.5e-4, utilizing a cosine decay schedule, and the optimizer employed is
 1995 AdamW.
 1996

1997 **Hyperparameters for Branch-train Mix (BTX).** For the training of the BTX router, we follow the
 1998 original implementation of it within ms-swift and its original paper to implement it. The relevant
 1999 hyperparameters for this setup include a training duration of 2 epochs, with a batch size of 2; this is
 2000 adjusted to 1 for the 7B and 8B models. The learning rate is established at 1.5e-6, utilizing a linear
 2001 decay schedule, alongside the AdamW optimizer, which is configured with a weight decay of 0.001.
 2002 The router's architecture consists of an input dimension derived from 2 layers of an FFN, with a
 2003 hidden dimension of 256, an output dimension corresponding to the number of experts, and a dropout
 2004 rate of 0.1. Warmup steps account for 5% of the total steps, and evaluations are conducted at every
 2005

1998 1000 steps. To ensure balanced representation, the router is trained on a dataset that equally samples
 1999 from all tasks, employing early stopping with a patience of 2 epochs based on validation accuracy.
 2000

2001 **Hyperparameters for Mediator.** For Mediator training, we utilize the same single-task finetuned
 2002 experts as delineated in Appendix E.2. The task-level router is constructed from the first 9 layers
 2003 of the pretrained LLM (with gradients stopped) and includes 2 additional FFN layers. The router
 2004 is trained on a balanced dataset with equal samples from each task domain to ensure unbiased task
 2005 routing. We evaluate the router performance every 1000 steps and use early stopping with patience
 2006 of 2 epochs based on validation accuracy. The training process for the router involves sampling
 2007 2000 examples from each task domain, specifically in mathematics, coding, question answering, law,
 2008 economics, instruction following, and medicine. The specific hyperparameters applicable to router
 2009 training encompass a duration of 2 epochs, and a batch size of 256, which is decreased to 128 for
 2010 the 7B and 8B models. The learning rate is set to 3e-4, accompanied by a cosine decay schedule,
 2011 and the optimizer remains as AdamW. The warmup ratio is defined as 10% of the total steps. The
 2012 router’s architecture features a frozen backbone comprising the initial 9 layers from the pretrained
 2013 LLM, along with 2 trainable FFN layers. These layers have a hidden dimension of 1280, with the
 2014 output dimension reflecting the number of experts, and a dropout rate fixed at 0.05.
 2015

2016 For router based selection, we use the temperature parameter β in Equation 4 as 1.5 to convert
 2017 the prediction rates into concrete merging parameters for each expert, which achieves the best
 2018 experimental results. This temperature scaling helps balance between being decisive in expert
 2019 selection while maintaining some degree of smoothness in the merging weights. A temperature of
 2020 1.5 empirically provides the optimal trade-off, where lower temperatures lead to more concentrated
 2021 weights but potentially miss useful signals from secondary experts, while higher temperatures result
 2022 in overly diffuse weights that don’t sufficiently leverage expert specialization.
 2023

2024 F THE VARIATIONS AND DETAILS OF DIFFERENT PARTS OF MEDIATOR

2025 In this section, we provide the detailed variations and implementation details of different parts of
 2026 Mediator. Some definitions and operations that appear in the main text may be re-defined in this
 2027 section for better clarity of reading.
 2028

2029 F.1 MEASURING PARAMETER CONFLICTS

2030 **Task Arithmetics.** We define the task arithmetics as the parameter difference between the finetuned
 2031 LLM θ_τ based on task τ and the pre-trained LLM θ , i.e., $\Delta_\tau = \theta_\tau - \theta$. Such a task arithmetics can
 2032 represent the update on the finetuned LLM θ_τ based on task τ . Given a pretrained LLM θ , one can
 2033 recover the finetuned LLM $\theta_\tau = \theta + \Delta_\tau$.

2034 **Denoising Parameters.** Because the finetuning directions on different tasks are various and stochastic,
 2035 there exist some elements in Δ_τ that do not influence the performance on task τ . Before measuring
 2036 the parameter conflicts (Yadav et al., 2023a; He et al., 2024b), we firstly denoise the parameters by
 2037 removing the elements in Δ_τ that do not influence the performance on task τ . We also model the
 2038 update directions of different elements as the Gaussian distribution $\mathcal{N}_{\text{UPD}}(\mu_{\text{UPD}}, \sigma_{\text{UPD}}^2)$, where μ_{UPD}
 2039 is the mean of the update direction and σ_{UPD}^2 is the variance.
 2040

2041 Based on the estimated μ_{UPD} and σ_{UPD} , we can regard the elements within range $(\mu_{\text{UPD}} - \sigma_{\text{UPD}},$
 2042 $\mu_{\text{UPD}} + \sigma_{\text{UPD}})$ as the elements that do not influence the performance on task τ . Thus, we can denoise
 2043 the parameters by removing the elements within range $(\mu_{\text{UPD}} - \sigma_{\text{UPD}}, \mu_{\text{UPD}} + \sigma_{\text{UPD}})$ (set as 0) and
 2044 obtain the new parameter arithmetic $\hat{\theta}_\tau = \theta + \hat{\Delta}_\tau$. In the deployment, these elements are saved with
 2045 their indexes and values for realistic sparsification thus saving memory.
 2046

2047 F.2 ADAPTIVE MERGING

2048 Inspired by the empirical observation in Figure 3 in Section 3, we propose to leverage the parameter
 2049 conflict distribution across different finetuned LLMs to adaptively merge the finetuned models.
 2050

2051 Practically, before merging, Mediator automatically calculates the conflicts d_l across different
 2052 finetuned LLMs. Then, Mediator models the conflicts as a Gaussian distribution $\mathcal{N}(\mu, \sigma)$. Then,

2052 for each layer index l , Mediator average layer parameters if the conflict d_l is less than the $\mu + \sigma$,
 2053 otherwise, Mediator Routing this layer. We denote the averaged layer parameters as ϕ_{AVG}^l and the
 2054 Routing layer parameters as ϕ_{UP}^l . Algorithm 1 shows this detailed process.
 2055

2056 **F.3 AVERAGING OPERATIONS**
 2057

2058 **Naive Average Operation.** The naive average operation \mathcal{M}_{AVG} is defined as:
 2059

$$2060 \quad \mathcal{M}_{\text{AVG}}(\theta_1, \theta_2, \dots, \theta_{|\mathcal{T}|}) = \frac{1}{|\mathcal{T}|} \sum_{\tau=1}^{|\mathcal{T}|} \theta_{\tau}, \quad (20)$$

$$2061$$

$$2062$$

2063 which regards all finetuned LLMs equally and utilizes the same weight for each finetuned LLM. Such
 2064 a simple average operation is easy to implement, without fabricated procedures, thus having low
 2065 computational overhead. However, different parameters may have different sensitivities to the final
 2066 merged model, which may lead to suboptimal performance.
 2067

2068 **Taylor Expansion.** The Taylor expansion is a powerful tool for approximating a function around a
 2069 specific point, and it is widely used in various fields, including model compression (Lee et al., 2019)
 2070 and previous works on model merging (Jhunjhunwala et al., 2023; Qu et al., 2022). We can utilize the
 2071 Taylor expansion to measure the sensitivity of each parameter that influences the model performance
 2072 on the downstream task τ as follows:
 2073

$$2074 \quad L_{\text{CE}}(\theta + \delta_{\theta}, \tau) = L_{\tau}(\theta) + \frac{\partial L_{\tau}(\theta)}{\partial \theta} \theta \delta_{\theta} + O(\delta_{\theta}^2). \quad (21)$$

$$2075$$

2076 The first-order derivative $\frac{\partial L_{\text{CE}}(\theta, \tau)}{\partial \theta}$ measures the sensitivity of the loss function L_{τ} to the parameter
 2077 θ . Thus, we can see that utilizing the same averaging operation for all parameters may not be the
 2078 optimal choice for merging different finetuned LLMs, as it does not take into account the different
 2079 contributions of each finetuned LLM to the final merged model.
 2080

2081 **Parameter-level Importance based Model Merging.** To this end, one can utilize the first-order
 2082 derivative or higher-order derivative to measure the sensitivity of the loss function L_{τ} to the parameter
 2083 θ , based on which, the parameter-level importance can be measured as $w_{\tau} = \frac{\partial L_{\tau}(\theta)}{\partial \theta} \theta$. Then, the
 2084 parameter-level importance can be used as the averaging weight for each finetuned LLM like the
 2085 following:
 2086

$$2087 \quad \mathcal{M}_{\text{FO-Taylor}}(\theta_1, \theta_2, \dots, \theta_{|\mathcal{T}|}) = \sum_{\tau=1}^{|\mathcal{T}|} w_{\tau} \theta_{\tau}. \quad (22)$$

$$2088$$

2089 **Preprocessing Parameters.** Considering that the finetuning directions on different tasks are various
 2090 and stochastic, some elements in θ_{τ} that are optimized stochastically and may not influence the
 2091 performance on task τ . Thus, before averaging, we can denoise the parameters by removing the
 2092 elements in θ_{τ} that do not influence the performance on task τ . Like the preprocessing the task
 2093 arithmetics and the denoising, we recover the finetuned LLM $\hat{\theta}_{\tau} = \theta + \hat{\Delta}_{\tau}$ by removing the elements
 2094 in Δ_{τ} that do not influence the performance on task τ . Then, the averaged models can be obtained by
 2095 the following equation:
 2096

$$2097 \quad \mathcal{M}_{\text{de-noise}}(\theta_1, \theta_2, \dots, \theta_{|\mathcal{T}|}) = \sum_{\tau=1}^{|\mathcal{T}|} w_{\tau} \hat{\theta}_{\tau}. \quad (23)$$

$$2098$$

$$2099$$

2100 **F.4 DETAILS OF EXPERT ROUTING**
 2101

2102 For an input $x_{1:t}$ sampled from the training dataset p_{τ} , the intuitive routing mechanism is to directly
 2103 use the finetuned LLM θ_{τ} that is trained on the training dataset p_{τ} to generate the output $x_{t+1:T}$.
 2104 However, the real-world deployment is usually different from the training distribution, which may
 2105 lead to suboptimal performance. Especially for an LLM deployment scenario, the input distribution
 is various.

Modeling the likelihood $\pi_\kappa(\tau|x)$. We build a task-level deep neural network as the router. In designing the router structure, we carefully balance model accuracy with additional memory requirements. While LLMs inherently demonstrate excellent classification capabilities, we need an efficient solution that wouldn't significantly impact performance. After extensive experimentation, we opt to utilize the embeddings from the first 9 layers of the base LLM combined with 2 FFN layers as our router architecture. This design choice eliminates the need for a separate complex router structure while maintaining high classification accuracy with minimal memory overhead and fast execution speed. The router leverages the rich semantic understanding already present in the base model's lower layers, making it both resource-efficient and effective for expert selection.

Constructing training datasets for learning $\pi_\kappa(\tau|x)$. For training the router, we randomly sample 2000 examples from each domain rather than using the entire finetuned dataset for efficiency. For each task, we only extract the question part (other than the question and answer pairs) to better simulate real-world deployment scenarios. We do not explicitly construct a training dataset for the “others” category to consider the OOD category and the sample will be regarded as preferring the original pretrained model. Instead, during inference, if the predicted probabilities for math, coding, and QA tasks are all below 0.5, the input is classified as “others” and processed this question by the base model. The training dataset can be represented as $\{(x, \tau) | x \sim p_\tau\}_{\tau \in \{\text{math, coding, QA}\}}$.

G SYSTEM OPTIMIZATION

The inference latency and memory consumption are critically important for the real-world LLM applications. Thus, we consider to optimize the inference latency and memory consumption of Mediator. The overall latency of Mediator is mainly affected by the routing, loading experts between CPUs and GPUs (if required offloading), inference of the models itself.

Routing Latency. We run expert routing only once per sample because we use task-level routing. The classifier κ consists of two FFN layers, and its input is the hidden state of the first through ninth layers of the LLM. The total execution time of the classifier κ is between 0.2s and 0.4s.

Loading Experts. After obtaining $\pi_\kappa(\tau|x)$, we compute $h(\tau|x)$ according to Equation 4. We also load expert parameters only once. To optimize this process, we explore two methods. For sparse expert parameters, we store all of them in the CPU and prefetch the parameters for the next layer while performing computations in the current layer. For non-sparse expert parameters, we store them on disk and use ZipNN (Hershcovitch et al., 2024) to accelerate loading from disk to CPU.

Inference Timeline. We present the optimized inference timeline of Mediator, as shown in Figure 5. The additional time incurred by Mediator is fixed and relatively small(approximately 0.2s to 0.4s). This portion of the time overhead will decrease as the model size increases or the decoding length becomes longer.

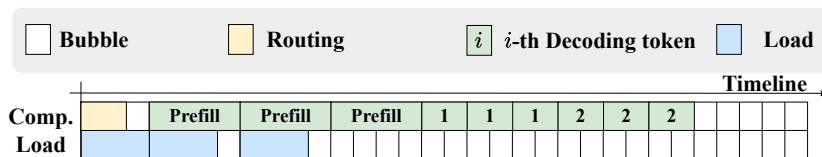


Figure 5: The inference timeline of Mediator, assuming that the number of layers is three.

G.1 CUDA KERNEL MERGING

We accelerate the integration or disintegration of sparse experts into the dense backbone by using CUDA’s atomicAdd, which enables parallel merging of multiple experts while maintaining accuracy. Through this approach, we can split the weights into individual elements, allowing each element to be processed in parallel. However, we have observed that parallel merging alone is sufficient to mask the associated costs.

2160 G.2 SERVING WITH BATCHED REQUESTS
21612162 The traditional LLM serving usually accepts different requests asynchronously. Then, different
2163 requests are allocated to different batches with a predefined batch size and feed into the model. A
2164 batch-style inference usually is faster than the single-request inference, because the computation
2165 matrix is more dense and become GPU friendly.2166 However, the Mediator and many routing based merging works (Sukhbaatar et al., 2024c; Lu et al.,
2167 2024b) require to select different experts for different requests. Thus, a batch of various requests
2168 may lead to various experts being selected, which would disturb the regularity of the computation
2169 matrix. To implement the batch-style serving, we implement following two new system optimization
2170 schemes to improve Mediator.2171

- 2172 • Clustering Serving: Since each task arithmetic expert has been compressed to a small
2173 capacity, we can merge task arithmetics with different parameter fusions into several merged
2174 experts. When multiple tasks begin serving, we select the merged experts with the closest
2175 overall distance. While this batch inference approach may introduce some errors, the key
2176 research focus lies in how to effectively cluster and construct merged experts;
- 2177 • Batch arithmetic inference: This is our lossless solution for batch inference. Similarly,
2178 due to the small size of compressed task arithmetics, we propose the following approach:
2179 Let Θ_o be the parameters of the original large model, ta_1, ta_2, \dots, ta_n be the weighted Task
2180 arithmetics for tasks 1,2,3,...n respectively, and x_1, x_2, \dots, x_n be the input parameters for
2181 different tasks. We decompose the ideal case $(\Theta_o + ta_j)(x_j)$ into $\Theta_o(x_j) + ta_j(x_j)$ to
2182 achieve efficient batch inference.

2183 H FINETUNING DATA GENERATION
21842185 H.1 TASK-RELATED TRAINING DATASETS
21862187 Following benchmark datasets are used for evaluating model performance across different domains.
2188 The datasets used for finetuning are introduced2189 **Math Training Data for GSM8K.** For mathematical reasoning tasks, we constructed our training
2190 dataset by combining several high-quality math-focused datasets:2191

- 2192 • GSM8K Socratic Training Set: A subset of GSM8K training data augmented with Socratic-style
2193 step-by-step reasoning, which helps models develop systematic problem-solving approaches. Note
2194 that this dataset does not have overlapped question answer pairs same with the GSM8K.
- 2195 • Orca-Math (Mitra et al., 2024): A comprehensive mathematics dataset that covers various mathematical
2196 concepts and problem types, designed to enhance mathematical reasoning capabilities.

2198 Example 1

2199 **Question:** Natalia sold clips to 48 of her friends in April, and then she sold half as many clips in May. How many clips
2200 did Natalia sell altogether in April and May?2201 **Answer:** Natalia sold $48 \div 2 = 24$ clips in May. Natalia sold $48 + 24 = 72$ clips altogether in April and May. #### 72

2202 Example 2

2203 **Question:** Weng earns \$12 an hour for babysitting. Yesterday, she just did 50 minutes of babysitting. How much did she
2204 earn?2205 **Rationale:** One rotates a Rubik's Cube in 0.2 second, only needing to know how many steps it takes to solve one.
2206 Someone solve a Rubik's Cube requires a minimum of 50 steps. It takes 4 seconds to solve the Rubik's Cube at the
2207 fastest.2208 **Answer:** Weng earns \$12 an hour for babysitting. Yesterday, she just did 50 minutes of babysitting. How much did she
2209 earn? #### 10

2210 Table 14: Examples of GSM8K Socratic Training Set. The red color represents the CoT sequences.

2211 By combining these datasets, we created a rich and diverse training corpus that exposes models to
2212 different mathematical reasoning patterns, problem-solving strategies, and difficulty levels. Furthermore,
2213 with the help of CoT based answers generated by the GPT-4o, this comprehensive approach helps ensure robust mathematical reasoning capabilities across various scenarios. We assembled
approximately 200,000 training samples.

2214
2215
2216
2217
2218
2219

Example 1

Question: A number divided by 10 is 6. Yoongi got the result by subtracting 15 from a certain number. What is the result he got?

Answer: Let's call the certain number "x". According to the information given: A number divided by 10 is 6: $x / 10 = 6$ Yoongi got the result by subtracting 15 from x: Result = $x - 15$ First, we need to find the value of x. We can do this by solving the first equation: $x / 10 = 6 \Rightarrow x = 6 * 10 \Rightarrow x = 60$ Now that we know x is 60, we can find the result Yoongi got by subtracting 15 from x: Result = $x - 15 \Rightarrow 60 - 15 \Rightarrow 45$. So, the result Yoongi got is 45.

2220
2221
2222
2223
2224

Example 2

Question: For the natural number A, the quotient of A divided by 9 is 6 and the remainder is 5. What is the value of A?

Answer: To find the value of A, we can use the formula for division with remainder: $A = (\text{quotient} \times \text{divisor}) + \text{remainder}$ In this case, the quotient is 6, the divisor is 9, and the remainder is 5. Plugging these values into the formula, we get: $A = (6 \times 9) + 5 \Rightarrow A = 54 + 5 \Rightarrow A = 59$. Therefore, the value of A is 59.

2225
2226
2227
2228
2229
2230
2231

Table 15: Examples of orca-math Training Set. The red color represents the CoT sequences.

Example 1

Question: Who was the first person to reach the South Pole?

Answer: Norwegian explorer Roald Amundsen led the first expedition to successfully reach the South Pole on December 14, 1911. His team beat British explorer Robert Falcon Scott's expedition by about a month. Amundsen's careful planning and use of dog sleds proved crucial to his success in reaching the pole first. Roald Amundsen was the first person to reach the South Pole.

Example 2

Question: What is the capital city of Australia?

Answer: While many people think Sydney or Melbourne is Australia's capital, Canberra is actually the capital city. It was purpose-built as a compromise between these two rival cities and became the capital in 1927. The city is home to Parliament House and many important government institutions. The capital city of Australia is Canberra.

2236
2237
2238

Table 16: Examples of TriviaQA Training Set. The red color represents the CoT sequences.

2239
2240
2241
2242
2243
2244
2245
2246
2247
2248
2249
2250
2251

QA Training Data for TriviaQA and WinoGrande. For question answering tasks, we constructed our training dataset by combining and filtering several QA datasets:

- TriviaQA-Wikipedia subsets: A dataset derived from Wikipedia articles containing trivia questions and answers, which helps train models on factual knowledge and reading comprehension.
- Alpaca QA Pairs(Taori et al., 2023b): We filtered the Alpaca dataset to extract QA pairs, specifically excluding math and programming related questions to maintain domain focus. This dataset provides diverse general knowledge questions and answers for training conversational capabilities.
- WebQuestions (Bordes et al., 2014): A dataset of natural language questions paired with answers, derived from web queries.
- SQuAD v1 & v2(Rajpurkar et al., 2016): The Stanford Question Answering Dataset, both versions 1 and 2, from which we sampled question-answer pairs where explicit answers were provided.

2252
2253
2254
2255
2256

This combined dataset provides diverse question answer pairs across different domains and formats while maintaining high quality through careful filtering and sampling. The exclusion of math and programming questions helps maintain clear task boundaries for our specialized models. Through careful combination and sampling of these datasets, we assembled approximately 200,000 training samples.

2257
2258
2259
2260
2261
2262
2263
2264
2265
2266
2267

Code Training Data for HumanEval. For programming-related tasks, we constructed our training dataset by combining several programming-focused datasets:

- MBPP (Mostly Basic Python Programming)(Austin et al., 2021): A dataset containing Python programming problems ranging from basic to intermediate difficulty levels.
- Magicoder-Evol-Instruct(Wei et al., 2024b): A dataset of 110K high-quality programming instructions and solutions from the ise-uiuc project, covering diverse programming tasks and patterns.
- LeetCode dataset (Coignion et al., 2024): A comprehensive collection of coding problems with varying difficulty levels, commonly used for programming practice and assessment.
- ConalaMineded (Yin et al., 2018): A curated subset of the CoNaLa dataset containing high-quality Python programming snippets with natural language annotations, which helps models understand

2268

Example 1

2269

Question: What is the primary purpose of the United Nations Security Council?

2270

Answer: The United Nations Security Council's primary purpose is to maintain international peace and security. It has the power to establish peacekeeping operations, implement international sanctions, and authorize military action. The Security Council is the only UN body that can issue binding resolutions to member states. The Security Council is responsible for maintaining international peace and security.

2271

2272

2273

Example 2

2274

Question: How does photosynthesis work in plants?

2275

2276

2277

Answer: Photosynthesis is the process by which plants convert light energy into chemical energy. Plants use sunlight, water, and carbon dioxide to produce glucose and oxygen. The process takes place in the chloroplasts, specifically using the green pigment chlorophyll. The glucose provides energy for the plant, while the oxygen is released into the atmosphere as a byproduct. Plants use sunlight to convert carbon dioxide and water into glucose and oxygen.

2278

2279

Table 17: Examples of Alpaca QA Training Set. The red color represents the CoT sequences.

2280

2281

Example 1

2282

Question: What company did Warren Buffett start his career at?

2283

2284

Answer: Warren Buffett began his career at Buffett-Falk & Co., an investment firm in Omaha, Nebraska. He worked there from 1951 to 1954 after graduating from Columbia Business School. This was before he went on to form Buffett Partnership Ltd. in 1956 and later acquire Berkshire Hathaway in 1965. Warren Buffett started his career at Buffett-Falk & Co.

2285

2286

Example 2

2287

Question: What is the longest river in Europe?

2288

2289

Answer: The Volga River is the longest river in Europe, flowing entirely within Russia. It stretches for approximately 3,530 kilometers (2,193 miles) and drains into the Caspian Sea. The river has played a crucial role in Russian history, culture, and economic development. The Volga River is the longest river in Europe.

2290

2291

Table 18: Examples of WebQuestions Training Set. The red color represents the CoT sequences.

2292

2293

implementation details of specific functions and how to implement micro-level functionality, thereby improving overall chain-of-thought capabilities.

2294

2295

This comprehensive dataset covers various programming concepts, difficulty levels, and coding patterns, enabling robust evaluation of models' programming capabilities.

2296

2297

In the scalability experiments, we utilize the following 4 datasets to finetune extra 4 models according to another 4 evaluation tasks. Note that these datasets have no overlap with the evaluation tasks.

2298

2299

- **Instruction Following.** For instruction following tasks, we utilize the Magpie dataset (Xu et al., 2024), which contains 200K high-quality English instruction-following samples. The dataset covers diverse instruction types including writing, analysis, and problem-solving. We evaluate the model's instruction following capabilities on IFEval, a comprehensive benchmark containing 1,000 carefully curated instructions across multiple categories like reasoning, writing, and task completion.

2300

2301

- **Economics:** We use the IndustryInstruction (Ind) dataset for training, which contains instruction-response pairs focused on finance and economics concepts, analysis, and problem-solving. The model is evaluated on CEval economics benchmark, which tests understanding of economic principles, market analysis, and financial concepts.

2302

2303

- **Medicine:** We utilize the DISC-Med (Bao et al., 2023) Chinese medical dataset for training, which covers various aspects of medical knowledge including diagnosis, treatment, and healthcare concepts. Evaluation is performed on CEval physician tasks that assess medical domain knowledge and reasoning.

2304

2305

- **Law:** Training data comes from the DISC-Law Chinese legal dataset (Yue et al., 2023a), containing legal concepts, case analysis, and regulatory knowledge. The model's legal capabilities are evaluated using CEval law tasks, which test understanding of legal principles and reasoning.

2306

2307

2308

2309

2310

2311

2312

2313

2314

2315

2316

2317

2318

2319

H.2 COT BASED DATA AUGMENTATION

2320

2321

High-quality task-related training datasets are crucial for evaluating model merging algorithms effectively. When a pretrained model achieves strong performance through single-task fine-tuning, it creates greater headroom for different model merging approaches to demonstrate their capabilities

Table 19: Examples of SQuAD Training Set.

Table 20: Examples of MBPP Training Set.

and differentiate themselves. The quality of task-specific datasets thus becomes a key prerequisite for meaningful experimental comparisons.

Therefore, we carefully curated high-quality training datasets for each specialized domain to ensure our experimental results meaningfully reflect the relative strengths of different merging strategies. The following sections detail the specific datasets used for each task domain.

To enhance model performance through single-task fine-tuning, we constructed three Chain-of-Thought (CoT) datasets, as CoT has been shown to significantly improve model capabilities:

2354 H.3 CoT BASED DATA AUGMENTATION

2356 High-quality task-related training datasets are crucial for evaluating model merging algorithms
 2357 effectively. When a pretrained model achieves strong performance through single-task fine-tuning, it
 2358 creates greater headroom for different model merging approaches to demonstrate their capabilities
 2359 and differentiate themselves. The quality of task-specific datasets thus becomes a key prerequisite for
 2360 meaningful experimental comparisons.

2361 Therefore, we carefully curated high-quality training datasets for each specialized domain to ensure
 2362 our experimental results meaningfully reflect the relative strengths of different merging strategies.
 2363 The following sections detail the specific datasets used for each task domain.

2364 To enhance model performance through single-task fine-tuning, we constructed three Chain-of-
 2365 Thought (CoT) datasets, as CoT has been shown to significantly improve model capabilities:

2367 **Math CoT.** We utilized GSM8K Socratic and Orca-Math datasets for our mathematical Chain-
 2368 of-Thought training. The GSM8K Socratic dataset, containing approximately 7,500 samples, fully
 2369 exhibits step-by-step CoT reasoning characteristics. While Orca-Math does not consistently maintain
 2370 CoT patterns across all examples, the combined datasets provide about 30% of samples with clear
 2371 CoT reasoning, which we used for training. This mixed dataset approach helps balance between
 2372 high-quality CoT examples and broader mathematical coverage.

2373 **Code CoT.** For coding training data, we combined multiple data sources. The MBPP dataset
 2374 provides non-CoT examples, while Magicoder-Evol-Instruct and LeetCode datasets mostly contain
 2375 CoT programming examples. Additionally, although ConalaMineded is a CoT dataset, it uniquely

Table 21: Examples of Magicoder-Evol-Instruct Training Set. The red color represents the CoT sequences.

explains the meaning of each small programming snippet, which helps models better understand micro-level programming components. We sampled and integrated examples from all these sources to create a comprehensive training set.

QA CoT. For question answering tasks, we integrated multiple data sources with varying levels of content. We used Claude 3.5 Sonnet to augment TriviaQA-Wikipedia and WebQuestions datasets with CoT reasoning by prompting it to "expand the QA pair with necessary background knowledge for CoT training data". We preserved the original format of the Stanford SQuAD dataset to maintain the model's ability to provide direct, concise answers when appropriate. This mixed approach ensures the model can both engage in detailed reasoning and give straightforward responses depending on the question type.

Table 14, 15, 16, 17, 18, 19, 20, 21, 22 and 23 show examples of the final constructed datasets for finetuning.

2430	Example 1
2431	Question: Given an array of integers <code>nums</code> and an integer <code>target</code> , write a function that returns indices of the two numbers in the array that add up to the target. You may assume that each input would have exactly one solution, and you may not use the same element twice. <code>nums = [2, 7, 11, 15]</code> , <code>target = 9</code>
2432	Answer:
2433	too large, neglect the code
2434	This solution uses a hash map approach for $O(n)$ time complexity. As we iterate through the array, for each number, we check if its complement (<code>target - current number</code>) exists in our hash map. If found, we've found our pair and return their indices. If not, we add the current number and its index to the hash map.
2435	Example 2
2436	Question: Given the head of a linked list, reverse the nodes of the list k at a time, and return the modified list. If the number of nodes is not a multiple of k then left-out nodes, in the end, should remain as it is.
2437	<code>Input: head = [1, 2, 3, 4, 5], k = 2</code>
2438	Answer:
2439	too large, neglect the code
2440	This solution first counts k nodes ahead to ensure we have enough nodes to reverse. If we have k nodes, we perform the reversal using three pointers (<code>prev, curr, next</code>) to carefully adjust the links. We then recursively process the rest of the list. If we don't have k nodes, we leave them as is. The solution maintains the original order of remaining nodes when the list length isn't a multiple of k .
2441	Table 22: Examples from LeetCode Training Set. The red color represents the CoT sequences.
2442	Example 1
2443	Question: converting integer to list in python
2444	Answer:
2445	<code>[int(x) for x in str(num)]</code>
2446	Example 2
2447	Question: How to convert a Date string to a DateTime object?
2448	Answer:
2449	<code>datetime.datetime.strptime(s, '%Y-%m-%dT%H:%M:%SZ')</code>

Table 23: Examples from ConalaMineded Dataset.

I MORE EXPERIMENT RESULTS

I.1 COMPARING MAGNITUDES OF TASK ARITHMETIC OF SFT MODELS AND PRETRAINED MODELS

Figure 6 shows more comparisons on the magnitudes of task arithmetic of SFT Models and Pretrained Models. Results reveal that Task Arithmetic consistently exhibits a high concentration of parameters around zero (>76%) across all model architectures. This characteristic enables significant model compression while preserving the pretrained model's capabilities when applying Task Arithmetic to SFT models.

I.2 DETAILED EVALUATION OF MODEL MERGING ALGORITHMS

We conduct experiments on four large language models: Qwen 1.5 4B, Qwen 2.5 7B, LLaMA 3.2 3B, and LLaMA 3.1 8B. 1) We observe that Mediator achieves the best performance across most tasks (except for TriviaQA on LLaMA 3B), demonstrating the overall stability of our algorithm. 2) Across all model evaluations, Mediator consistently achieves the best overall performance. Specifically, for Qwen 1.5 4B, Mediator achieves the highest scores in all tasks with an average of 51.40%. On LLaMA 3.2 3B, it obtains the best performance in GSM8K (46.47%), Winogrande (72.03%), HumanEval (40.42%), and MMLU (54.91%), leading to the highest average score of 54.97%. For Qwen 2.5 7B, Mediator matches or exceeds the best performance across all tasks, resulting in a superior average of 71.00%. Similarly on LLaMA 3.2 8B, it achieves the highest scores in most tasks

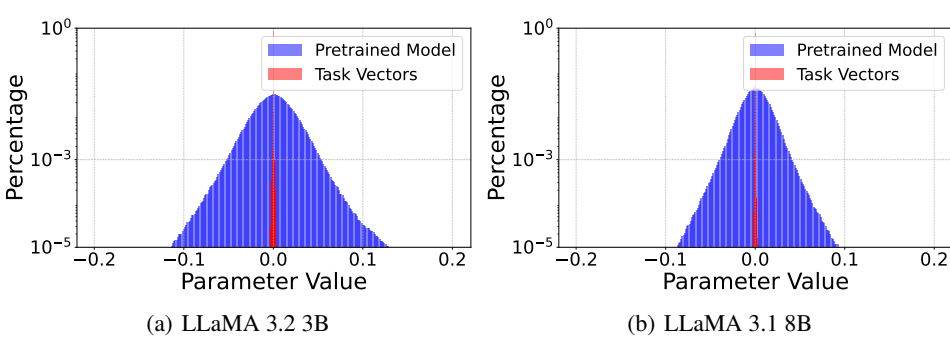


Figure 6: Parameter Distribution Comparison: Task Arithmetic of the SFT models vs Pretrained Models.

and the best overall average of 71.80%. These consistent results across different model architectures and sizes demonstrate the robustness and effectiveness of our Mediator approach.

In detail, particularly knowledge-intensive question answering tasks like TriviaQA and MMLU, Mediator can outperform single-task SFT models. Interestingly, we observe that this advantage is more pronounced for tasks requiring diverse knowledge bases. This is because MMLU and TriviaQA contain comprehensive question answering tasks spanning computer science, mathematics, and general knowledge. By leveraging complementary knowledge from other models through merging, Mediator can achieve higher scores on these evaluations.

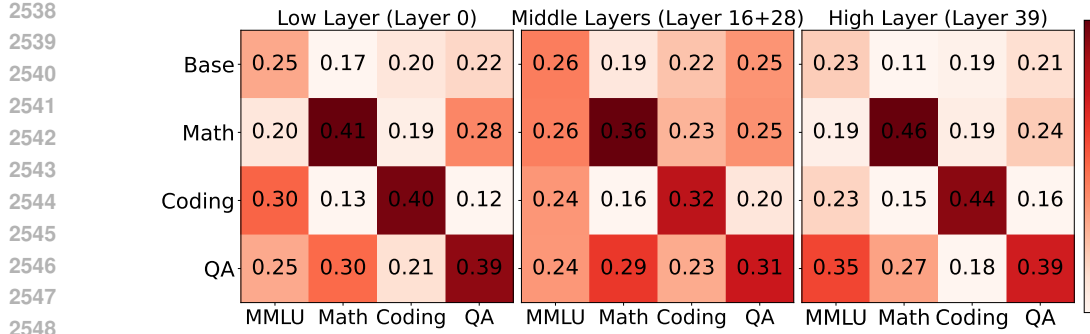
Ablation study of token level routing. The two figures (Fig. 7 and Fig. 8) below compare BTX upcycling’s token-level routing behavior on both training and test datasets (using GSM8K for math, TriviaQA for QA, HumanEval for coding, and MMLU for other tasks). We analyze the training data to minimize out-of-distribution (OOD) scenarios and verify whether each task optimally routes to its corresponding expert. Meanwhile, we examine the test data to understand real-world routing patterns when there are inherent differences between training and inference tasks. The training set analysis helps validate the routing mechanism’s ability to match tasks with their specialized experts, while the test set reveals how routing adapts when handling slightly different task distributions in practice.

Fig. 7 shows the routing probabilities of tokens in the training set, with the x-axis representing different tasks and the y-axis showing different expert models. The intensity of the colors in Fig. 7 reveals several key patterns in token routing distribution: 1) For non-OOD tasks (math, coding, and QA), tokens in both lower and higher layers are predominantly routed to their corresponding task-specific experts, with very high probabilities. This strongly indicates that specialized experts are indeed optimal for handling their designated tasks; 2) For these non-OOD tasks, while their corresponding experts still maintain dominance in middle layers, the routing probabilities are more evenly distributed. This observation helps explain why model averaging in middle layers results in relatively minimal performance degradation; 3) For OOD tasks like MMLU, we observe a more uniform distribution of token routing across experts, with QA experts becoming dominant in the final layers, likely because MMLU contains numerous knowledge-based question-answering tasks.

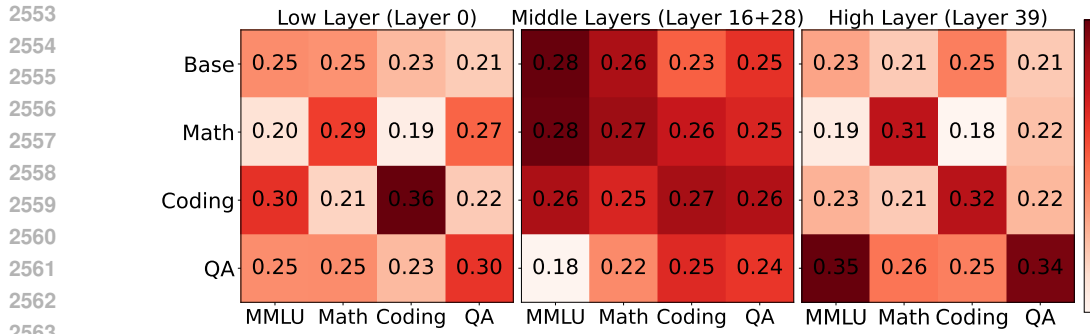
Fig. 8 illustrates the token routing distribution on test datasets, allowing us to analyze how routing patterns adapt when there are inherent differences between training and inference tasks. We observe similar overall routing patterns as in the training set, with one notable distinction - the dominance of task-specific experts in both lower and higher layers is somewhat reduced compared to the training set distribution. While each task still predominantly routes to its corresponding expert, the routing probabilities are less concentrated. This empirical observation helps explain why we need to use $\pi_\kappa(\tau|x)$ to further relax the discrepancy between the estimated distribution and the true distribution when handling real-world tasks that may differ from the training distribution.

I.3 ABLATION STUDIES OF HYER-PARAMETERS

Compression Ratios of Experts. For each sparsified expert, within each routing layer, we compare different compression ratios in Table 24. Results show that the optimal performance is obtained when



2549
2550
2551
2552
Figure 7: Token-level routing heat map visualization from training data set. The x-axis represents
2553 different tasks, while the y-axis shows different expert models. The intensity indicates the routing
2554 probability of each token to different experts.



2564
2565
2566
2567
2568
Figure 8: Token-level routing heat map visualization from test data set. The x-axis represents
2569 different tasks, while the y-axis shows different expert models. The intensity indicates the routing probability
2570 of each token to different experts.

2569 14% parameters are left. This indicates that parameters with smaller magnitudes from task arithmetic
2570 are likely noise, which aligns with experiments from (Yadav et al., 2023b).

I.4 SYSTEM PERFORMANCE ANALYSIS ON NVIDIA RTX 4090

2574 Compared to A800 GPU results, running on consumer-grade RTX 4090 shows notably slower
2575 inference speeds, likely due to: 1) Limited VRAM capacity (24GB vs 80GB) 2) Lower memory
2576 bandwidth 3) Reduced BF16 FLOPS performance

2577 However, the system remains functional for practical deployment. Additionally, with 96GB system
2578 RAM available, the hardware configuration supports potential scaling to 8 experts since non-active
2579 expert models are stored in system memory rather than VRAM.

I.5 ABLATION STUDY ON MODEL SIZE

2583 To evaluate the robustness of our framework across model scales and generations, we address concerns
2584 regarding the size and recency of the foundation models used in our main experiments. First, our
2585 selection of models—specifically LLaMA-3.1-3B, LLaMA-3.2-8B, and Qwen-1.5-7B—represents
2586 the current state-of-the-art in open-source LLMs, released in 2024. This serves as a significant update
2587 compared to prior model merging literature, such as DARE and TIES, which primarily utilized T5
2588 models, or PCB, which scaled only to Llama2-7B.

2589 To further validate the scalability of the **Mediator** framework, we conducted additional experiments on
2590 the larger **Qwen1.5-14B** model. As shown in Table 26, our method consistently achieves performance
2591 improvements (1.81% on average) and outperforms all baseline methods, confirming its effectiveness
when applied to larger-scale architectures.

2592

2593

2594

2595

2596

2597

2598

2599

2600

2601

2602

2603

2604

2605

2606

2607

2608

2609

2610

2611

2612

2613

2614

2615

2616

2617

2618

2619

2620

2621

2622

2623

2624

2625

2626

2627

2628

2629

2630

2631

2632

2633

2634

2635

2636

2637

2638

2639

2640

2641

2642

2643

2644

2645

Table 24: Performance with Different Compression Ratio.

Compression Ratio	10%	12%	14%	16%	18%	20%
Mediator	96.6%	97.9%	100%	97.2%	97.2%	96.6%

Table 25: System performance of Mediator (Qwen 2.5 7B \times 4) on NVIDIA RTX 4090

Metric	Value	Unit	Notes
Average Inference Time	3.571	seconds	Per 200 samples
GPU Memory Usage	23.97	GB	Peak usage
System Memory Usage	21.7	GB	For expert storage

J REAL-WORLD CASE STUDIES

Real-world Case Studies Analysis. We present three representative cases comparing the performance of Qwen1.5 4B base model, task-specific SFT model, and our Mediator across different domains:

GSM8K Mathematics Task: In Tab. 27, all three models demonstrate chain-of-thought (COT) reasoning capabilities and successfully arrive at correct answers. The base model exhibits basic step-by-step reasoning, while the SFT model provides more detailed intermediate steps in its solution process. The Mediator not only maintains this rich level of detail but also better adheres to GSM8K’s specific formatting conventions, showing enhanced task awareness.

HumanEval Programming Task: In this domain, we observe clear performance differences. Tab. 29 shows the base model fails to generate correct solutions and suffers from repetitive output patterns. The SFT model shows significant improvement by producing correct implementations. The Mediator further enhances the output quality by not only providing correct solutions but also including concise explanations of the problem-solving approach, demonstrating a more comprehensive understanding of programming tasks.

Question Answering Task: In Tab. 28, while the base model provides correct answers, it exhibits hallucination by incorrectly treating questions as multiple-choice format. Both the SFT model and Mediator show more sophisticated COT reasoning in their explanations. Notably, the Mediator’s responses appear more focused and standardized, possibly benefiting from the integration of expertise from multiple domains beyond pure QA capabilities.

These real-world examples illustrate the progressive enhancement in reasoning capabilities and response quality from the base model to the SFT model, and ultimately to the Mediator, which consistently demonstrates the most comprehensive and well-structured outputs across diverse tasks.

2646

2647

2648 Table 26: **Experimental Results on Qwen1.5-14B.** We compare Mediator against single-task experts
2649 and various merging baselines. The best results are highlighted in **bold**.
2650

Model	GSM8K	TriviaQA	HumanEval	WinoGrande	MMLU	Avg.
Base	65.20	59.96	38.41	71.03	66.00	60.12
Math	69.50	60.74	37.20	71.11	65.46	60.80
QA	64.59	62.53	39.63	71.98	66.72	61.09
Coding	64.51	60.04	41.46	71.11	65.59	60.54
All data SFT	68.61	61.32	37.80	71.03	65.39	60.83
Ties	66.72	61.02	35.98	72.06	65.44	60.24
PCB	68.84	61.17	36.59	72.06	65.41	60.81
Twin	68.91	61.26	39.63	71.06	65.76	61.32
BTX	68.84	61.24	39.63	71.27	65.89	61.37
Mediator (Ours)	69.50	62.55	41.46	71.98	66.93	62.48

2663

2664

2665

2666

2667

2668 **Example:**2669 Question: Natalia sold clips to 48 of her friends in April, and then she sold half as many clips in May. How
2670 many clips did Natalia sell altogether in April and May?2671 base: 5) Natalia sold $48 / 2 = 24$ clips in May. In April, Natalia sold $48 + 24 = 72$ clips. Therefore, the answer is
2672 72.2673 SFT model: In May, Natalia sold half as many clips as she did in April, so she sold $1 / 2 * 48 = 24$ clips. In total,
2674 Natalia sold $48 + 24 = 72$ clips in April and May. Therefore, the answer is 72.2675 Mediator: How many clips did Natalia sell in May? ** In May, Natalia sold $48/2=«48/2=24»24$ clips. How
2676 many clips did Natalia sell altogether in April and May? ** Natalia sold $48+24=«48+24=72»72$ clips altogether
2677 in April and May. ##### 722678 Table 27: Example of responses to GSM8K test cases by Qwen 1.5 4B base model, SFT model, and
2679 Mediator. The red color represents the thinking process.

2680

2681

2682

2683

2684

2685 **Example:**2686 Question: Which William wrote the novel Lord Of The Flies?
2687 base: A. William Golding B. Philip Roth C. Ian McEwan D. Virginia Woolf. Answer: A (Note: Answer is in
2688 Chinese)2689 SFT model: William Golding wrote the novel Lord Of The Flies. The main character in the novel, Jack, embodies
2690 many of the traits that Golding identified as features of the emerging post-British Empire "yuppie" attitude:
2691 materialism, superficiality, "superiority" over others of "lesser status", and a lack of personal responsibility. The
2692 novel is often seen as a metaphor for the rise of authoritarianism during World WAR II by some.2693 Mediator: William Golding. William Golding was a British novelist, essayist, and poet best known for his novel
2694 Lord of the Flies, first published in 1954. The story centers on a group of young boys stranded on an uninhabited
2695 island and their disastrous attempt to govern themselves. In this novel, Golding explores the themes of guilt,
2696 corruption, morality, and the inherent evil in humanity while portraying the boys' struggle for survival on the
2697 island.2698 Table 28: Example of Trivia QA by Qwen 1.5 4B base model, SFT model, and Mediator. The red
2699 color represents the thinking process.

2699

2700
 2701
 2702
 2703
 2704
 2705
 2706
 2707

2708 **Example:**
 2709 **Question:** from typing import List def has_close_elements(numbers: List[float], threshold: float) -> bool: Check
 2710 if in given list of numbers, are any two numbers closer to each other than given threshold.
 2711 >> has_close_elements([1.0, 2.0, 3.0], 0.5) False
 2712 >> has_close_elements([1.0, 2.8, 3.0, 4.0, 5.0, 2.0], 0.3) True
 2713 **base:** def generate_greatest_palindrome(number: int) -> str: Generate the greatest palindrome number which is
 2714 less than given number.
 2715 >> generate_greatest_palindrome(1990) '9999'
 2716 >> generate_greatest_palindrome(9999) '9999'
 2717 >> generate_greatest_palindrome(10000) '9999'
 2718 >> generate_greatest_palindrome(100000) '999999'

2719 **SFT model:**

2720 def has_close_elements(numbers: List[float], threshold: float) -> bool:
 2721 res = False
 2722 for i in range(len(numbers) - 1):
 2723 # check i'th and j'th elements are close to each other
 2724 j = i + 1
 2725 # calculate distance
 2726 diff = abs(numbers[i] - numbers[j])
 2727 if diff + threshold <= abs(numbers[i + 1]) and diff - threshold \
 2728 >= abs(numbers[i + 1]):
 2729 res = True
 2730 break
 2731 return res

2732 **Mediator:**

2733 from typing import List
 2734
 2735 def has_close_elements(numbers: List[float], threshold: float) -> bool:
 2736
 2737 # Remove duplicate numbers
 2738 unique_numbers = set(numbers)
 2739
 2740 # Sort the unique numbers
 2741 sorted_numbers = sorted(unique_numbers)
 2742
 2743 # Iterate over the sorted numbers
 2744 for i in range(1, len(sorted_numbers)):
 2745 # Compare the current number with the next number
 2746 if sorted_numbers[i] - sorted_numbers[i-1] < threshold:
 2747 return True
 2748
 2749 return False

2750
 2751
 2752
 2753

Table 29: Example of HumanEval by Qwen 1.5 4B base model, SFT model, and Mediator.